DISSERTATION

THE ROLES OF IRON, THE INFRAPATELLAR FAT PAD, AND DIETARY FACTORS IN THE HARTLEY GUINEA PIG MODEL OF SPONTANEOUS OSTEOARTHRITIS

Submitted by

Lauren Radakovich

Department of Microbiology, Immunology, and Pathology

In partial fulfillment of the requirements

For the Degree of Doctor of Philosophy

Colorado State University

Fort Collins, Colorado

Fall 2018

Doctoral committee:

Advisor: Kelly Santangelo

Christine Olver
Amy MacNeill
Michelle Foster
Michael Pagliassotti

Copyright by Lauren Beck Radakovich 2018

All Rights Reserved

ABSTRACT

THE ROLES OF IRON, THE INFRAPATELLAR FAT FAD, AND DIETARY FACTORS IN THE HARTLEY GUINEA PIG MODEL OF SPONTANEOUS OSTEOARTHRITIS

Osteoarthritis (OA) is the most prevalent musculoskeletal disorder across the world, affecting close to 300 million people. The disease manifests as degeneration and loss of articular cartilage, synovial hyperplasia, formation of osteophytes, subchondral bone remodeling, and joint space narrowing. These changes result in decreased range of motion as well as painful mobility in affected individuals. The knee joint is the most commonly afflicted joint. Osteoarthritic changes may develop secondary to a localized injury, referred to as post-traumatic OA. Degenerative changes can also develop without an inciting cause, which is referred to as spontaneous, or primary OA. Spontaneous OA is an insidious disease that is associated with aging, and, more recently, with obesity. The mechanisms contributing to disease development are not yet fully characterized, which has impeded implementation of successful treatment options. Currently, there are no treatments that are able to restore degraded cartilage. Thus, most patients with symptomatic knee OA undergo costly total knee joint replacement surgeries. The aims of this dissertation were to explore the roles that aging-associated iron accumulation, the infrapatellar fat pad, and calorie restriction with various diets may play in OA development. These studies were performed in the Hartley guinea pig, one of the only small animal models of spontaneous OA. One study was performed in Strain 13 guinea pigs, a strain that is OA-resistant.

Iron is an element that acts as a double-edged sword. It is essential for oxidative phosphorylation and heme synthesis, yet its redox potential means it has the capacity to incite

oxidant damage when present in excess. As there is no direct excretion mechanism for iron, it tends to accumulate slowly within tissues over time. This cellular iron accrual has been implicated in many degenerative diseases associated with aging, but its potential role in spontaneous OA has not been well-studied. In our first studies, we demonstrated that systemic iron levels have an influence on OA. We were able to induce bony and cartilage lesions in OA-resistant Strain 13 guinea pigs by systemic administration of iron dextran. Immunohistochemistry (IHC) indicated higher levels of lipid peroxidation in cartilage, menisci, the infrapatellar fat pad (IFP), and synovium in the iron overload animals. Special stains revealed that iron content was significantly higher in the IFP in these animals, which we propose serves as a local depot of oxidant damage to the knee joint. In a parallel study, we fed OA-prone Hartley guinea pigs an iron deficient diet to determine if reducing systemic iron levels may have a protective effect on the knee joint. Cartilage lesions were significantly lower in the iron deficient diet group compared to controls. Likewise, IHC for lipid peroxidation revealed less oxidant damage in the iron deficient pigs. However, no differences were noted in knee joint iron content, so the exact mechanisms for the lessened OA remain unclear.

Because the iron overload study pointed to the IFP as a potential iron depot, we wanted to further characterize how this adipose tissue contributes to overall knee joint homeostasis. First, we demonstrated that quantitative iron content in the IFP was increased in aged, osteoarthritic guinea pigs compared to young, healthy animals. Gene expression data collected suggested that dysregulated iron trafficking, particularly increased expression of ZIP14 – which has been linked to pathologic iron uptake in other conditions – may be contributing to this aging-associated increase of iron in the IFP. Because of our suspicion that the IFP may be inciting local oxidant damage to the knee, we surgically removed it from a set of young Hartley guinea pigs. An

identical sham procedure was performed in the contralateral limb. Four months post-surgery, animals were collected to evaluate OA in both limbs. Both cartilage and bony OA scores were markedly decreased in the IFP removal limb compared to the sham surgery limb. It is possible that removal of the IFP removed a source of local inflammatory mediators and iron, which resulted in lessened OA. As the IFP was replaced by a thick band of fibrous connective tissue, increased joint stability was also considered a contributing factor. Future studies will more closely examined contributions of biomechanical factors that may be at play.

Finally, we aimed to determine how dietary manipulations may influence *early* OA, as previous studies suggest that calorie restriction may improve *end-stage* OA. Additionally, many studies have shown high fat diet (HFD)-induced obesity plays a role in OA development due to the inflammatory nature of excess adipose tissue. In our study, we demonstrated that calorie restriction with a low fat regular chow diet, but not a calorie restricted HFD, delayed onset of OA in Hartley guinea pigs. In fact, the HFD group had higher levels of systemic inflammation than the restricted regular chow group. The HFD group had similar levels of inflammation and OA scores as obese animals. Thus, we concluded that the pro-inflammatory nature of a HFD supersedes any positive effects of calorie restriction in the onset of spontaneous OA.

ACKNOWLEDGEMENTS

I would like to thank many people for making this research possible. First and foremost, I owe my most sincere gratitude to my advisor, Kelly Santangelo, for her tireless efforts in helping me both in the lab and in ensuring my growth as a clinical pathologist and scientist. She welcomed me with open arms at the beginning of this journey and has treated me as an equal from day one. She has been an incredible mentor, advisor, collaborator, and friend for the past five years. Thank you so much for taking me under your wing as your first graduate student. It has been through your support and unwavering positive attitude that I have achieved so much. I would also like to thank Christine Olver for her guidance along the way and in my training as a clinical pathologist. She has been there many times to offer a fresh perspective and "therapeutic chocolate" in times of stress and self-doubt. My committee members have provided invaluable insight during this journey, and thank you for patiently listening to many presentations of my data. I admire each and every one of you. My colleagues Mary Afzali and Lindsey Burton have been instrumental in bringing many of these projects to fruition and in helping me stay sane throughout this process. For their help and companionship, I am incredibly grateful. Undergraduate students, especially Lauren Culver and Maggie Campbell were integral to my success in chipping away at these projects. And of course, I would like to thank my loving husband, Tony for his never-ending support, sense of humor, and unconditional love throughout this process. He has been there with me through all the triumphs and failures in vet school, during my clinical pathology residency, and now this PhD. Without him, I would not be where I am today.

TABLE OF CONTENTS

LIST OF TABLES

LIST OF FIGURES

CHAPTER 1

LITERATURE REVIEW

1.1 Importance of Osteoarthritis.

Osteoarthritis (OA) is a degenerative disease of joints that is hallmarked by loss of articular cartilage, formation of osteophytes, synovial hyperplasia, and thickening of subchondral bone[1]. These changes often result in decreased range of motion, and, therefore, contribute to inhibited and sometimes painful mobility for affected individuals. The loss of the ability to move freely and without pain is a key problem leading to a decreased quality of life in those suffering from OA[2]. As with many degenerative diseases, the biggest risk factor associated with OA is age[3]. However, obesity is closing in on age as one of the most prominent risk factors contributing to development of this disease[4]. Other identified risk factors associated with OA in people include female sex, African American race, and physically demanding jobs with frequent knee bending[3,5–7].

In general, there are two broad categories of OA. First, there is primary OA, which is also commonly referred to as spontaneous OA or naturally-occurring OA. In spontaneous OA, which is the main focus of this dissertation, the onset and/or predisposing cause of disease is unknown. In other words, there is no defined event that incites OA pathology. This is in contrast to secondary or post-traumatic OA (PTOA) where a single event, usually a traumatic injury to the joint, initiates onset of the degenerative changes[8,9]. In addition to having a clear inciting incident, individuals with PTOA often develop chronic changes similar to those seen in spontaneous OA[9].

PTOA commonly affects younger individuals, athletes, and military personnel, while spontaneous OA affects older individuals[8,9].

Unfortunately, in the case of primary OA, the mechanisms leading to the onset and progression of this debilitating disease are poorly understood. There are likely numerous complex factors at play contributing to OA, which are addressed in more detail, below. In addition to the lack of understanding of the pathogenesis of spontaneous OA, there are currently no treatment options that are able to restore damaged cartilage to normal structure or function. Rather, treatment is aimed at symptom modification and pain relief[10]. Of relevance, cartilage is an avascular tissue, and, as such, faces unique difficulties in repair compared to other tissue types[11,12]. Because of this, most patients with end stage disease either endure symptomatic relief with chronic use of anti-inflammatory medications, or they may undergo costly total joint replacement surgery. Notably, these surgeries cost the United States over $185 billion a year[13]. Further, pain management with anti-inflammatories often comes with a host of unwanted side effects and may not provide satisfactory pain relief[14]. Thus, more research is needed to fill knowledge gaps in our understanding of OA. Better comprehension of OA may lead to more treatment options that may restore damaged cartilage or prevent cartilage breakdown from occurring in the first place.

1.2 Current Understanding of Osteoarthritis Pathogenesis.

Spontaneous OA has historically been considered a “wear and tear” disease of joints due to mechanical breakdown of cartilage over time. However, we now know that inflammation plays an essential role to disease pathogenesis[15]. Nonetheless, the complex pathogenesis leading to OA remains loosely defined, and there is much we still do not understand. In the case of

PTOA, recent studies suggest that injury to the joint stimulate the release of inflammatory cytokines such as IL-1, IL-4, IL-13, and TNF, as well as matrix-degrading metalloproteinases (MMPs) from chondrocytes, synoviocytes, and osteoblasts[16–18]. Once MMP activity is underway, chondrocytes undergo hypertrophy while simultaneously losing their ability to produce cartilage matrix[17]. At the same time, chondrocytes release vascular endothelial growth factor (VEGF), which can lead to increased vascularization of the synovium and the whole joint[19,20]. Along with this destruction of cartilage matrix and vascularization, subchondral bone also undergoes pathologic remodeling, which can lead to the formation of cysts and osteophytes[18].

In aging individuals, chondrocytes, like other cells, exhibit increased production of inflammatory cytokines. Advanced glycation end products (AGEs) – proteins and lipids that have been glycated due to sugar exposure – are implicated in this process. With age, AGEs accumulate in articular cartilage and bind to chondrocyte receptors that increase secretion of pro-inflammatory cytokines and VEGF[21–23]. Another factor possibly contributing to the increased inflammatory status of chondrocytes is "inflammaging," where systemic levels of inflammatory cytokines slowly increase with age[24]. Inflammaging has been implicated in a variety of aging-associated diseases including Alzheimer's, atherosclerosis, type II diabetes, cancer, and heart disease[25]. Inflammaging has also been implicated in spontaneous OA[24]. This steady rise in pro-inflammatory mediators and oxidants is persistent, low-grade, and considered non-resolving[25]. Circulating levels of IL-6, specifically, exhibit a strong and robust association with age-related disease and mortality[26]. Of note, higher levels of IL-6 were found in individuals with knee joint OA and were associated with a higher risk of disease progression[27]. Studies examining the possibility of local inflammaging within the joint are needed.

1.3 Effects of Obesity, Diet, and the Infrapatellar fat pad.

A major risk factor associated with both inflammaging and development of OA is obesity[24]. Historically, it was believed that increased load-bearing on joints was the driving factor of the OA seen in obesity. However, because these individuals often experience OA in non-weight-bearing joints, such as the hands, increased load cannot entirely explain the link between OA and obesity[28]. The low-grade systemic inflammation associated with obesity is now considered a major contributor to disease pathogenesis[29]. Likewise, as people age, muscle mass decreases while fat mass increases. This increased fat mass, even without overt obesity, may contribute to systemic inflammaging and OA in aging people[30]. Inflammation from adipose tissue is primarily attributed to infiltrating macrophages[31]. Other factors contributing to an pro-inflammatory state in obese individuals include enhanced translocation of lipopolysaccharide from the gastrointestinal tract to the bloodstream[32] and stimulation of the innate immune response by circulating saturated fatty acids[33]. Increased leptin, an adipokine that is dysregulated in obesity, promotes inflammation through stimulation of IL-1, tumor necrosis factor (TNF), and IL-6[34]. Leptin has also been shown to promote OA by increasing activity of MMPs and aggrecanases that degrade the cartilage matrix[33,35]. A large study investigating the contribution of adipose mass to levels of systemic inflammatory cytokines found that obese individuals with knee OA had increased circulating IL-6[36]. Additionally, those study participants who lost at least 10% of their fat mass demonstrated a decrease in their IL-6 levels, as well as decreased knee pain[36]. Together, these findings lend support to the role of obesity-related systemic inflammation in the pathogenesis of OA.

Numerous animal studies have investigated the mechanisms behind obesity-driven knee OA. Most of these studies utilize a high fat diet (HFD) to induce obesity[32,37–43]. HFDs used in

these rodent studies are typically comprised of 40-60% fat, with animal-based saturated fats as the primary component. While most of these studies employ an injury to incite OA, they all provide convincing evidence that HFD-induced obesity results in worsened OA. A common finding in these HFD studies is that an increased fat mass, not overall body weight, is the key factor associated with worsened OA[32,37,38,40,43].

In addition to systemic obesity, local adipose tissue in the knee joint, the infrapatellar fat pad (IFP), likely also plays a role in OA pathogenesis. The IFP is the largest adipose depot within the knee joint, but its exact purpose remains poorly understood. Functions of the IFP are thought to include distribution of synovial fluid across the joint as well as mechanical shock absorption[44–46]. Due to presence of leukocytes within the IFP, it is also primed to be a source of inflammatory mediators that contribute to OA[41,45–53]. One study found that IFPs from women with knee joint OA secreted more than twice the amount of IL-6 compared to subcutaneous thigh fat from the same individuals[52]. Another study showed that IFP volume increased with age and was correlated to increasing knee joint OA in people[54]. An *in vitro* study demonstrated that human articular cartilage explants displayed increased MMP activity when cultured in media conditioned with IFP-derived adipocytes collected from individuals with knee joint OA[55]. Collectively, these studies provide evidence of the role the IFP plays in OA pathogenesis. Additional studies are needed to further clarify our understanding of how the IFP contributes to knee joint health and OA in aging and obese people.

1.4 Rodent Models of Osteoarthritis.

As naturally-occurring OA takes many years to develop in humans, animal models have been crucial to our understanding of the disease. Complicating matters further is that the disease

course in humans can be unpredictable, symptoms frequently appear late in the course of disease, and radiographic outcomes do not always correlate with clinical signs[56,57]. While numerous animal models are available to study OA, there is no single universally accepted model that most accurately reflects human disease[58].

Animal model selection usually depends on whether spontaneous OA or PTOA is being investigated. There are a variety of models to study PTOA, typically utilizing mice and rats[58]. Methods to induce PTOA include destabilization of the medial meniscus, meniscectomy, transection of the anterior cruciate ligament or collateral ligaments, creation of an articular cartilage groove defect, and non-invasive models of ligament injury[15]. Benefits of studying PTOA include reproducibility in a laboratory setting and rapid onset of disease[58]. However, many of these models do not recapitulate the pathology seen in human primary OA, which is the predominant form of degenerative arthropathy.

While mice and rats are excellent models of PTOA, these rodents do not typically develop spontaneous OA. There are two major rodent models of primary OA: the Hartley guinea pig and the STR/ort mouse. The STR/ort mouse is an inbred strain that develops OA-like lesions early in life, particularly in males[59]. However, this strain may not be directly translational, as studies point to an inherent defect in endochondral ossification as the major driver of their OA pathology[59]. The biggest cons to using mice are the small size of tissues, and mouse cartilage lacks the three distinctive zones of cartilage present in humans[58]. Benefits include the fast course of disease, cost, and readily available reagents. Many studies employ genetically modified mice to examine the role that single genes may play in the pathogenesis of primary OA[15]. These models have provided important information regarding specific genetic contributions to the development of OA. Nonetheless, spontaneous OA is a polygenic disease process, and

experiments in knockout mice may oversimplify the pathology, thus limiting their translatability[15].

The Hartley guinea pig may provide the best representation of the pathologic changes seen in human spontaneous OA[15]. These animals have many advantages, including pathology that closely mimics that seen in humans[60], larger tissue size, and cartilage structure similar to humans[58]. They have also been used to study inflammation within the joint[61]. Another strain of guinea pig commonly used in OA research is the Strain 13 guinea pig. Unlike the Hartley guinea pig, Strain 13 animals are considered OA-resistant[61,62]. Thus, they are a valuable comparison strain to Hartleys.

Specific to iron metabolism, which is a major focus of this dissertation, guinea pigs have a more similar sequence and tissue distribution of hepcidin (discussed in more detail in "Iron Homeostasis" section, below) to humans compared to other rodents[63]. Additionally, they have a dietary requirement for vitamin C, similar to humans[64]. This may be an important consideration in studies exploring oxidant damage, as vitamin C is a natural antioxidant. Limitations of using guinea pigs include increased cost and general lack of commercially available laboratory reagents.

1.5 Current Outcome Measures of Osteoarthritis.

In animal models of OA, histopathology remains the gold standard for evaluation of pathologic joint changes[65]. Other commonly used outcome measures include imaging, biomechanics, pain assessment, and gait outcomes[15]. Over the years, numerous histopathologic scoring systems have been devised. These scoring schemes were based on human pathology and, thus, were modified to better fit animal models[15]. There were inherent limitations to these early

grading schemes, so the Osteoarthritis Research Society International (OARSI) formed a working group in 2010 to develop standardized scoring systems to grade OA in animal models[66]. The goal of this working group was to create a grading system that was simple, useful, and that would allow for comparison of results across studies[67]. In the guinea pig, OARSI guidelines include the grading of articular cartilage surface integrity, cartilage proteoglycan content, chondrocyte cellularity, presence of osteophytes, and integrity of the tidemark[60].

Apart from histology, radiographic imaging is a mainstay in the diagnosis and monitoring of progression of OA. These modalities allow for visualization of bony changes associated with OA. In people, plain X-ray radiographs are commonly used in clinical practice to demonstrate joint space narrowing and presence of osteophytes[68]. Drawbacks to plain radiography include lack of ability to evaluate cartilage and meniscal changes and lack of sensitivity to detect subtle and early changes associated with OA[15,69]. Computed tomography (CT) scans create 3D reconstructions of bony structures from many 2D image slices. MicroCT is commonly utilized in animal studies and provides excellent visualization of subchondral bone changes such as sclerosis and the presence of cysts[15,70]. Contrast-enhanced microCT also permits visualization of cartilage changes[70].

Magnetic resonance imaging (MRI) addresses the limitations of radiography by allowing visualization of cartilage, menisci, synovium, and ligaments[71]. Additionally, MRI can be used to monitor changes in water and glycosaminoglycan content within the cartilage[15]. Because of this enhanced ability to evaluate non-invasively many structures of the joint and to detect early OA, MRI is on-course to replace plain radiography and potentially CT scans in the clinic. High cost is the most limiting factor affecting its widespread use currently[72,73]. MRI is increasingly being used in studies of animal models of OA[15].

1.6 Iron Homeostasis.

This section contains original material from "Pigments: Iron and Friends" written by Lauren Radakovich and Christine Olver published in Veterinary Clinics of North America Small Animal Medicine *in January 2017 used with permissions by providing the following Science Direct link: https://doi.org/10.1016/j.cvsm.2016.07.002*

1.6.1 Functions of Iron.

Iron is an element essential for life and maintaining normal organism function. In mammals, the vast majority of iron is used to synthesize hemoglobin, the oxygen-carrying protein in erythrocytes. It is also necessary for the production of myoglobin, oxidative phosphorylation within mitochondria, DNA synthesis, and making iron-sulfur containing proteins[74]. While iron is critical for survival and its deficiency can lead to anemia, it is also dangerous in high amounts as it can promote free radical damage. It plays a central role in the Fenton reaction, where oxidation-reduction (redox) reactions with hydrogen peroxide release hydroxyl and hydroperoxyl radicals[75,76]. These reactive oxygen species (ROS) promote lipid peroxidation and DNA damage.

1.6.2 Iron Absorption.

Because iron is necessary for life but is also toxic in excess, mammals have evolved an intricate system for its regulation and availability. Surprisingly, mammals have no designated mechanism for iron excretion. Rather, total body iron is regulated by controlling how much is absorbed through the gastrointestinal (GI) tract. Iron can be absorbed in either heme (from animal sources) or non-heme (from plant sources) forms. Each form is transported across the enterocyte's apical membrane by a transport protein. Once within the enterocyte cytoplasm, iron

may be stored within ferritin, a cytosolic protein that can bind thousands of Fe^{3+} particles, thus maintaining iron in a soluble and non-toxic form. If the body is iron-replete, iron will remain within enterocytes as ferritin and be lost with normal sloughing of the GI tract epithelial surface. If there is a need for iron, as with iron deficiency or anemia, the ingested iron will be transported through the basolateral side of the enterocyte via ferroportin, the only cellular iron exporter identified to date[77]. After passing through ferroportin, iron is oxidized to the ferric form by hephaestin, a ferroxidase on the basolateral enterocyte membrane, to mediate binding of iron to the plasma protein transferrin.

1.6.3 Iron Transport, Uptake, and Recycling.

Transferrin is the transport protein that carries iron throughout the bloodstream to reach its targets, primarily the erythroid cells of the bone marrow. Each unit of transferrin can carry two molecules of ferric (Fe^{3+}) iron[78]. Iron must be bound to transferrin within the blood to prevent oxidant damage. Once iron-bound transferrin reaches the bone marrow, it binds to rubriblasts (the earliest erythrocyte precursors) via the transferrin receptor (TfR1). The resulting complex is internalized within an endosome, ultimately resulting in the release of iron from transferrin. Iron exits the endosome while the empty transferrin receptor is recycled to the exterior of the cell where it can then bind more iron, if needed[79].

Macrophages within the splenic red pulp also play a major role in regulating iron availability. Most of the iron arriving at the bone marrow is recycled from these macrophages. As erythrocytes become senescent, they are cleared from the blood via erythrophagocytosis by macrophages**.** Macrophages also have receptors CD163 and CD91 to scavenge iron from haptoglobin-bound hemoglobin and hemopexin-bound heme, respectively. Macrophages can

also endocytose transferrin-bound iron via TfR1 (CD71). Once senescent red blood cells, heme, or hemoglobin are endocytosed, heme is degraded by heme-oxygenase 1 (HO-1) to release iron (and biliverdin), which is then exported from the endosome via DMT1. Likewise, when transferrin-bound iron binds to TfR, the complex is internalized, acidification of the endosome results in the reduction of iron, promoting its release from transferrin. The ferrous iron exits the endosome via DMT1 while TfR is returned to the cell membrane[80]. Once iron is present in macrophages, it has two potential fates: 1) it can be exported through ferroportin where it is oxidized by ceruloplasmin (a ferroxidase similar to hephaestin) to then bind transferrin, or 2) iron can be stored in the macrophages cytoplasm in ferritin. Should ferritin stores become maximally filled, then hemosiderin begins to accumulate, as described below.

1.6.4 Iron Storage and Regulation of Iron via Hepcidin.

Excess iron is stored as ferritin, primarily in the liver. Ferritin is a protein complex comprised of numerous heavy (H) and light (L) chains, which form a protective shield around iron to prevent free radical damage. The H chain has ferroxidase activity, keeping iron in the ferric state, which is less able to participate in the deleterious Fenton reaction. The L chain is involved in electron transfer to allow iron release from ferritin when there is peripheral demand[81]. Iron stores, in the form of hemosiderin, are also present in the spleen and in the bone marrow of most mammalian species. These stores serve as a backup source of iron should there be unexpected blood loss. Iron stores may also be present in increased numbers in areas where local hemorrhage has occurred, such as in hematomas or within the local lymph node near an injured site. Hemosiderin is another storage form of iron that is a complex of ferritin and denatured ferritin. It is a non-soluble form of iron that forms when there is iron overload.

Essentially, ferritin becomes oversaturated with iron molecules, resulting in damage to ferritin. This damage allows iron to come into contact with redox reactive molecules in the cell cytoplasm, initiating free radical damage. The cell's response to this free radical damage is autophagy, where the damaged ferritin is engulfed by lysosomes. Damaged and degraded ferritin within lysosomes is classified as hemosiderin[82]. The body relies on iron stores to support hemoglobin synthesis when iron becomes scarce, as seen with an iron-poor diet or chronic external blood loss.

When iron stores reach a maximum level and further absorption carries the risk of ROS formation, the liver is stimulated to produce hepcidin, the "master iron regulator"[83]. Hepcidin, encoded by the *Hamp* gene, is a peptide secreted by the liver in response to high total body iron levels. Hepcidin binds to ferroportin, resulting in its internalization and degradation. Subsequently, ingested iron cannot be exported from enterocytes, thus no iron is absorbed into the bloodstream. Likewise, iron cannot be exported from macrophages or hepatocytes. The result is a decreased amount of iron present in the bloodstream available to bone marrow erythroblasts.

Hepcidin is also induced by systemic inflammation, primarily through interleukin-6 (IL-6) activation. IL-6-induced production of hepcidin is an attempt by the body to sequester iron from potential invading pathogens. If inflammation is chronic, *functional* iron deficiency often develops. This term refers to ongoing iron sequestration within macrophages and duodenal enterocytes, thus limiting iron bioavailability to the bone marrow. Eventually, this iron sequestration can lead to anemia. This inflammation-induced anemia is termed anemia of chronic disease (ACD) or anemia of inflammation. Hepcidin production is inhibited when iron deficiency, tissue hypoxia, and anemia are present[84]. In the absence of hepcidin, ferroportin

remains on enterocyte, hepatocyte, and macrophage membranes, thus allowing iron to be readily absorbed and cycled throughout the body.

1.7 Iron in Aging and Osteoarthritis.

Progressive iron accrual has been linked to many aging-associated chronic diseases, due to the toxic effects of iron ions in tissues over time[85]. Age-related conditions in which excessive or improperly handled iron is a risk factor include sarcopenia, type II diabetes, neurodegenerative disorders, atherosclerosis, and numerous cancers[86]. Additionally, iron overload in joints has long been implicated in arthropathies associated with hereditary hemochromatosis[87] (HH), rheumatoid arthritis (RA)[88,89], traumatic arthropathy, and hemophilic arthropathy[90]. In these conditions, excess iron can accumulate from two sources: blood that enters the joint from either trauma or inflamed synovium, and/or exchange from the labile non-heme iron pool[89,91]. Regardless of the mechanism, several human studies have shown hemosiderin deposits in cartilage and synovium, as well as increased ferritin (the major storage form of iron) in the synovial fluid of affected joints[88,89]. Iron-overloaded synoviocytes release pro-inflammatory cytokines, including interleukin-1β (IL-1β), IL-6, and tumor necrosis factor[92], that stimulate the catabolic activity of chondrocytes. Iron also has a direct effect on cartilage by inducing hydroxyl radical-driven chondrocyte apoptosis and breakdown in matrix components[93,94]. However, the possible role iron accumulation may play in the onset and progression of osteoarthritis has not been well-explored.

Because iron has emerged as a major contributor in other diseases associated with aging, it is prudent to consider it may also be driving the onset and progression of spontaneous OA. Limited studies have examined iron status in the context of spontaneous OA. One such study

found that serum ferritin levels increased with age and that men with knee OA had higher serum ferritin concentrations that men without knee joint OA. Further analysis demonstrated that men with higher serum ferritin levels had a four-fold greater risk of having radiographic knee joint OA compared to age-matched controls with normal serum ferritin levels[95]. Another study revealed that OA patients had significantly higher synovial fluid ferritin concentrations when compared to patients without OA, indicating that local iron production within the joint space may contribute to the disease[93].

1.8 Global Hypothesis and Rationale.

The research described in this dissertation aims to firmly establish iron's role in the pathogenesis of OA. As such, the global hypothesis of this work is that aging-associated iron accrual in knee joints contributes to the onset and progression of primary OA by inciting oxidant damage (Figure 1.1). Additional goals were to determine the contributions of the IFP to the knee joint and to assess the effects of a Western-style high fat diet on the onset and progression of disease in a Hartley guinea pig model of primary OA. Lastly, we aimed to develop a clinically-relevant OA scoring system to be applied to radiographic microCT images, similar to what is done in human medicine. Based on our hypothesis, we believe limiting ingestion of foods high in iron content as well as limiting overall fat consumption may be useful in the prevention of primary OA in people.

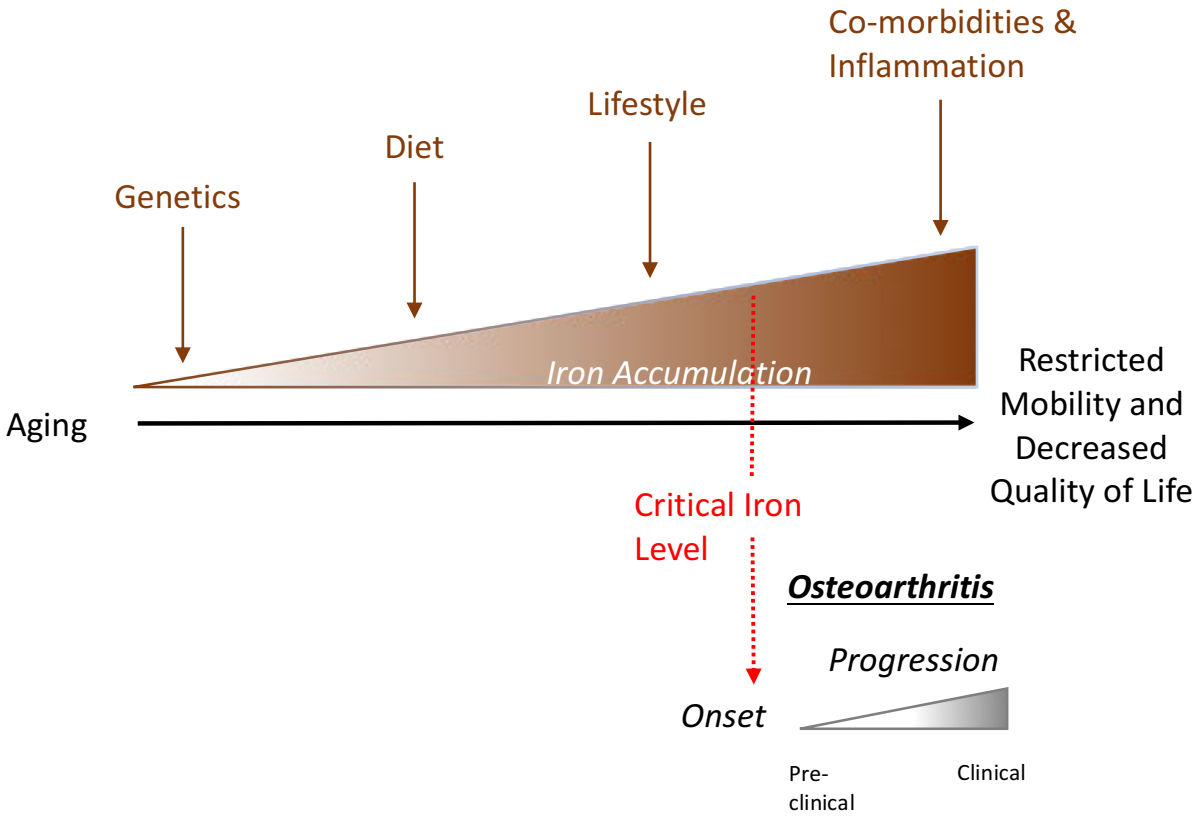

Figure 1.1 – Global hypothesis of this dissertation. We theorize that, throughout aging, there is progressive accumulation of iron that is influenced by endogenous and exogenous factors. Specific to OA, there is a "critical iron level" above which joint tissue cannot compensate for iron-related oxidant damage, which results in OA onset and progression. Of note, this "critical iron level" may be unique to each individual and can be reached at varying ages.

CHAPTER 2

DEVELOPMENT OF A MICROCOMPUTED TOMOGRAPHY SCORING SYSTEM TO CHARACTERIZE DISEASE PROGRESSION IN THE HARTLEY GUINEA PIG MODEL OF SPONTANEOUS OSTEOARTHRITIS[1]

2.1 Introduction.

Osteoarthritis (OA) is the most widespread form of arthritis, with estimates that at least 10-15% of those over age 60 suffer from the disease[96]. OA is thus a leading cause of pain and disability across the globe[97], with the knee identified as the most commonly affected joint. Unfortunately, the individual and economic burden of OA is expected to increase as people continue to live longer and lifestyle factors that contribute to OA, such as inactivity and obesity, continue to rise[96,98].

OA is characterized by loss of articular cartilage, subchondral bone sclerosis, and synovial hyperplasia and inflammation[1]. Eventually, these changes lead to loss of normal joint function, resulting in decreased mobility, pain, and poor quality of life[99]. Although great strides have been made in understanding the underlying mechanisms that contribute to OA, its pathogenesis is still not completely understood. In particular, there is a lack of understanding of the inciting and underlying triggers of spontaneous OA, which is the predominant form of disease and occurs without prior trauma to the joint. Other than symptomatic pain relief and

[1] Article used with permission from Taylor and Francis (www.tandfonline.com); published in the December 2017 issue of *Connective Tissue Research.*

total joint replacement, treatment options for OA are limited and an active area of investigation[100–102].

Numerous animal models have been employed to aid in the study of human OA[15,58,103]. These include small animals models, such as mice, rats, guinea pigs, and rabbits, as well as large animal models, including dogs, small ruminants, and horses[58,103]. One outbred rodent species with spontaneous OA is the Hartley guinea pig, which has joint pathology, especially in the knee, that mimics that seen in humans[15,58,103,104]. Other advantages of the Hartley guinea pig are its physiologic requirement for exogenous vitamin C[64], which is identical to people, and the ability to collect larger tissue samples than smaller mouse and rat models. As the Hartley guinea pig is an accepted model for both spontaneous and post-traumatic OA, the Osteoarthritis Research Society International (OARSI) has developed guidelines on the histologic examination of knee joints from these animals[60].

Of note, histopathology is the predominant outcome measure used in animal models of OA, as it is considered the gold standard for laboratory work [15]. In contrast, radiographic analysis, typically using X-ray radiographic images, is practical and readily available in the medical community, making it the main descriptor of joint pathology. This presents a potential dichotomy when comparing basic and clinical research, as it is not clinically feasible to do histopathologic assessment of knee joints on human patients outside of total joint replacement surgery.

Two-dimensional (2D) radiographic images of OA patients are interpreted using a variety of clinical features, such as presence and location of osteophytes, subchondral bone changes, and articular bone lysis[105]. Of note, 2D radiography is not often employed for animal work and, instead, microcomputed tomography (microCT) is utilized[106]. MicroCT, a form of advanced

radiography, provides high resolution images and the ability to view both 2D and 3D reconstructions of bony structures. It is primarily used in research settings to quantitatively evaluate bony features such as subchondral bone sclerosis, subchondral bone volume fraction (BV/TV), trabecular thickness, and bone tissue mineral density (TMD), particularly in rodent models such as guinea pigs [107–109]. Similar to traditional radiography, microCT can be performed longitudinally *in vivo*, allowing researchers to follow OA progression in live animals and direct appropriate harvest time points in studies[70,110].

While quantitative microCT measurements provide valuable information, it would be complementary to apply a clinically-oriented evaluation of microCT images from these animals in a manner similar to human radiographic findings. Although microCT is not frequently used in the human clinical setting, OA features assessed on radiographs can be readily applied to 2D microCT images. Thus, the main objective of the current study was to create and utilize a new whole joint scoring system to evaluate microCT images from Hartley guinea pigs as they age from 2 to 15 months old. We also compared and contrasted the benefits and limitations of this new grading scheme to both histologic grading and quantitative microCT measurements, such that there is rationale to include this clinically-based grading scheme in our repertoire of tools used to describe OA.

2.2 Materials and Methods

Animals.

All procedures were approved by the university's Institutional Animal Care and Use Committee and were performed in accordance with the NIH Guide for the Care and Use of Laboratory Animals. Thirty male Hartley guinea pigs were acquired from a commercial vendor

(Charles River Laboratories, Wilmington, MA) to allow harvest at the following ages: 2 months (pre-OA), 3 months (OA onset), 5 months (early OA), 9 months (moderate OA), and 15 months (severe OA)[60]. Group size and power were determined using the statistical software at www.stat.uiowa.edu/~rlenth/Power. Based upon previous work and pilot studies, histologic assessment of OA was used as the principle outcome. Using a within group error of 0.5 and a detectable contrast of 1.0 in a linear regression model, power associated with a Tukey/HSD post-test (alpha = 0.05) was calculated as 0.9 with a sample size of 6 per experimental group. All animals were purchased one month prior to target ages and maintained at Colorado State University's Laboratory Animal Resources housing facilities. Animals were monitored daily by a veterinarian and provided with a full screening to ensure animals were healthy prior to harvest. All guinea pigs were singly-housed, as is suggested for males, in solid bottom cages. They were provided regular guinea pig chow (Harlan Teklad 7006) fortified with vitamin C (800 mg/kg) and vitamin D (2.4 IU/g). Food and water were provided *ad libitum*.

Specimen Collection.

At time of harvest, guinea pigs were anesthetized and maintained with a 1.5 to 3% mixture of isoflurane and oxygen. Thoracic cavities were opened, and blood was collected via direct cardiac puncture using a 20-gauge butterfly catheter for full complete blood count and biochemistry evaluation (data not shown). This data, coupled with a complete necropsy, confirmed that animals did not have concurrent morbidities. Anesthetized animals were then immediately transferred to a carbon dioxide chamber for euthanasia. Left hind limbs were removed at the coxofemoral joint and fixed in 10% neutral buffered formalin for 48 hours. Right

hind limbs were used for an unrelated study. After 48 hours, limbs were placed in phosphate buffered saline (PBS), at which time limbs were imaged with microCT.

Quantitative MicroCT Measurements.

Knee joints were scanned in PBS using the Inveon microPET/CT system (Siemens Medical Solutions, Malvern PA), with a voxel size of 18 micrometers, a voltage of 100 kV, and an exposure time of 2356 ms. All quantitative microCT measurements (Table 2.1) were performed using ImageJ software (Research Service Branch, National Institutes of Health, Bethesda, MD). Thresholds were determined optically using the edge detection method[111]. For analysis of tibial subchondral trabecular bone, a region with an area of 1.04 x 1.04 x 0.52 mm^3 was selected as the region of interest (ROI), as previously described [107,112]. For analysis of femoral subchondral trabecular bone, a cuboid region of trabecular bone with size of 1.5 x 1.5 x 0.5 mm^3 was identified, as published [112]. Example ImageJ photos with regions of interest highlighted are provided in Figure 2.1. Bone TMD (g/cm^3), BV/TV, trabecular thickness (mm), and trabecular spacing (mm) were quantified for both medial and lateral tibial subchrondral trabecular bone, and medial and lateral subchondral trabecular bone in the femoral condyles. Bone TMD was calibrated using phantoms of known hydroxyapatite density embedded in epoxy.

Whole Joint Scoring System for MicroCT.

In conjunction with a board-certified veterinary radiologist (AJM), we developed a novel, clinically-oriented scoring system to assess whole joint microCT radiographic images in this species. Key features of this grading scheme (Table 2.2) are radiographic assessments typically utilized in day-to-day evaluation of human OA, including presence and location of osteophytes,

subchondral bone changes, and articular bone lysis[113]. Features of the proposed grading system are similar to the Kellgren-Lawrence score, which is the most widely used classification for radiographic analysis of human OA in clinical practice and is commonly applied in research settings[114]. In this human scheme, a score of 0 (no OA) to 4 (most severe OA) is assigned and is based on joint margin osteophytes, joint space narrowing, subchondral bone sclerosis, small cyst-like lesions in the subchondral bone, and altered shape of bone ends[114]. Similar to the OARSI histologic score (described below), the microCT grading scheme scored whole knee joints in their entirety. This same radiologist then assessed all anatomical structures across all planes and serial sections of 2D microCT image stacks. Images were scored in duplicate in a random order, blinded to age group. A perfect intraclass correlation coefficient of 1.0 for intra-reviewer consistency was calculated.

OARSI recommended histopathologic assessment of OA.

After legs were scanned for microCT, PBS was removed and replaced with 12.5% ethylenediaminetetraacetic acid (EDTA) at pH 7 for decalcification. The EDTA solution was replaced every 3-5 days for 4-6 weeks, based on age, until legs were appropriately decalcified. Coronal slices of the knees at the level of the medial tibial plateau were sectioned, as previously described[60]. Samples were paraffin embedded and a 5-micron intact central section was stained with Toluidine Blue, as recommended by the OARSI guidelines[60]. Medial and lateral femoral condyles, as well as medial and lateral tibial plateaus, were scored using a semiquantitative grading scheme outlined by OARSI[60]. This semiquantitative histopathologic grading scheme is based on articular cartilage structure, proteoglycan content, cellularity, tidemark integrity, and presence of osteophytes. Scores for medial and lateral tibia, as well as medial and lateral femur,

were assigned and summed for a total knee joint OA score. Scores pertinent to the medial and lateral aspects of the knee, only, were also calculated. Scores were performed in a blinded fashion by two independent reviewers (LBR and KSS). An intraclass correlation coefficient for inter-reviewer consistency was calculated at 0.92, which was considered excellent. Scores from each of the four anatomic locations were summed to obtain a total knee joint OA score for each guinea pig. Due to rare, imperfect coronal sectioning of the joints, not all compartments at the level of the medial tibial plateau could be adequately scored for every guinea pig. If any single structure was not appropriately sectioned for scoring, that animal was excluded from the analysis for OARSI histology scoring for the total joint score.

Statistical analysis.

Data for total body weights, quantitative microCT measurements, microCT OA scores based on the novel grading scheme, and OARSI histology scores were subjected to, and passed, normality testing via the Kolmogorov-Smirnov test. Data were compared between the five age groups using parametric ordinary one-way ANOVA analyses followed by Tukey's multiple comparisons tests to allow for adjusted P values. Pearson's correlation coefficients were calculated between the whole joint microCT scoring system, histology scores, and quantitative microCT measurements. Statistical significance was set at $P < 0.05$. All statistical analyses were performed with GraphPad Prism (La Jolla, CA, USA).

2.3 Results.

General description of animals.

Guinea pigs in all groups remained clinically healthy and gained weight as expected for this species when fed ad libitum. Mean weight was 598.9 grams for the 2-month old group, 747.3 grams for the 3-month old group, 901.8 grams for the 5-month old group, 1031 grams for the 9-month old group, and 1016 grams in the 15-month old group. Significant differences in weight and weight ranges are presented (Figure 2.2).

Quantitative microCT measurements.

All 6 animals in each age group were included in this aspect of the study. Mean values (and 95% confidence interval) for each of the quantitative microCT measurements can be found in Table 2.1. Significant differences among the five age groups were found for: BV/TV, trabecular thickness, and trabecular spacing in the medial tibial subchondral trabecular bone; and tibial and femoral cortical thickness. BV/TV decreased with age in the medial tibial compartment (overall ANOVA $P = <0.0001$: $P < 0.05$ for 2 months vs 5 months; $P < 0.01$ for 2 months vs both 9 and 15 months, and 3 months vs 5 months; $P < 0.001$ for 3 months vs both 9 and 15 months). Similar decreasing trends with advancing age were noted for the medial femoral and lateral tibial compartments ($P = 0.0857$ and $P = 0.0555$, respectively). Trabecular thickness in the medial tibial compartment increased from 2 months to 5 months, and then remained stable (overall ANOVA $P = 0.0080$: $P <0.05$ for 2 months vs both 3 and 5 months). Trabecular spacing in the medial tibial compartment followed the same trend ($P = 0.0492$), although there were no significant differences noted on multiple comparison analysis of the age

groups. Cortical thickness of the tibia increased after 2 months of age (overall ANOVA P = 0.0156: $P < 0.05$ for 2 months vs both 3 and 5 months).

Whole joint microCT scoring scheme.

As above, all 6 animals in each age group were included in this analysis. No microCT pathology (score of 0) was noted in the 2 or 3-month old age groups. The mean score was 4.2 (95% confidence interval [CI] 2.6 - 5.7) for the 5-month old group, 4.5 (95% CI 2.4 - 6.6) in the 9-month old group, and 11.8 (95% CI 11.4 - 12.3) in the 15-month old group. Individual scores and statistical differences are found in Figure 2.2.

In the 5-month old group, all animals had small osteophytes (<1mm) on either the patella or femur. Two animals in this group had osteophytes present on both the patella and femur. In the 9-month old group, all animals had small osteophytes on the patella and/or femur. Additionally, 3 animals in this group also had radiographic evidence of subchondral bone sclerosis and subchondral bone cystic changes. In the 15-month age group, all 6 animals had large osteophytes (≥1mm) present on the patella, femur, and tibia. All 6 animals also had evidence of subchondral bone sclerosis and subchondral bone cystic changes. Five animals exhibited articular bony lysis. Representative sagittal and coronal microCT images from each age group are presented (Figure 2.3).

OARSI histology score.

All 6 animals in the 2-month old age group were evaluated, but only 5 animals in each of the remaining age groups were included in the total joint analysis due to skew in the sectioning of the joints (n=26, total). Data pertinent to animals with individual intact medial and lateral

compartments (n=26 and n=27, respectively) were similar to that for the total joint evaluation (data not shown).

The OARSI total joint scores were significantly different among the age groups (P = 0.0001). As expected, mean OA scores progressively increased with age and were statistically different between every age group, with the exception of the 2 and 3 month old groups (Figure 2.2). Mean OARSI scores for all four knee joint compartments were 0.375 (95% CI -0.1 - 0.9), 1.2 (95% CI 0.8 - 1.6), 10.8 (95% CI 6.9 – 14.6), 26.2 (95% CI 16.9 – 35.5), and 40.4 (95% CI 30.3 – 50.5) for the 2, 3, 5, 9, and 15 month old groups, respectively. In general, scores from the medial compartment were higher than those from the lateral compartment.

Representative lesions from each age group are presented (Figure 2.4). In both the 2 and 3-month old groups, mild articular surface irregularities and slight proteoglycan loss in the superficial zone were the most common lesions observed. Proteoglycan loss was more severe in the 5-month old group, and occasional fissures were present in the articular cartilage surface. Mild hypocellularity in the superficial zone was also commonly noted in this age group. In the 9-month old group, proteoglycan loss with more accentuated hypocellularity coupled with regions of chondrocyte clustering were noted. Tidemark duplication was also common in the 9-month olds. All of above mentioned lesions were present in the 15-month old group, but to a more severe extent. In some animals, there was complete loss of articular cartilage at this late age.

Correlations between quantitative microCT measurement, the whole joint microCT scoring scheme, and OARSI OA scores.

Medial tibial BV/TV and whole joint microCT scores demonstrated a moderate negative correlation ($r = -0.61$, 95% confidence interval -0.79 to -0.31, $P < 0.0001$). Moderate to strong correlations were present between medial tibia BV/TV and OARSI OA scores ($r = -0.72$, 95% confidence interval -0.86 to -0.46, $P < 0.0001$). No significant correlations were found for remaining quantitative microCT measurement.

The whole joint microCT-based clinical OA scoring system demonstrated strong correlation to OARSI OA grading, with a Pearson coefficient of 0.89 (95% confidence interval 0.76 to 0.95) ($P < 0.0001$). Similar correlations were noted when OARSI scores from only the medial or lateral compartments were compared to the microCT score ($r = 0.88$ and 0.82, respectively).

2.4 Discussion.

To the authors' knowledge, this is the first study to utilize a clinically-based, whole joint microCT grading scheme in a rodent model of OA, with a focus on the Hartley guinea pig model of spontaneous disease. Other studies have examined quantitative microCT measurements and histology simultaneously in guinea pigs [107–109,112], but we aimed to implement a translational approach to disease assessment. To this end, we have demonstrated that our grading scheme is a useful tool that provides important and complementary data to existing outcome measures in the evaluation of OA. Indeed, this new scoring system strongly correlates to OARSI-based histologic grading. Increasing severity of osteophytes, subchondral bone sclerosis and cystic

changes, and articular bone lysis detected by microCT were associated with increasing severity of articular cartilage surface lesions and proteoglycan loss seen on histology.

Advantages of microCT include 3-dimensional visualization of the joint (vs. 2-dimensional views on histology), the ability to evaluate living specimens in a longitudinal fashion, and more sensitive detection of subtle bony lesions that tend to occur early in OA disease progression[115,116]. As discussed further, below, it is advantageous that these multiplanar reconstructions of the intact organ can be made in an endless number of angles for complete evaluation of the entire joint.

One particular benefit of microCT highlighted in the current study is the increased ability to detect osteophytes. With whole joint microCT, all animals in the 5, 9, and 15-month old groups (18 animals total) had visible osteophytes. However, only one animal had visible osteophytes detected by histology. Osteophytes are an optional category to include in OARSI scoring of knee joints, as they may be missed depending on the plane of section obtained[60]. Because sectioning for OA grading focuses on coronal sectioning through the medial tibial plateau, osteophytes present elsewhere in the joint, particularly on the patella, may be missed. Also, imperfect trimming of knee joint tissue may result in histologic sections lacking representative lesions from all compartments of the joint (both medial and lateral tibial and femoral regions), as occurred with a few animals in the current study. Furthermore, coronal sectioning precludes histologic sagittal examination of the same joints. Finally, because the joint remains intact for microCT, many different views from the same animal can be evaluated. In particular, this allows assessment of the patella, a structure often excluded from histologic OA grading but considered relevant in clinical evaluation of human patients[117]. Of note, evaluation of the patella can provide important clinical information in regards to overall knee OA, including

presence of osteophytes, sclerosis, and chronic remodeling[117]. Here, we have demonstrated that the patella became severely affected in the progression of OA in this guinea pig strain, which provides yet another similarity between this species and humans [117].

As expected, OA total knee joint scores based on the OARSI scale increased with advancing age in the Hartley guinea pigs. Very mild changes, such as minor articular surface undulations or minimal proteoglycan loss, were noted at 2 months in a few animals. Histologic evidence of OA was consistently present by 3 months of age, as has been described in other studies examining age-dependent changes in articular cartilage in Hartleys[108,109,118]. Others have reported no obvious cartilage damage by 3-4 months of age[107,119], while another study saw no significant difference in OA scores in Hartley guinea pigs between 4 and 5 months of age[120]. In our project, dramatic increases in severity of histologic OA were noted between the 5 and 9-month, as well as the 9 and 15-month, groups. Investigating additional time points between these ages would more clearly highlight when these changes occur, as well as the specific changes that contribute to the overall OARSI score. Of note, the current work is strengthened by the fact that all four knee joint compartments were scored according to OARSI recommendations, and the sum of the four regions was used as a total knee joint OA score. Other studies vary on whether only a single compartment is scored (typically the medial tibial region) or if a subset are scored and combined. It is recognized, however, that dedicating an entire joint to histology is not always practical in studies where tissue is needed for other assays.

Interestingly, statistical differences in histologic OA scores were found between every group, while whole joint microCT OA scores did not worsen between 5 and 9 months of age. It is possible that bony changes are most striking during both the early and later phases of OA, with cartilage changes occurring continuously throughout disease progression. While both are

typically present in patients with end-stage OA, cartilage degeneration and bony changes are considered separate mechanistic events[121]. Thus, as emphasized in our work, it is important to simultaneously examine cartilage and bone changes in animal models of OA to gain a complete picture of the disease.

Most OA studies employing microCT describe quantitative morphometric measurements, such as BV/TV, bone TMD, and subchondral bone trabecular thickness and spacing, as major outcome measures. These quantitative measurements were performed in the current study, with the majority of statistical differences focused on the medial tibial compartment. Overall, BV/TV in the medial tibial subchondral trabecular bone decreased with age and increasing OA severity. In the 3-month age group, BV/TV of the medial tibial subchondral trabecular bone was higher than that of the lateral tibial subchondral trabecular bone, a finding previously reported in 3-month Hartley guinea pigs of undesignated sex[107]. Another study examining OA in female Hartley guinea pigs at 1, 3, 6, and 9 months of age found that BV/TV of the tibia was highest at 3 months of age and then remained constant[108]. It is not known, however, if this particular study examined the tibia in its entirety, or if medial and lateral compartments were considered separately. Rat and rabbit studies of secondary, trauma-induced OA also showed that BV/TV decreased in both the femur and tibia in injured legs (with more severe OA) compared to sham control legs[122,123]. As bony remodeling results in weakened bone with reduced bone volume – especially in the medial tibia – in both spontaneous and secondary OA in animal models[122,123], the decreasing BV/TV in this study is not surprising. Conversely, however, a recent human study of 14 tibial samples showed that subchondral bone volume increased with advancing OARSI histologic score for cartilage degeneration[124]. These discrepant results may reflect

differences in BV/TV based on the stage of OA evaluated, as microCT is typically only performed on samples from end-stage human patients undergoing knee replacement surgery.

Many OA studies using microCT as a major outcome measure have also focused on bone TMD. Of note, manuscripts vary on whether TMD is measured in the tibial subchondral plate or tibial subchondral trabecular bone. Further, microCT methodologies and analysis software are often different among studies and this may explain the lack of consensus amongst studies regarding TMD and OA. No statistical differences were detected for TMD in any of the four knee joint compartments as guinea pigs aged in the present study; however, highest TMD for all four compartments were present at 3 months of age, tended to decrease at 5 months, and then remained stable thereafter. A previous study examining TMD changes in female Hartley guinea pigs at various ages found that tibial subchondral TMD increased with age and was stable by 9 months[118]. Another study comparing male Hartley guinea pigs to the OA-resistant GOHI/SPF strain found femoral subchondral bone TMD was lower in the Hartleys[112]. A different study comparing male and female Hartleys to female OA-resistant Strain 13s found tibial subchondral TMD was similar between male Hartleys and female Strain 13s, yet was increased compared to female Hartleys[125]. Likewise, female Hartleys have higher tibial subchondral plate TMD than OA-resistant Bristol Strain 2 guinea pigs[107]. In a rabbit injury-induced model of OA, both tibial and femoral TMD were decreased in the injured limb[123], while no differences in TMD were found in a rat model of injury-induced OA[122]. Standardization of methods and location within the bone (subchondral trabecular bone vs subchondral plate) for TMD measurement may allow for more meaningful comparisons amongst studies.

One hurdle of the current study was the inability to assess weight-bearing joint space narrowing, a key radiographic feature assessed clinically in human OA patients[114]. Fixation of

limbs prior to microCT scanning results in artificial shrinkage of the joint space, making this measurement invalid. Furthermore, even when *in vivo* microCT is available, laboratory animals must be anesthetized, which precludes normal weight bearing of the knee joint. Thus, joint space narrowing is especially challenging, if not impossible, to obtain accurately in many animal models of OA. Another limitation of the proposed whole joint microCT grading scheme is the inability to assess soft tissue structures of the knee joint, such as cartilage and menisci. As such, it is important to evaluate joints using multiple modalities, including microCT and histology, that provide complementary data.

Of note, there are advanced imaging methods available that can provide information regarding both bone and soft tissue changes, bridging the gap between microCT and histology. In particular, Equilibrium Partitioning of an Ionic Contrast (EPIC) and other related forms of contrast-enhanced microCT exist, but are not yet as commonly used as more traditional microCT. These modalities utilize ionic contrast agents that electrochemically interact with cartilage matrix components, resulting in a nonuniform partitioning of the agent throughout the cartilage. This partitioning is then visualized and is reflective of articular cartilage defects and proteoglycan content [126–128]. Contrast-enhanced microCT should be used in future studies, as the lack of cartilage visualization is a major drawback of traditional microCT in OA assessment. Assessment of cartilage in conjunction with bony changes using a single imaging modality may also strengthen our proposed whole joint microCT score.

In summary, we have shown that a whole joint microCT OA scoring system provides data complementary to OARSI histologic OA scores and quantitative microCT parameters in a guinea pig model of spontaneous OA. Although not yet demonstrated, this scheme may also be applicable in other species used to study OA. This clinically-oriented microCT grading scheme,

particularly in conjunction with histology, may also be more comprehensive than individual microCT or histologic outcome measurements, alone. Future work would include an evaluation of additional species and models utilized in OA research, as well as both male and female animals.

Table 2.1 – Quantitative microCT values in age group guinea pigs. Mean values and 95% confidence intervals are provided.

		2 month	3 month	5 month	9 month	15 month	P-value
Bone Volume/Total Volume	**MT**	0.6318 (0.5794,0.6843)	0.6737 (0.5723,0.7750)	0.5013 (0.3882,0.6145)	0.447 (0.3939,0.4954)	0.4643 (0.4049,0.5237)	**<0.0001**
	LT	0.6057 (0.4190,0.7923)	0.5422 (0.4211,0.6633)	0.4567 (0.3604,0.5529)	0.4353 (0.3262,0.5445)	0.4155 (0.3210,0.5100)	0.0555
	MF	0.5292 (0.4533,0.6050)	0.5438 (0.4633,0.6244)	0.5385 (0.4695,0.6075)	0.4587 (0.4125,0.5049)	0.4443 (0.3299,0.5588)	0.0857
	LF	0.4507 (0.3722,0.5291)	0.4852 (0.4415,0.5288)	0.4887 (0.4087,0.5687)	0.4373 (0.4187,0.4560)	0.4175 (0.3330,0.5020)	0.2561
Bone Tissue Mineral Density (g/cm^3)	**MT**	2.682 (2.121,3.243)	2.653 (1.923,3.383)	2.550 (2.461,2.638)	2.209 (2.061,2.357)	2.494 (2.416,2.572)	0.2868
	LT	2.671 (2.126,3.217)	2.650 (1.925,3.375)	2.508 (2.384,2.632)	2.206 (2.036,2.364)	2.511 (2.411,2.639)	0.2946
	MF	2.681 (2.104,3.258)	2.648 (1.910,3.386)	2.527 (2.384,2.669)	2.200 (2.143,2.292)	2.525 (2.461,2.603)	0.3057
	LF	2.692 (2.115,3.270)	2.634 (1.902,3.365)	2.517 (2.386,2.648)	2.223 (2.061,2.385)	2.521 (2.435,2.606)	0.3460
Trabecular Thickness (mm)	**MT**	0.1775 (0.1546,0.2004)	0.2133 (0.1948,0.2319)	0.2123 (0.1860,0.2387)	0.1825 (0.1694,0.1956)	0.1902 (0.1706,0.2097)	**0.0080**
	LT	0.1707 (0.1626,0.1787)	0.1765 (0.1653,0.1877)	0.1847 (0.1623,0.2070)	0.1770 (0.1543,0.1997)	0.1755 (0.1479,0.2031)	0.7887
	MF	0.1905 (0.1679,0.2131)	0.2117 (0.1905,0.2328)	0.2303 (0.1963,0.2644)	0.1935 (0.1766,0.2104)	0.2055 (0.1497,0.2613)	0.2246
	LF	0.1683 (0.1501,0.1865)	0.1873 (0.1721,0.2026)	0.2118 (0.1838,0.2399)	0.2085 (0.1586,0.2584)	0.1997 (0.1474,0.2520)	0.2106
Trabecular Spacing (mm)	**MT**	0.2427 (0.2043,0.2811)	0.2305 (0.1997,0.2613)	0.3038 (0.2238,0.3839)	0.2800 (0.2480,0.3120)	0.3052 (0.2394,0.3709)	**0.0492**
	LT	0.2150 (0.1808,0.2492)	0.2518 (0.2247,0.2790)	0.2813 (0.2401,0.3226)	0.2608 (0.2083,0.3184)	0.2485 (0.2151,0.2819)	0.0634
	MF	0.2430 (0.2206,0.2654)	0.2467 (0.2217,0.2716)	0.2710 (0.2422,0.2998)	0.2640 (0.2460,0.2820)	0.3682 (0.08492,0.6514)	0.3973
	LF	0.2705 (0.2294,0.3116)	0.2715 (0.2460,0.2970)	0.2877 (0.2591,0.3162)	0.2993 (0.2627,0.3359)	0.2735 (0.2334,0.3136)	0.5006

MT, medial tibia; LT, lateral tibia; MF, medial femur; LF, lateral femur; T, tibia; F, femur. In the P-value column, bolded numbers are statistically significant. P-value represents significance of overall one-way ANOVA analysis.

Table 2.2 – Guinea Pig Whole Knee Joint MicroCT OA Scoring System.

MicroCT Finding	**Score**
Presence of osteophytes	0 = none 1 = small osteophyte (< 1mm) 3 = large osteophyte (≥1 mm)
Location of osteophytes	1 = medial and/or lateral tibia 2 = patella 3 = medial and/or lateral femur
Subchondral bone cystic changes	0 = no 1 = yes
Subchondral bone sclerosis	0 = no 1 = yes
Articular bone lysis	0 = none 1 = yes
Intra-articular soft tissue	0 = normal 1 = increased

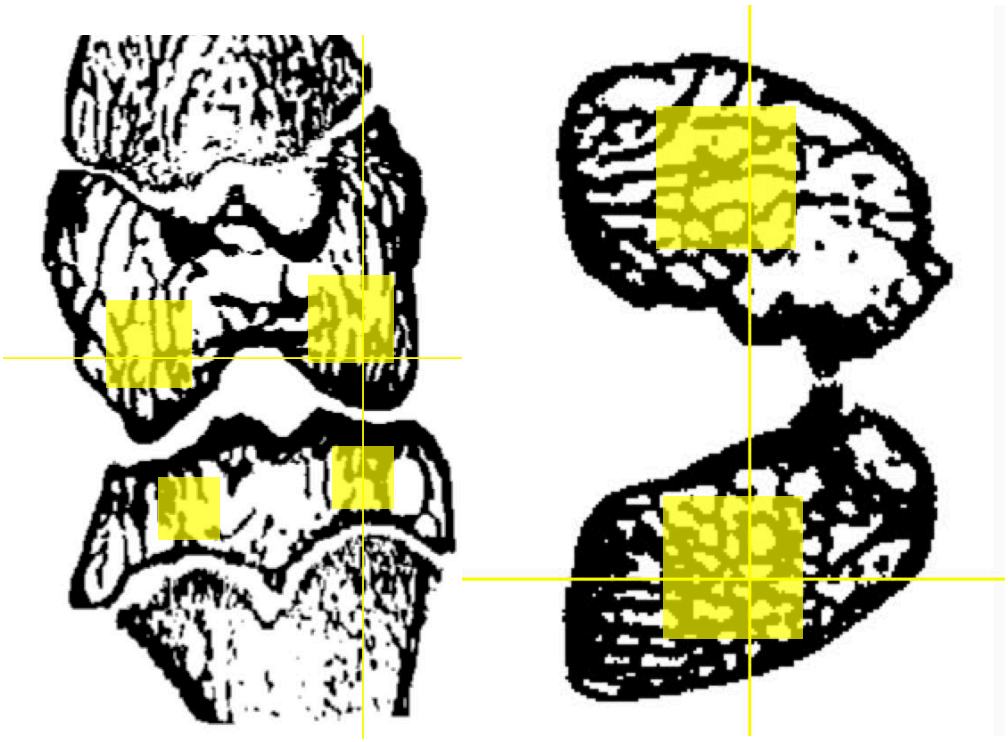

Figure 2.1 – Regions of interest for conventional microCT. Representative coronal (left) and transverse (right) microCT images produced by ImageJ software. Regions of interest in the subchondral trabecular bone utilized to determine quantitative microCT measurements are defined by the yellow squares.

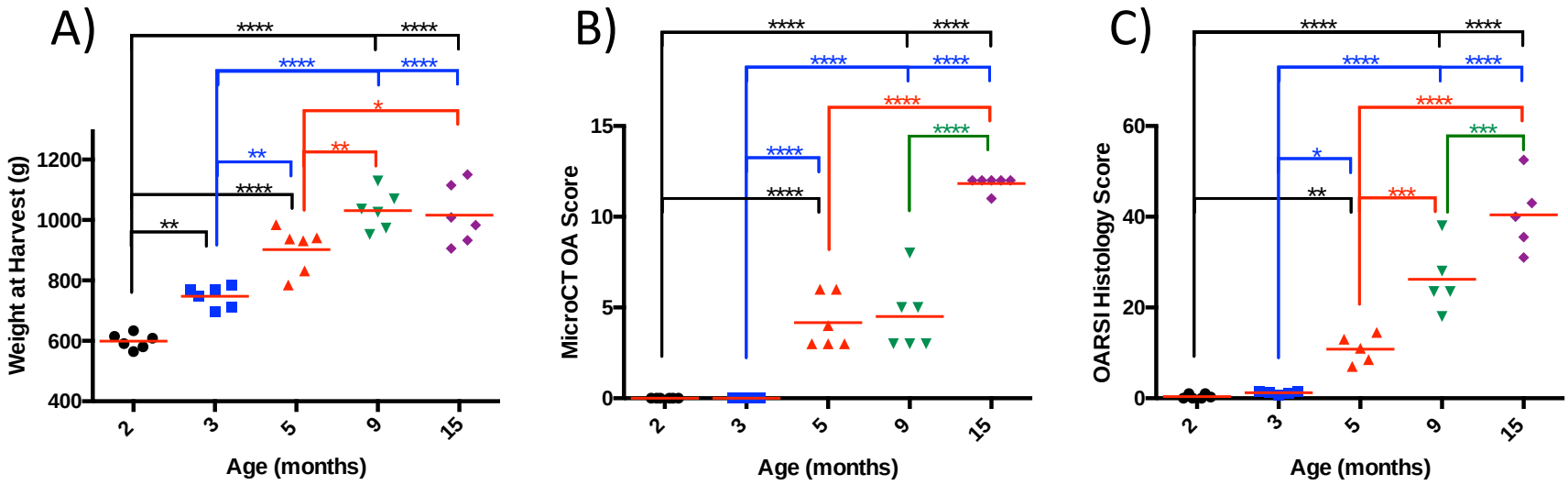

Figure 2.2 – Body weights, microCT OA scores, and histologic OA scores. (A) Total body weight (in grams, g) for each age group of guinea pigs. (B) Comparison of total knee joint OA scores using the novel microCT grading scheme. (C) Comparison of total knee joint OARSI OA scores using toluidine blue-stained histology slides among the five age groups. Red lines indicate the mean value for each group. * $P \leq 0.05$, ** $P \leq 0.01$, *** $P \leq 0.001$, **** $P \leq 0.0001$.

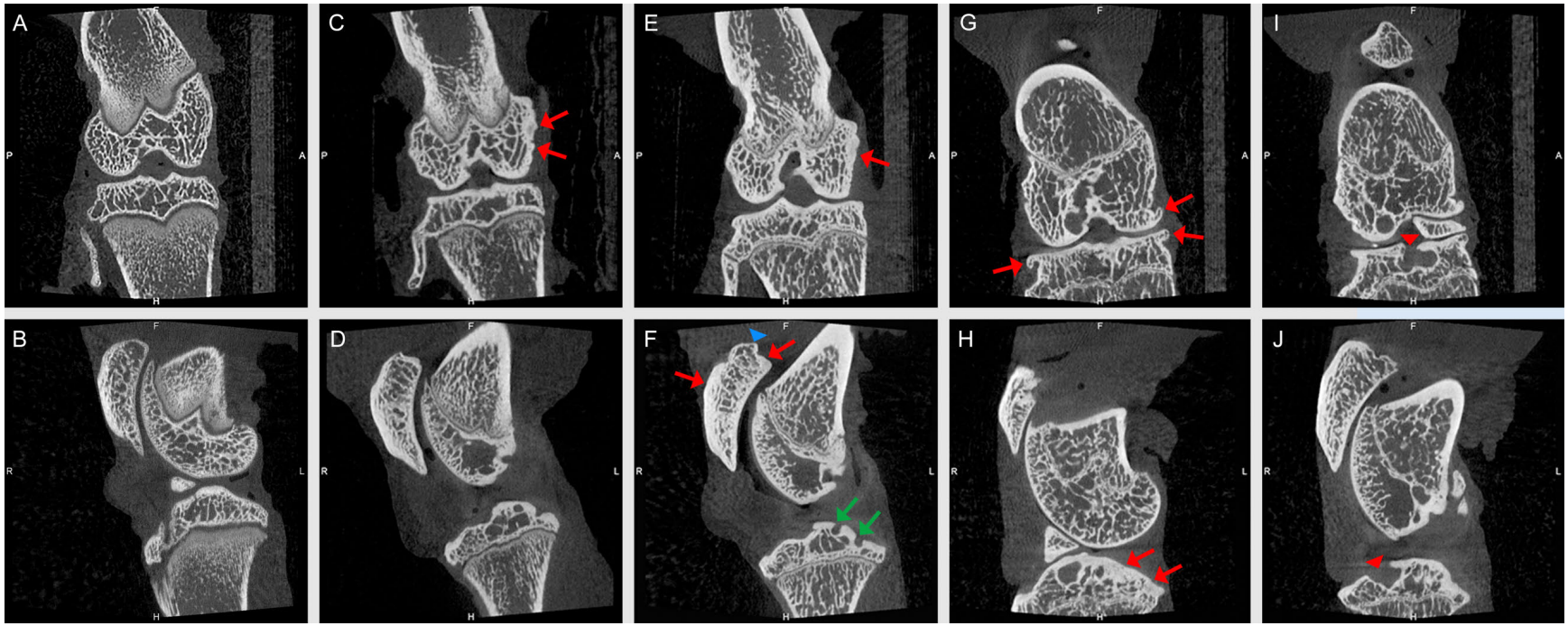

Figure 2.3 – Example microCT images from each age group. (A) Dorsal and (B) sagittal reconstructions from a 2 month old Hartley guinea pig with no clinically significant OA lesions. This animal received a microCT OA score of 0. (C) Dorsal reconstruction from a 5 month old Hartley guinea pig. Sclerosis and small osteophytes are present on the medial femoral condyle (red arrows). and mild sclerosis of the central tibial plateau (D) Sagittal reconstruction from the same 5 month old guinea pig. Mild sclerosis of the cranial aspect of the patella and caudal tibial condyle is present. The small articular cystic changes are artifact due to the angle of the multiplanar reconstruction, which was selected to highlight the entire patella. This animal received a microCT OA score of 4. (E) Dorsal reconstruction from a 9 month old Hartley guinea pig. There is sclerosis and small osteophytes present on the medial femoral condyle (red arrow). (F) Sagittal reconstruction from the same 9 month old guinea pig. There is sclerosis along the cranial margin of the patella and at the proximal caudal end of the patella (red arrows). A large osteophyte is present on the patella (blue arrow). There are 2 cystic areas in the tibia that extend to the articular surface (green arrows). This animal received a microCT OA score of 5. (G) Dorsal reconstruction from a 15 month old Hartley guinea pig. There are 3 large osteophytes (red arrow) on the medial and lateral tibial plateau and on the medial femoral condyle. (H) Sagittal section from the same guinea pig. There is moderate subchondral sclerosis (outlined by red arrows) along the caudal tibia. (I) Dorsal reconstruction from a different plane of section from

the same 15 month old guinea pig. Osteophytes on both medial and lateral tibial plateau and medial femoral condyle are still visible. There is cystic change with articular lysis (red arrow) in the tibial plateau. Subchondral bone sclerosis is also evident in the tibial plateau. (J) Sagittal reconstruction from the same animal. There is marked articular lysis of the tibial plateau (red arrow). This animal received a microCT OA score of 12.

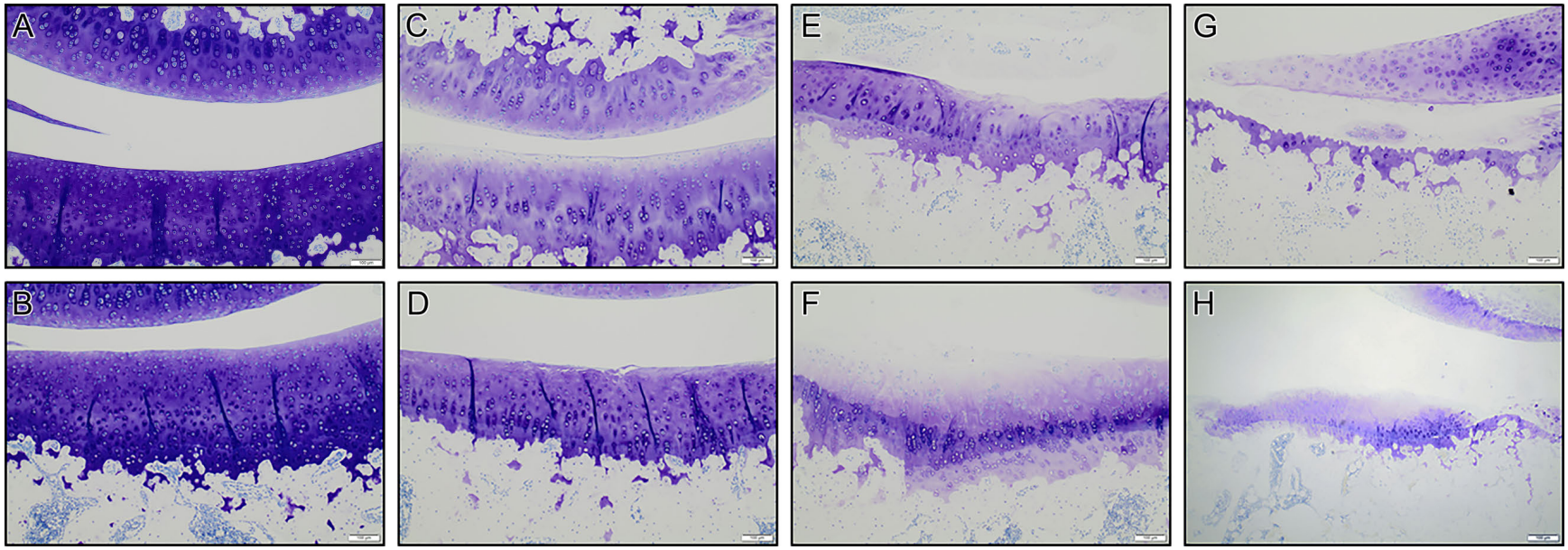

Figure 2.4 – Photomicrographs of histologic OA lesions seen in each age group. All photos are at the medial tibial surface. A) 2 month old with medial tibial OARSI score of 0; B) 3 month old with mild surface undulation, medial tibial OARSI OA score of 0; C) 5 month old demonstrating superficial proteoglycan loss, medial tibial OARSI OA score of 4; D) 5 month old showing articular cartilage fibrillation, medial tibial OARSI OA score 5; E) 9 month old showing proteoglycan loss into the middle zone and loss of superficial cartilage, medial tibial OARSI OA score 8; F) 9 month old demonstrating more diffuse proteoglycan loss into the deep layer with tidemark duplication, medial tibial OARSI OA score 10; G) 15 month old showing complete loss of articular cartilage, medial tibial OARSI OA score of 17; H) Another 15 month old demonstrating loss of articular cartilage and proteoglycan loss, medial tibial OARSI OA score of 18. Toluidine blue stain.

CHAPTER 3

SYSTEMIC IRON OVERLOAD INDUCES OSTEOARTHRITIS IN DISEASE-RESISTANT STRAIN 13 GUINEA PIGS

3.1 Introduction.

Iron is a ubiquitous element that plays a key role in numerous metabolic processes in living organisms including hemoglobin synthesis and oxidative phosphorylation. While iron is essential for life, excess levels are potentially toxic due its ability to induce oxidant damage via the Fenton and Haber Weiss reactions[75,129]. Intriguingly, there is no direct excretion mechanism for iron despite this propensity to create deleterious reactive oxygen species. As such, iron levels are controlled by limiting its absorption in the gastrointestinal tract via actions of the peptide hormone hepcidin. When total body iron stores are replete, the liver is stimulated to produce hepcidin, which binds to and degrades the only known cellular iron export protein, ferroportin[77]. Hepcidin is also produced secondary to inflammation, specifically in response to interleukin-6 (IL-6)[84]. When ferroportin is degraded, iron can no longer be exported from enterocytes, macrophages, and other cell types to enter the bloodstream. As a result, iron becomes sequestered within cells. When hepcidin production is prolonged, as can occur with chronic inflammation, ongoing cellular iron sequestration and accumulation may exhaust normal cellular defenses and incite free radical formation.

Progressive iron accrual has been linked to many aging-associated chronic diseases, due to the toxic effects of iron ions in tissues over time[85]. Age-related conditions in which excessive or improperly handled iron is a risk factor include sarcopenia, type II diabetes,

neurodegenerative disorders, atherosclerosis, and numerous cancers[86.] Additionally, iron overload in joints has long been implicated in arthropathies associated with hereditary hemochromatosis[87] (HH), rheumatoid arthritis (RA)[88,89], traumatic arthropathy, and hemophilic arthropathy[90]. In these conditions, excess iron can accumulate from two sources: blood that enters the joint from either trauma or inflamed synovium, and/or exchange from the labile non-heme iron pool[89,91]. Regardless of the mechanism, several human studies have shown hemosiderin deposits in cartilage and synovium, as well as increased ferritin (the major storage form of iron) in the synovial fluid of affected joints[88,89]. Iron-overloaded synoviocytes release pro-inflammatory cytokines, including interleukin-1β (IL-1β), IL-6, and tumor necrosis factor[92], that stimulate the catabolic activity of chondrocytes. Iron also has a direct effect on cartilage by inducing hydroxyl radical-driven chondrocyte apoptosis and breakdown in matrix components[93,94]. However, the possible role iron accumulation may play in the onset and progression of osteoarthritis has not been well-explored.

Spontaneous osteoarthritis (OA), also known as primary OA, is a painful condition affecting millions of people across the world[97]. Despite its widespread prevalence, mechanisms contributing to OA remain poorly understood. Advancing age is the largest risk factor for development of spontaneous OA[96]. Because iron has emerged as a major contributor in other diseases associated with aging, it is prudent to consider it may also be driving the onset and progression of spontaneous OA.

Limited studies have examined iron status in the context of spontaneous OA. One such study found that serum ferritin levels increased with age and that men with knee OA had higher serum ferritin concentrations that men without knee joint OA. Further analysis demonstrated that men with higher serum ferritin levels had a four-fold greater risk of having radiographic knee

joint OA compared to age-matched controls with normal serum ferritin levels[95]. Another study revealed that OA patients had significantly higher synovial fluid ferritin concentrations when compared to patients without OA, indicating that local iron production within the joint space may contribute to the disease[93].

Because of this intriguing link between iron, aging, and OA, the current study set out to definitively establish iron's role in the pathogenesis of spontaneous OA. We aimed to demonstrate a direct relationship between excess cellular iron accumulation and OA. For this study, we hypothesized that administration of exogenous iron to an OA-resistant guinea pig (Strain 13 guinea pigs) would incite OA pathology.

3.2 Materials and Methods.

Animals.

All procedures were approved by the university's Institutional Animal Care and Use Committee and were performed in accordance with the NIH Guide for the Care and Use of Laboratory Animals. Twenty-two Strain 13 guinea pigs (13 males, 9 females) were purchased at 8 weeks of age and maintained at Colorado State University's Laboratory Animal Resources housing facilities. Animals were monitored daily by a veterinarian. All animals were housed individually in solid bottom cages. Animals were provided regular guinea pig chow (Teklad Global Guinea Pig Diet #2040, Madison, WI), hay cubes, and water *ad libitum*.

Iron dextran injections.

Twelve guinea pigs (7 males, 5 females) were allocated to the experimental iron overload group. Ten animals (6 males, 4 females) were allocated to the control group. To induce systemic

iron overload, animals in the experimental group were administered 400 mg/kg of iron dextran solution intraperitoneally once weekly for a total of four weeks – a dose previously utilized in the guinea pig[130]. Animals in the control group were given 400 mg/kg of a dextran solution intraperitoneally once weekly for four weeks. All injections were initiated when animals were 12 weeks of age. Injections were administered under isoflurane gas anesthesia, with administration sites alternated between the lower left and lower right abdominal quadrants.

Specimen collection.

Animals were harvested at 16 weeks of age. Body weights were recorded at time of harvest. Animals were anesthetized with a mixture of isoflurane and oxygen. Thoracic cavities were opened, and blood was collected with 20-gauge butterfly catheter via direct cardiac puncture. Anesthetized animals were immediately transferred to a carbon dioxide chamber for euthanasia. Hind limbs were removed at the coxofemoral joint. The left limb was placed into 10% neutral buffered formalin for 48 hours and then transferred to PBS for microcomputed tomography (microCT) analysis. Prior to microCT imaging, femur length was measured using calipers. After microCT, limbs were transferred to a 12.5% solution of ethylenediaminetetraacetic acid (EDTA) at pH 7 for decalcification. EDTA was replaced twice weekly for 6 weeks.

Microcomputed tomography of knee joints.

Knee joints were scanned in PBS using the Scanco microCT system (Scanco uCT80, Scanco Medical AG, Bruttisellen, Switzerland) with an isotropic voxel size of 18um. Built-in software (Scanco Medical AG IPL v4.05, Bruttisellen, Switzerland) was used to evaluate bone

volume fraction (BV/TV), trabecular number, trabecular thickness, trabecular spacing, and mean tissue mineral density of bone. These parameters were measured in trabecular bone for the following regions of interest (ROI) in each animal: medial tibia, lateral tibia, medial femur, and lateral tibia. Regions of interest were drawn with the cylinder tool. Fifty image slices were used to create the femoral and tibial ROIs. Clinical features of OA were scored by a veterinary radiologist using a whole joint grading scheme, as previously described[131].

Histologic grading of OA using OARSI recommendations.

After decalcification, three sagittal slices were made through each knee joint. Mid-sagittal slices were made for histologic evaluation of the IFP. Sagittal slices through the medial and lateral femoral condyles were made to assess OA changes in four sites: medial tibia, lateral tibia, medial femur, and lateral femur. Samples were paraffin embedded and a 5-micron section was stained with Toluidine Blue. Medial and lateral femoral condyles along with medial and lateral tibial plateaus, were scored using the recommended published guidelines[60]. This semiquantitative histopathologic grading scheme is based on articular cartilage structure, proteoglycan content, cellularity, tidemark integrity, and presence of osteophytes. Scores were performed in a blinded fashion by two independent pathologists (LBR and KSS). Scores from each of the four anatomic locations were assessed separately, and they were summed to obtain a total knee joint OA score for each guinea pig.

Complete blood count and serum biochemical profile.

At the time of harvest, an aliquot of whole blood collected via cardiac puncture was allocated to 0.5 mL EDTA microtubes for complete blood count (CBC). CBCs were performed

at the CSU Clinical Pathology Laboratory using the Advia 120 hematology analyzer (Siemens, Munich, Germany) with instrument settings and software specifically designed for guinea pig samples. Blood films were manually reviewed, and a leukocyte differential count was performed by a veterinary clinical pathologist (LR). Remaining blood was placed in red top glass tubes, allowed to clot for 30 minutes, and then centrifuged at 5,000 x g for 15 minutes for serum collection. Serum was aliquoted to cryovials and stored at -80°C for future analysis. One aliquot of serum was not frozen and submitted to the Colorado State University (CSU) Clinical Pathology Laboratory for serum biochemical analysis, including serum iron measurement, using the Roche Cobas 6000 (Basel, Switzerland).

Perl's Prussian blue staining of internal organs and liver iron quantitation.

Sections of liver and spleen were placed into 10% neutral buffered formalin at the time of harvest. After 48 hours, formalin was removed and replaced with 1X PBS solution. After left hind limbs were decalcified and knees were trimmed for histologic analysis, remaining femur and tibia long bones were cut longitudinally to obtain sections of bone marrow. These sections of liver, spleen, and bone marrow were paraffin-embedded and 5-micron sections were stained with Perl's Prussian blue to highlight tissue iron load. Iron quantitation was performed via atomic absorption spectroscopy (AAS) on 200-gram samples of formalin-fixed liver tissue by the CSU Toxicology Laboratory. Iron levels were reported as parts per million (ppm) dry weight.

Enhanced iron staining of knee joints.

To identify small amounts of iron in joint tissues, an enhanced staining protocol was used, as previously described[132]. Unstained sections of knee joints were heated at 60°C

overnight. Slides were briefly deparaffinized by immersion into a gentle xylene substitute (SafeClear). After drying, slides were immersed in a solution of 1% potassium ferrocyanide, 0.05N hydrochloric acid, and 5% polyvinylpyrrolodione for 60 minutes. They were then incubated in a 0.3% hydrogen peroxide and 0.01M sodium azide solution for 75 minutes. After rinsing in PBS, slides were transferred to a diaminobenzidine (DAB) solution. After rinsing and drying, slides were coverslipped using Permount. Negative control slides for each joint were made by following the described protocol without incubation in the potassium ferrocyanide solution. Four representative photographs of cartilage from each slide were used to make a single composite photograph for each animal. A single photo of the infrapatellar fat pad was taken for each animal. Nikon Elements software (Tokyo, Japan) was used to quantify surface area of iron-positive areas on the cartilage composite and IFP photographs.

Immunohistochemistry of knee joints for 4-hydroxynonenal.

Immunohistochemistry (IHC) was performed on sections of knee joints using a polyclonal rabbit antibody to 4-hydroxynonenal (4HNE) (Abcam ab46545) at a dilution of 1:200. Prior to incubation with primary antibody, slides were incubated in citrate buffer overnight at 55°C for antigen retrieval, as recommended for skeletal tissues[133]. Slides were incubated in primary antibody overnight at 4°C, followed by a 30-minute incubation with a biotinylated goat anti-rabbit secondary antibody. Exposure to secondary antibody, alone, did not result in any positive immunostaining. Sections were counterstained with hematoxylin, coverslipped, and viewed by light microscopy. At least four sections from each joint were examined for immunostaining in chondrocytes, matrix, menisci, synovium, and within the IFP.

Statistical analyses.

Data for total body weights, femur length, bone morphometric measurements, CBC values, serum biochemical values, liver AAS, and surface area of iron staining on knee joint photographs passed normality testing via the D'Agostino Pearson omnibus test and were compared using parametric t tests. Histologic and whole joint microCT OA scores were not normally distributed. These data sets were compared using non-parametric Mann Whitney U tests. Statistical significance was set at $P < 0.05$. All statistical analyses were performed with GraphPad Prism (La Jolla, CA, USA).

3.3 Results.

General description of animals.

Animals in the iron dextran group exhibited skin hyperpigmentation as a result of the iron overload. Despite these findings, all animals appeared clinically healthy, and no changes in behavior were noted. Most guinea pigs in the iron overload study gained weight as expected, and there was no statistical difference in total body weight between the overload group and the dextran control group (Figure 3.1). Mean total body weight was 775.6 grams in the dextran control group and 711.9 grams in the iron overload group. When stratified by sex, there was no significant difference in total body weight for the males; however, the females in the iron overload group had a significantly decreased body weight compared to female controls (data not shown). Mean body weight for the female iron overload animals was 571.4 grams while dextran controls mean body weight was 733.5 grams ($P = 0.0317$). Femur lengths between the iron overload and dextran control groups was also similar (Figure 3.1), indicating iron overload did

not alter skeletal growth in these animals. No differences in femur length were found when stratified by sex (data not shown).

Quantitative microCT measurements.

Mean values (and 95% confidence interval) for each of the quantitative microCT measurements are listed in Table 3.1. In this study, significant differences were found for the following parameters: BV/TV in the lateral tibia, trabecular number in the lateral tibia and lateral femur, trabecular thickness in the lateral tibia, and trabecular spacing in the medial tibia. No differences in bone tissue mineral density were noted in any anatomic region of interest. Lateral tibial BV/TV and trabecular thickness were decreased in the iron overload group compared to dextran controls. Trabecular number was decreased in the lateral tibia, yet increased in the lateral femur in the iron overload group. Trabecular spacing was mildly decreased in the medial tibia of the iron overload group.

Whole joint microCT OA scores.

The whole joint microCT OA scores provides a global assessment of bony changes observed in the tibia, femur, and patella in each animal. OA scores were higher in the iron overload group (Figure 3.2). Mean score in this group was 4.5 compared to 1.6 in the dextran control group. One animal in the iron overload group had no evidence of bony lesions and received a score of 0. Remaining animals in this group had scores ranging from 2-8. Conversely, in the dextran control group, five animals had no radiographic evidence of OA with scores of 0. Remaining animals in the dextran control group ranged from 2-5. Representative microCT images are provided in Figure 3.3. Of the 10 animals in the dextran control group, 5 had small

osteophytes present on the tibia. Two of these 5 also had small osteophytes on the femur. No evidence of patellar osteophytes, subchondral bone cysts, or subchondral bone sclerosis were noted in any animal in the dextran control group. In the iron overload group, 11 out of 12 animals had small osteophytes on both the tibia and femur. Two female animals also had large osteophytes on their femurs. Similar to the dextran group, no animals in the iron overload group had evidence of subchondral bone cysts or subchondral bone sclerosis.

OARSI histology score.

Histologic OA scores, which focus primarily on cartilage changes, were higher in the iron overload group compared to dextran controls (Figure 3.2). Mean total joint score was 20.0 (95% CI 17.34 – 22.66) in the iron overload group and 3.875 (95% CI 2.833 – 4.917) in the dextran control group ($P < 0.0001$). When medial and lateral compartments were analyzed separately, the same pattern was noted (data not shown). Mean score for the medial compartment was 11.9 (95% CI 9.48 – 14.32) in the iron overload group while it was 1.889 (95% CI 0.84 – 2.94) in the dextran control group ($P < 0.0001$). Mean score for the lateral compartment was 8.11 (95% CI 5.28 – 10.95) in the iron overload group and 2.11 (95% CI 1.40 – 2.82) in the dextran control group ($P = 0.0002$). Representative photomicrographs demonstrating articular cartilage in the medial compartment are depicted in Figure 3.4. Figure 3.4A shows normal, healthy cartilage in a dextran control animal. Figure 3.4B shows an area on the tibial surface with a mildly irregular articular surface, loss of proteoglycan content into the middle layer of cartilage, and chondrocyte loss.

Complete blood count and serum biochemistry.

There were several key differences in CBC and serum biochemical values between the iron overload and dextran control group animals. Concerning erythrocyte indices, iron overload did not result in a difference in hematocrit (Figure 3.5) or in the cellular hemoglobin concentration mean (CHCM, Figure 3.5). However, iron overload did result in a change in mean red blood cell volume (MCV, Figure 3.5). Relative to controls, iron overloaded animals had smaller, microcytic red blood cells. MCV in the iron overload group was 69.14 (95% CI 64.76 – 73.53) while it was 72.90 (95% CI 71.98 – 73.82) in the dextran group ($P = 0.0291$). Serum iron levels were also much higher in the iron overload group (Figure 3.5). Mean serum iron was 939.1 μg/dl (95% CI 476.0 – 1,402) in the overload group and 281.9 μg/dl (95% CI 265.2 – 298.6) in the dextran group ($P = 0.0008$).

There were also several changes to suggest increased systemic inflammation in the iron overload group. Platelet counts and total white blood cell counts were both higher in the iron overload group (Figure 3.5). Mean platelet count was 544,100 cells/μL (95% CI 500,200 – 588,000) in the iron overload group and 462,900 cells/μL (95% CI 410,600 – 515,200) in the dextran group ($P = 0.0179$). Mean WBC count was 7,175 cells/μL (95% CI 6,138 – 8,212) in the iron overload group and 3,930 cells/μL (95% CI 3,220 – 4,640) in the dextran group ($P < 0.0001$). On serum biochemistry, an inflammatory pattern of lower albumin coupled with increased globulins was present in the iron overload group as well (Figure 3.5). Mean serum albumin was 2.5 g/dl (95% CI 2.333 – 2.667) in the iron overload group and 2.87 g/dl (95% CI 2.774 – 2.966) in the dextran group ($P = 0.0002$). Mean serum globulin concentration was 2.113 g/dl (95% CI 1.926 – 2.299) in the iron overload group and 1.880 g/dl (95% CI 1.742 – 2.018) in the dextran group ($P = 0.0307$).

Perl's Prussian blue staining of internal organs & liver iron quantitation.

In order to demonstrate tissue iron levels in the iron overloaded and dextran control animals, samples of liver, spleen, and bone marrow were stained with Prussian blue. This stain highlights iron, specifically that in the form of hemosiderin. The liver is a major organ dedicated to iron storage. The spleen and bone marrow are also iron-rich, due to the presence of macrophages that participate in red blood cell turnover and iron storage, respectively. Figure 3.6A and 3.6C depict a strong blue color, indicating presence of abundant iron in the iron overload group liver and spleen, respectively. In contrast, very little detectable blue staining is observed in the dextran control liver and spleen (Figure 3.6B, D). Similar staining properties were noted in the bone marrow (not pictured). To quantitate the amount of iron present in the liver, AAS was performed on a sample from each animal in both the iron overload and dextran groups. Liver iron content was significantly different between the two groups. Mean liver iron in the overload group was 10,448 ppm (95% CI 7,870 – 13,025) and 1,214 ppm in the dextran control group (95% CI 518.7 – 1,909) ($P<0.0001$) (Figure 3.7).

Enhanced iron staining of knee joints.

Because iron levels in joint tissues were expected to be low, even in the face of iron overload, an enhanced stain with increased sensitivity compared to Perls' Prussian blue stain was utilized. Staining in cartilage and the IFP was quantified and compared separately between treatment groups. Surface area of iron staining in cartilage was similar between the dextran control and iron overload groups. However, surface area was significantly higher in the IFP of the iron overload group (Figure 3.8). Surface area of iron staining in cartilage was 69.44 square microns (95% CI 61.32 – 77.57) in the dextran group and 67.17 square microns (95% CI 59.63 –

74.70) in the iron overload group (P = 0.6538). Meanwhile, surface area of iron staining in the IFP was 37.22 square microns (95% CI 31.94 – 42.50) in the dextran group and 53.00 square microns (95% CI 49.96 – 56.04) in the iron overload group (P < 0.0001).

IHC for 4HNE in knee joints.

Protein expression of 4HNE, a marker of lipid peroxidation, was present within the meniscus and chondrocytes in the superficial zone of cartilage of the iron overload group (Figure 3.9). No staining was noted in chondrocytes or menisci in the dextran control group. 4HNE immunostaining was present within the synovium and IFP in both the dextran control and iron overload groups. However, staining intensity was notably increased in the iron overload group. No staining was noted within the extracellular cartilage matrix.

3.4 Discussion.

In the current study, we demonstrated that experimental iron overload induced knee joint OA in disease-resistant Strain 13 guinea pigs. This work firmly establishes that iron overload is detrimental to knee joint health and should be considered a key player in the development of spontaneous OA. While we did not note any changes in demeanor over the course of the study, animals in the iron overload group exhibited skin hyperpigmentation. Because of this marked change in skin color, we harvested the animals after one month of iron administration to ensure proper animal welfare. Although females in the iron overload group had a significantly decreased body weight compared to dextran females, there was no difference in femoral length, indicating iron overload did not alter skeletal growth of these animals. In regards to these sex differences, it is possible the females were more sensitive to the hazardous effects of iron compared to males,

although the reason for this requires more investigation. In humans, it is men who are more prone to higher systemic iron levels (e.g. serum ferritin) with age, as women experience years of recurrent mild blood loss due to menstruation. Thus, women are relatively iron deficient compared to men until menopause, when ferritin levels begin to increase[134].

Both bony and cartilage lesions associated with OA were markedly increased in the iron overload group. These changes are especially striking given the young age (16 weeks) and OA-resistant nature of the Strain 13 guinea pigs used in this study. While Strain 13 animals are not immune to OA, they typically exhibit minimal to mild lesions at 12 months of age, and, therefore, are often referred to as OA-resistant[135]. This is in contrast to the Hartley guinea pig, a strain that develops OA lesions starting at 3 months of age and is considered a natural model of this disease[135].

Using the whole joint microCT scoring system, nearly all animals in the iron overload group exhibited osteophytes on both the femur and tibia. Osteophytes are bony outgrowths that arise from the periosteum at joint margins and are commonly found in osteoarthritic joints[136]. They form early in the development of disease under the influence of transforming growth factor beta (TGFß), and may be a source of pain[137,138]. Osteophytes are thought to provide added stability to joints with OA[139] although their true function is incompletely understood. In our Strain 13 animals, we would not expect joint laxity or mechanical problems to be present that may promote osteophyte formation. It may be possible that iron overload triggers a biochemical event that incites osteophyte formation. Indeed, osteophytes are commonly present in humans with systemic iron overload due to hemochromatosis[140]. The link between iron overload and osteophyte formation may lie in the BMP/SMAD signaling pathways shared by TGFß and the

iron regulator hepcidin[141,142]. Despite utilizing similar signaling pathways, the potential connection between iron and osteophyte formation has not been explored.

Aside from OA changes noted using the clinically-oriented grading scheme, we also found several changes in more conventional microCT values. These changes were predominantly found in the lateral tibia. This site exhibited decreased bone volume fraction, trabecular thickness, and trabecular number in the iron overload group. Iron excess can induce osteoarthritic changes; however, it can also cause osteoporosis and osteopenia characterized by bone loss and decreased bone mineral density[143,144]. The reason for these dichotomous actions and what drives OA in some patients and bone loss in others remains unclear. Several studies have shown that excess iron exerts inhibitory effects on osteoblasts while simultaneously increasing the bone resorptive activity of osteoclasts[145-148]. A study in iron overloaded mice linked excess ROS formation with bone loss[148]. ROS induce NF-kB and downstream pro-inflammatory cytokines such as TNF and IL-6, which can stimulate osteoclast formation[148,149]. While we found no differences in bone mineral density in the iron overloaded guinea pigs, this may be due to short-term nature of study. Differences may emerge with a longer time course of iron overload. Based on our findings, there is evidence for concurrent OA and changes consistent with osteopenia in iron overloaded guinea pigs. The complex interaction and balance between iron overload and bony changes warrants further investigation.

To characterize systemic effects of iron dextran administration, we collected blood, serum, and several tissues for analysis. As expected, serum iron levels were increased in the iron overload group. As iron is integral to heme formation, erythrocyte values on CBC were examined. Interestingly, the mean cell volume (MCV) of erythrocytes was decreased in the iron overload group with no changes noted in total hematocrit or mean cell hemoglobin

concentrations. Decreased MCV, or microcytosis, is a finding typically associated with iron deficiency, not overload. However, experimental iron overload (via a high iron diet) caused copper deficiency in rats[150]. Because copper is intimately linked to iron homeostasis, copper deficiency can result in microcytosis[151]. It is possible that the iron overload guinea pigs in the current study became copper deficient, leading to microcytosis. Another possibility is that the microcytosis developed secondary to inflammation and the iron-restricting effects of hepcidin. In future studies, measurement of serum or tissue copper and hepcidin levels should be performed to characterize the cause of the microcytosis.

In addition to erythrocyte values, several other blood and serum parameters were examined. There were several indicators of increased levels of systemic inflammation in the iron overload group. They had increased total leukocyte counts as well as increased platelet counts. Increased platelets, while non-specific, is commonly associated with inflammation, as cytokines, particularly IL-6, stimulate thrombopoiesis,[152] and this has been demonstrated experimentally in guinea pigs[153]. On serum biochemistry, iron overload animals had lower albumin levels coupled with increased globulins, a pattern indicative of inflammation. Albumin is a negative acute phase protein, while globulins are positive acute phase proteins[154], so they often exhibit an inverse relationship in the presence of inflammation. Another consideration for the lower albumin concentrations is possible decreased production due to liver insufficiency in the iron overload group. Hepatic dysfunction is linked to iron overload[155] and cannot be entirely ruled out in the current study.

To further characterize the extent of iron overload systemically and locally within the knee, we performed specialized histochemical stains in major organs involved with iron homeostasis and knee joints, respectively. To this end, Perls' Prussian blue stain was done on

sections of liver, spleen, and bone marrow from each animal. Results from these stains confirmed the marked degree of iron overload in the treated group compared to controls. Liver iron quantitation via AAS further confirmed these findings. As preliminary studies in our lab revealed that Perls' Prussian blue stain lacked sensitivity to detect the expected small amount of iron present in knee joints (data not shown), an enhanced stain was used. Results from the enhanced iron stain illustrated that there was, indeed, increased iron within the knee joints of the iron overload group. Differences in iron staining were attributed to accumulation within macrophages in the infrapatellar fat pad (IFP). No differences were noted in cartilage iron staining between the groups. The IFP has emerged as an important player in knee joint homeostasis[156]. The IFP is comprised of a network of adipocytes, fibroblasts, and leukocytes[44,47]. Therefore, it is prone to be a source of inflammatory mediators that may contribute to OA[41,45–47,53,157–161]. While it has not been described in the IFP specifically, iron accumulation within adipose tissue macrophages occurs with states of chronic inflammation, such as obesity[162]. In the current work, iron accrual within IFP macrophages was drastic and was likely a primary source of oxidants within the knee joint. Indeed, IHC for 4HNE, a marker of oxidant damage, lends support to this suspicion, as there were higher levels of immunostaining in cartilage, menisci, synovium, and the IFP in the iron overload group.

This study provides data linking iron overload to development of OA in disease-resistant Strain 13 guinea pigs. Specifically, iron accumulation within the IFP likely acts as a local depot triggering pro-oxidant and inflammatory damage to many tissues in knee joints. A limitation of this work is the marked degree of iron overload that is likely not biologically relevant in normal, healthy aging animals. However, this proof-of-principle study aimed to pinpoint iron as a direct contributor to the pathogenesis of primary OA. Future work will examine tissue iron load in

untreated aging animals, particularly in OA-prone Hartley guinea pigs. Similarly, it is prudent to determine whether a decrease in iron load, via diet or chelation, may prevent OA lesions or delay their onset. Studies examining iron trafficking pathways within joint tissues are also needed to increase our understanding of how this element contributes to development of primary OA in animals and humans.

Table 3.1 – Conventional microCT values in dextran and iron overload animals.

		Dextran	Iron Overload	P-value
Bone Volume/Total Volume	**MT**	0.4142 (0.3717,0.4567)	0.4223 (0.3868,0.4578)	0.7456
	LT	0.4227 (0.3971,0.4483)	0.3817 (0.3628,0.4006)	**0.0081**
	MF	0.4543 (0.4451,0.4635)	0.4342 (0.4054,0.4629)	0.1911
	LF	0.3829 (0.3539,0.4120)	0.3797 (0.3565,0.4028)	0.8439
Trabecular Number (1/mm)	**MT**	4.443 (4.257,4.630)	4.519 (4.334,4.705)	0.5321
	LT	5.040 (4.770,5.310)	4.608 (4.407,4.808)	**0.0081**
	MF	3.866 (3.754,3.978)	3.986 (3.853,4.118)	0.1490
	LF	3.626 (3.425,3.826)	3.979 (3.825,4.132)	**0.0047**
Trabecular Thickness (mm)	**MT**	0.1174 (0.1106,0.1242)	0.1148 (0.1079,0.1216)	0.5589
	LT	0.1093 (0.1046,0.1140)	0.1006 (0.0979,0.1032)	**0.0012**
	MF	0.1242 (0.1197,0.1287)	0.1192 (0.1125,0.1259)	0.2055
	LF	0.1104 (0.1069,0.1139)	0.1072 (0.1042,0.1103)	0.1420
Trabecular Spacing (mm)	**MT**	0.2286 (0.2177,0.2394)	0.2010 (0.1864,0.2156)	**0.0030**
	LT	0.2027 (0.1870,0.2184)	0.2122 (0.1993,0.2251)	0.3031
	MF	0.2117 (0.2027,0.2208)	0.2077 (0.1975,0.2716)	0.5208
	LF	0.2362 (0.2205,0.2518)	0.2209 (0.2064,0.2355)	0.1288
Bone Tissue Mineral Density (g/cm^3)	**MT**	875.6 (865.3,885.9)	877.0 (864.8,889.2)	0.8523
	LT	880.9 (873.6,888.1)	875.7 (867.9,883.5)	0.3002
	MF	900.3 (893.6,907.1)	909.6 (895.4,923.9)	0.2371
	LF	888.6 (882.5,894.8)	896.7 (888.2,905.3)	0.1167

MT, medial tibia; LT, lateral tibia; MF, medial femur; LF, lateral femur

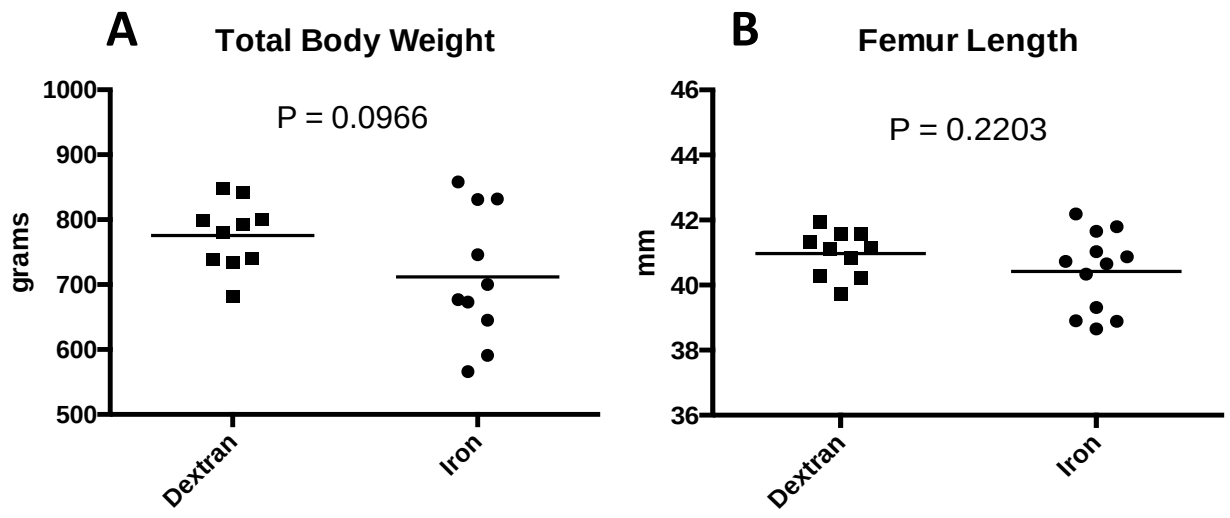

Figure 3.1 – Body weights and femur lengths in dextran and iron overload animals. Total body weight (A) and femur length (B) for dextran control and iron overload animals. Black line represents mean value.

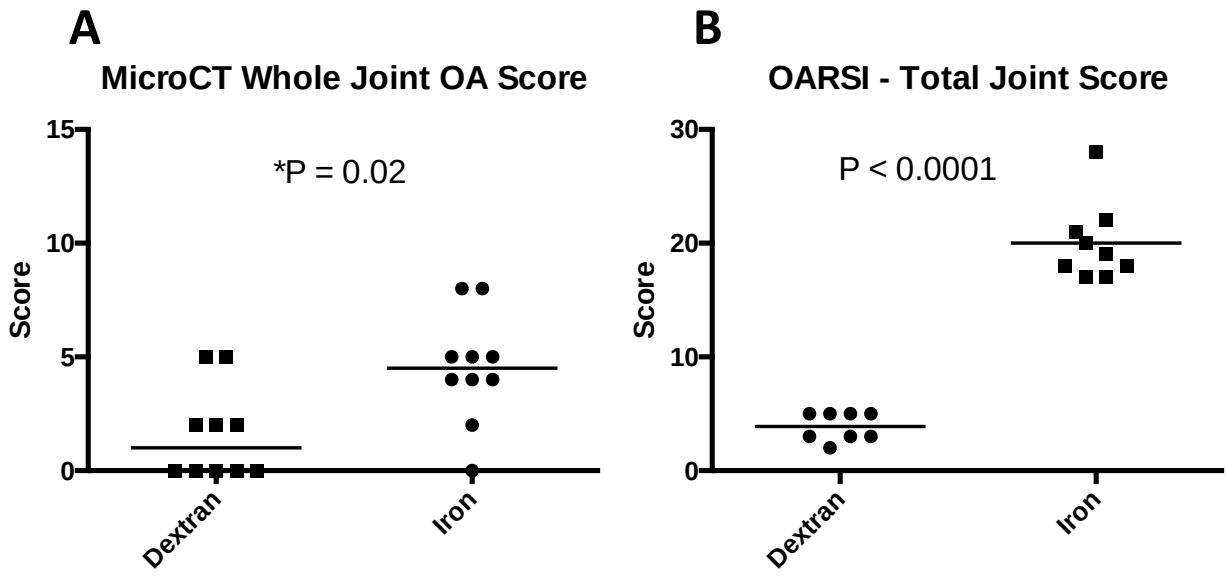

Figure 3.2 – MicroCT and OARSI histologic OA scores in dextran and iron overload animals. MicroCT whole joint OA score (A) and histologic OA score (B) for dextran control and iron overload groups. Black line represents mean value.

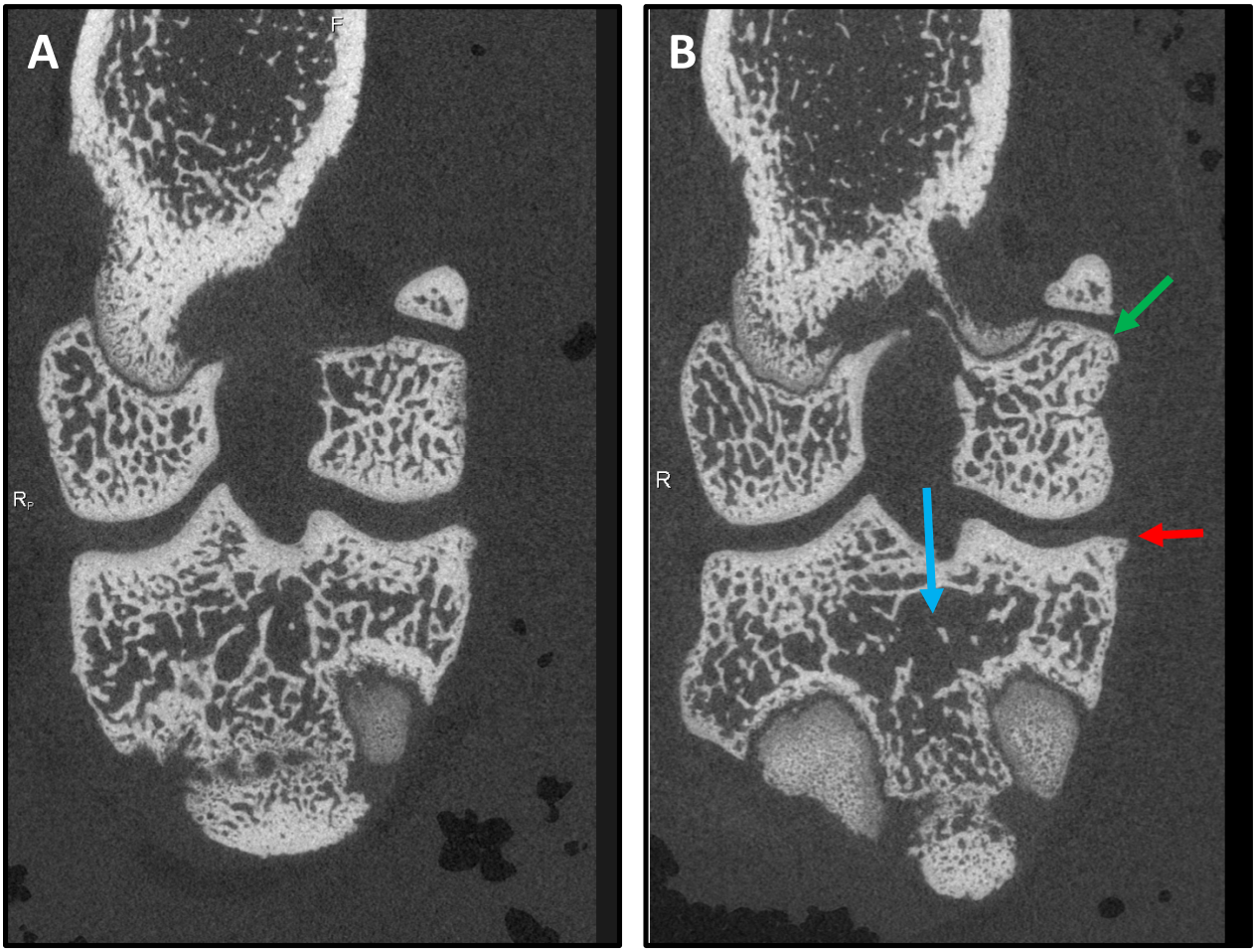

Figure 3.3 – Example images of microCT lesions. Representative microCT images from a dextran control guinea pig (A), and an iron overload guinea pig (B). Note the presence of osteophytes on the medial tibia (red arrow) and medial femur (green arrow), and a subchondral cyst (blue arrow).

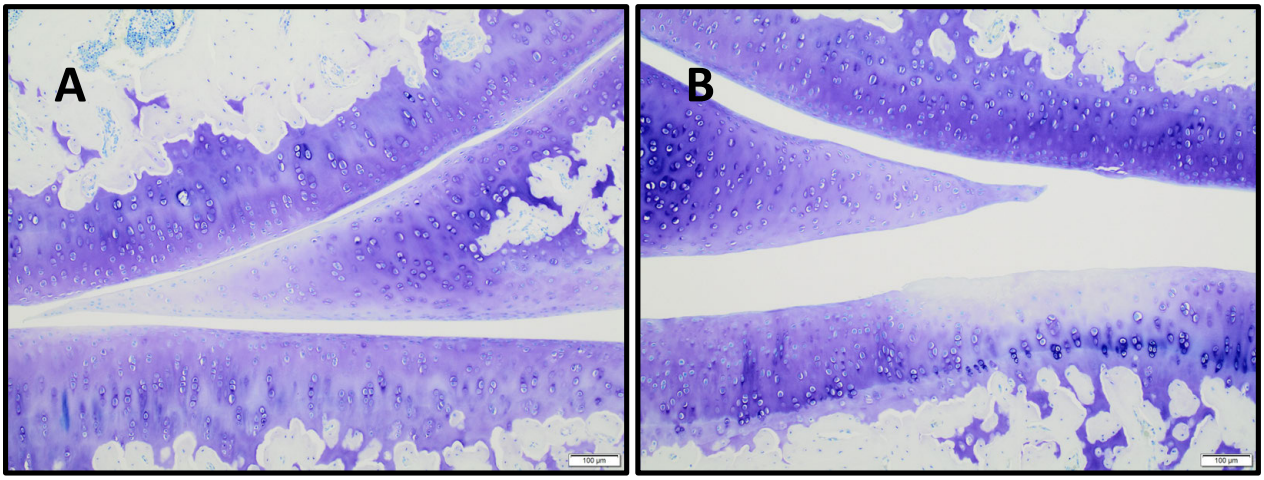

Figure 3.4 – Example photomicrographs of histologic lesions. Toluidine blue stained photomicrographs of medial compartment. A) Representative photomicrograph from an animal in the dextran group (medial compartment OARSI score of 0). B) Representative photomicrograph from an animal in the iron overload group (medial compartment OARSI score of 12).

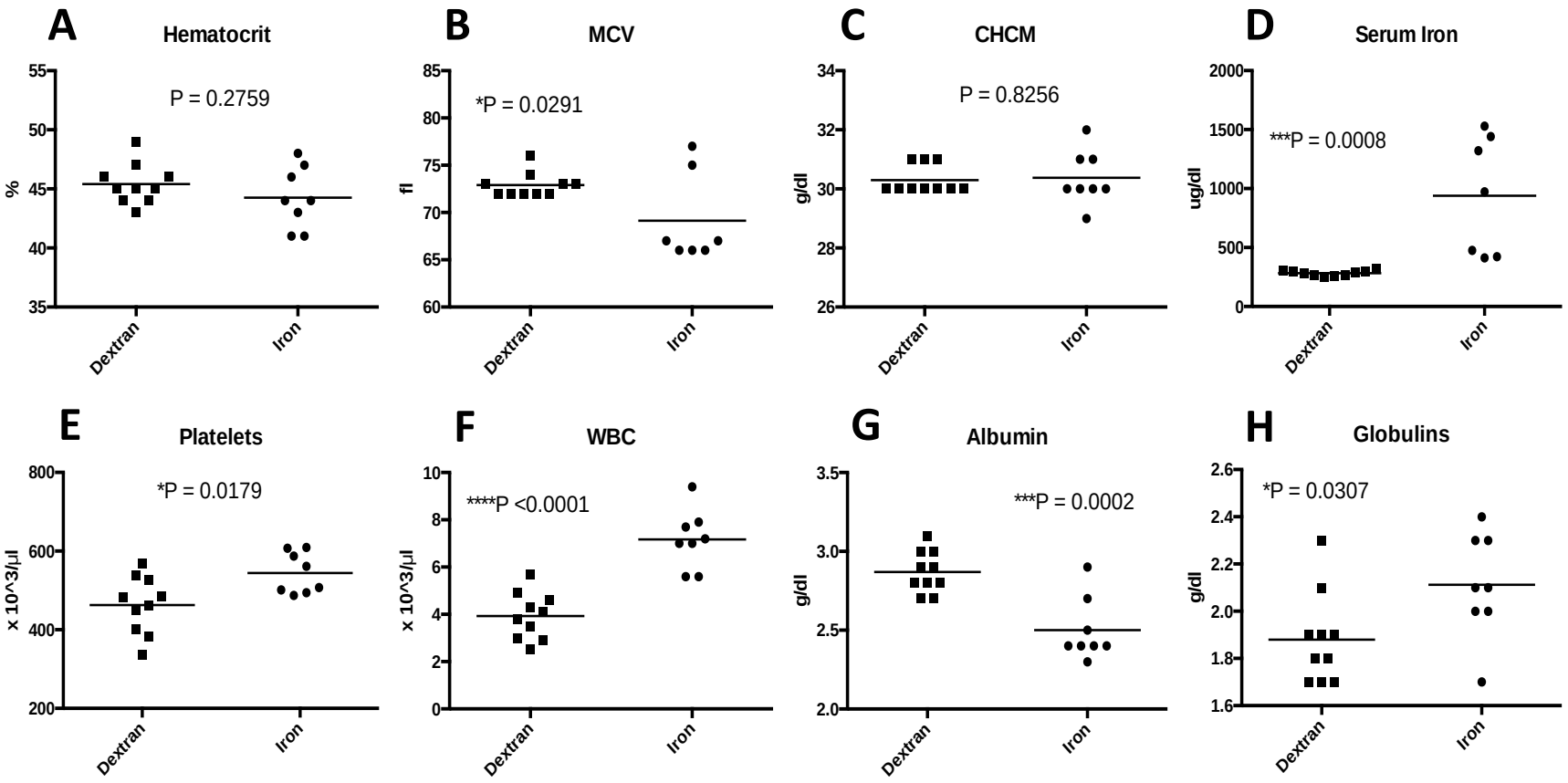

Figure 3.5 – CBC and biochemistry data from dextran and iron overload animals. Select CBC and serum biochemical values from dextran control and iron overload groups. A) hematocrit, B) mean red blood cell volume, C) cellular hemoglobin concentration mean, D) serum iron, E) platelet count, F) white blood cell count, G) serum albumin, and H) serum globulins. Black line represents mean value.

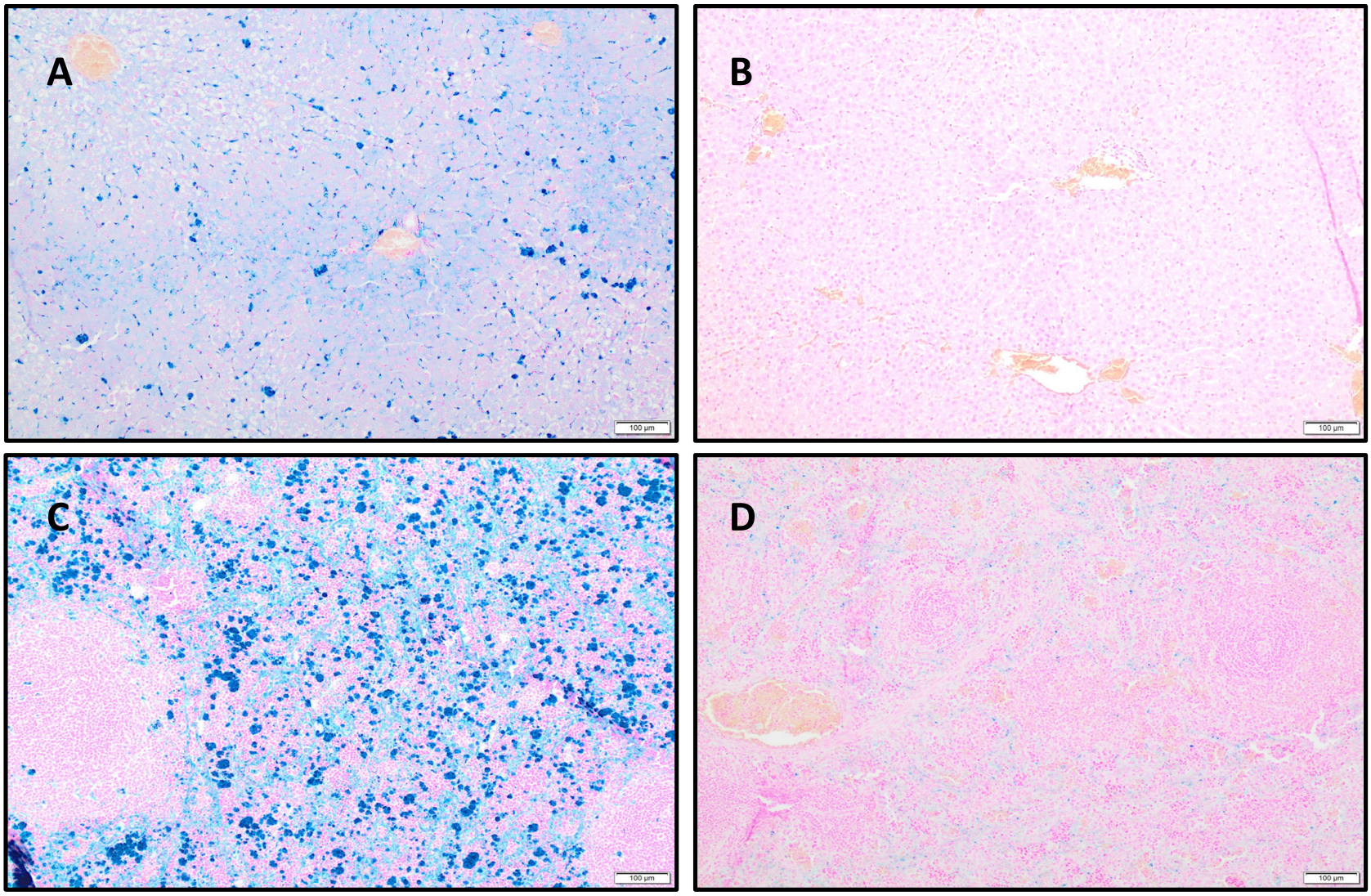

Figure 3.6 – Perls' Prussian blue photos of liver and spleen in dextran and iron overload animals. Representative Prussian blue photos from A) liver from an animal in the iron overload group, B) liver from an animal in the dextran control group, C) spleen from an animal in the iron overload group, and D) spleen from an animal in the dextran control group.

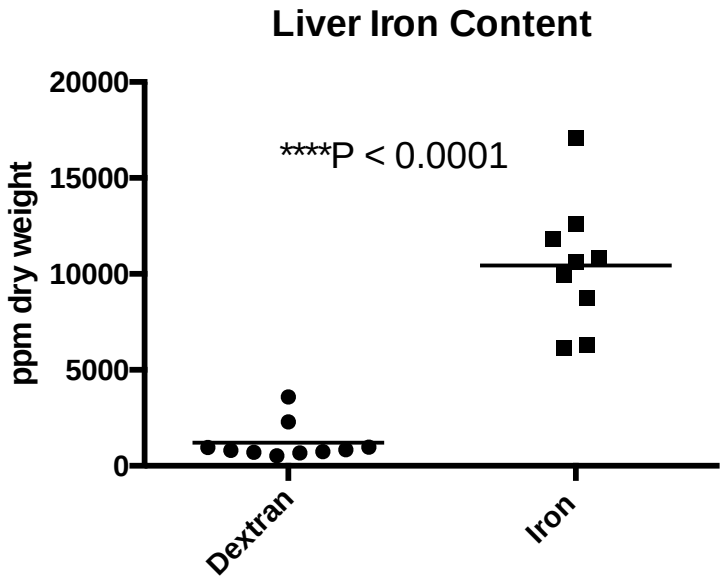

Figure 3.7 – Quantitative liver iron content in dextran and iron overload animals. Iron content reported as parts per million dry weight of liver in the A) dextran control group, and B) iron overload group. Black line represents mean value.

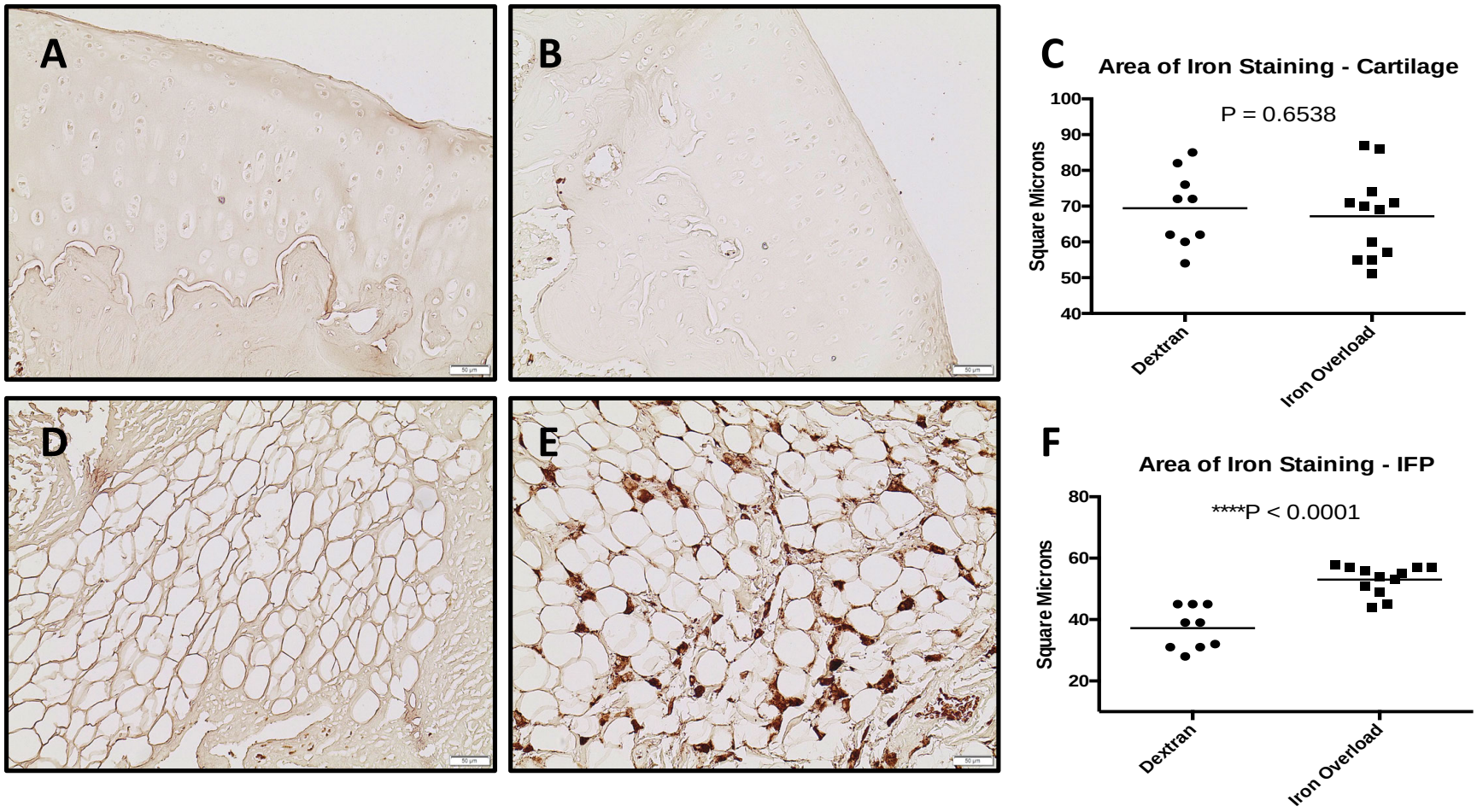

Figure 3.8 – Enhanced iron staining of knee joints in dextran and iron overload animals. Iron staining in the cartilage of a dextran control animal (A), cartilage of an iron overload animal (B), IFP of a dextran control animal (D), and IFP of an iron overload animal (E). (C) and (F) demonstrate area of iron staining in the cartilage and IFP.

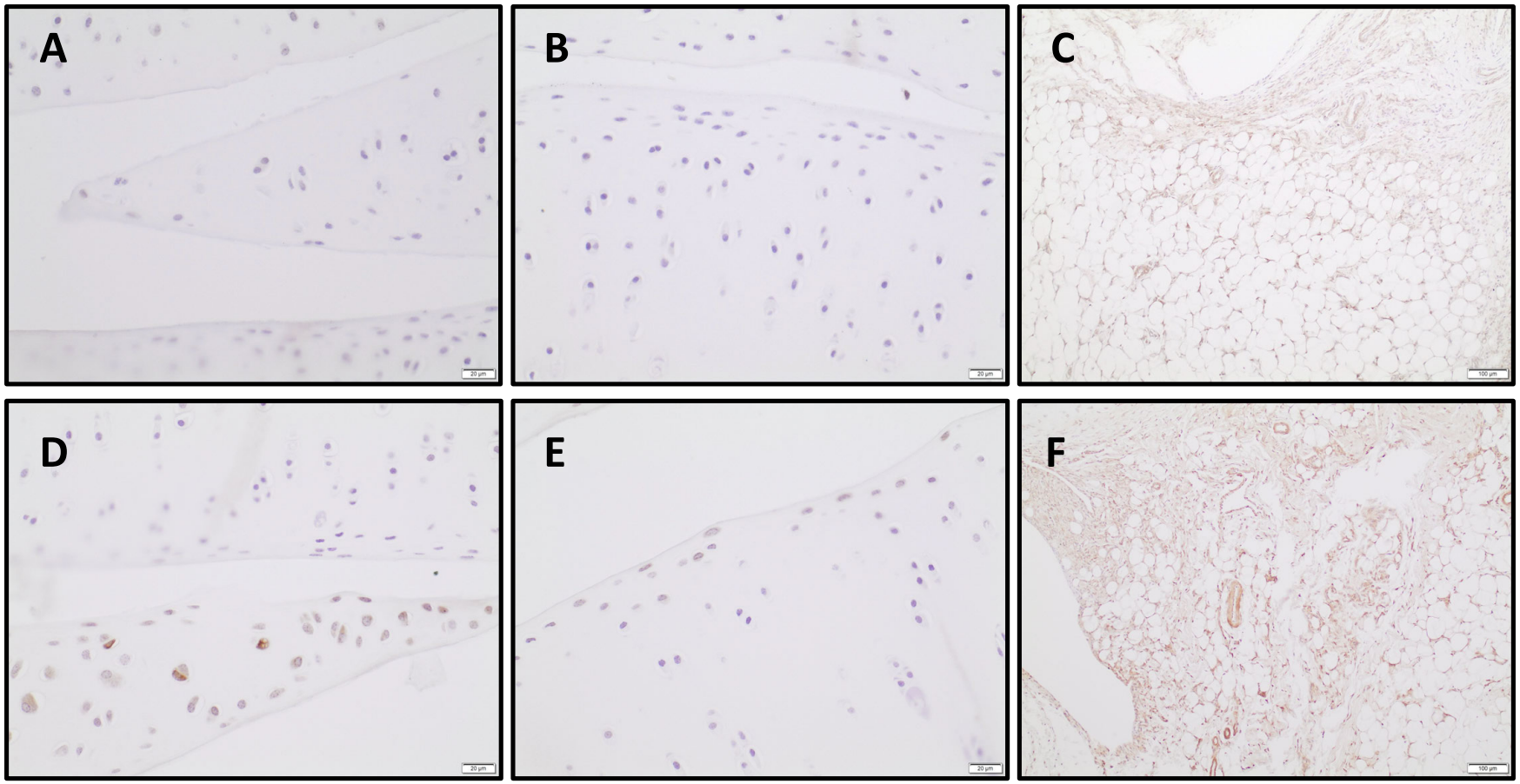

Figure 3.9 – 4-hydroxynonenal immunohistochemistry in dextran and iron overload animals. 4HNE immunostaining in dextran control meniscus (A), tibial cartilage (B), and IFP and synovium (C). 4HNE immunostaining in iron overload meniscus (D), tibial cartilage (E), and IFP and synovium (F).

CHAPTER 4

SYSTEMIC IRON DEFICIENCY LESSENS OSTEOARTHRITIS SEVERITY IN DISEASE-PRONE HARTLEY GUINEA PIGS

4.1 Introduction.

Iron is an element that is critical to normal organismal function. Primarily, it is used to synthesize hemoglobin for normal oxygen transport in mammals, but it also has roles in oxidative phosphorylation and production of iron-sulfur clusters within the mitochondria. Although iron is essential for life, it also has the ability to induce tissue injury when it is present in excess amounts or is not properly handled by cells[163]. This is due to iron's propensity to participate in the free radical producing Fenton and Haber Weiss reactions[75,129]. Despite this potential for tissue injury, there are no direct iron excretion mechanisms present in mammals other than normal desquamation of skin and gastrointestinal epithelium[164]. Thus, in normal individuals, iron levels are controlled by limiting its intestinal absorption. This is regulated by hepcidin, a peptide hormone produced by the liver. Hepcidin is produced in iron replete states as well as in response to systemic inflammation[84]. In the presence of hepcidin, ferroportin, the only known iron export protein, is degraded[77]. This prevents iron within enterocytes, as well as within hepatocytes and macrophages, from being exported to the bloodstream. When hepcidin production is prolonged, as can occur with chronic inflammation[165], iron becomes sequestered within cells and can accumulate[166,167].

Due to the lack of an excretion mechanism, progressive iron accumulation in tissues over time seems to be an inevitable process associated with aging. In fact, many chronic aging-related

diseases have been linked to the toxic effects of iron accrual over time[85]. Examples of such diseases include type II diabetes, sarcopenia, atherosclerosis, neurodegenerative diseases, and various cancers[86]. Furthermore, excess iron in joint tissues has long been linked to arthropathies associated with hereditary hemochromatosis[87], rheumatoid arthritis[88,89], and hemophilic arthropathy[90]. Studies have shown increased iron levels in cartilage, synovium, as well as synovial fluid in these conditions[88,89]. *In vitro* studies have demonstrated that iron-loaded synoviocytes secrete pro-inflammatory cytokines that, in turn, stimulate chondrocyte matrix metalloproteinase activity[92]. Additionally, iron is able to directly cause chondrocyte apoptosis through induction of hydroxyl free radical formation[93,94].

Though iron has been studied in the arthropathies described above, its possible role in driving spontaneous, aging-associated osteoarthritis (OA) has not been well-explored. Spontaneous OA is a widespread, painful condition affecting millions across the globe[97]. Unfortunately, mechanisms underlying development of this debilitating disease are poorly understood. To date, one human study showed that higher serum ferritin (a storage form of iron) levels in men were associated with a 4-fold increased risk of having radiographic evidence of knee joint OA[168]. Another study found increased ferritin levels in the synovial fluid of patients with OA compared to those without the disease[93]. Because iron has been implicated in many other diseases related to aging, we hypothesize its accumulation in joint tissues may be contributing to development of spontaneous OA.

To directly assess this intriguing link between iron and OA, we performed two proof-of-principle studies. In the first study, described in a companion manuscript, we demonstrated that induction of systemic iron overload, via administration of iron dextran, resulted in early onset and worsened severity of OA in a disease-resistant Strain 13 guinea pigs. Here, we assessed the

ability of systemic iron depletion, using an iron deficient diet, to prevent or delay the onset and/or progression of OA. For this study, we hypothesized that consumption of an iron deficient diet would mitigate OA in disease-prone Dunkin-Hartley guinea pigs.

4.2 Materials and Methods.

Animals.

All procedures were approved by the university's Institutional Animal Care and Use Committee and were performed in accordance with the NIH Guide for the Care and Use of Laboratory Animals. Twelve male Dunkin-Hartley guinea pigs were purchased from a commercial vendor (Charles River Laboratories, Wilmington, MA) at 8 weeks of age and maintained at Colorado State University's Laboratory Animal Resources housing facilities for an additional 19 weeks. Animals were monitored daily by a veterinarian. All animals were housed individually in solid bottom cages and fed *ad libitum*, as described below.

Iron deficient and control diets.

For this part of the study, six animals were placed on either an iron deficient or iron sufficient (control) diet. Due to their fastidious nature, guinea pigs were transitioned from a regular chow diet (Teklad Global Guinea Pig Diet #2040, Madison, WI) to either the iron deficient or iron sufficient (control) diet over 2 weeks by mixing the diets. They were fully switched to the experimental diets at 12 weeks of age. These diets were specially formulated from Harlan Teklad and were identical in composition with the exception of iron content. The iron sufficient diet contained 0.735 g/kg of ferric citrate as the source of iron while the deficient diet was formulated without added ferric citrate. Animals were fed these diets for a duration of

19 weeks. Food and water were provided *ad libitum*. Fleece material was used to prevent consumption of bedding, a common behavior of coprophagic guinea pigs, as all available bedding options contained high levels of iron (data not shown).

Specimen collection.

Animals were harvested at 31 weeks of age. Body weights were recorded at time of harvest. Animals were anesthetized with a mixture of isoflurane and oxygen. Thoracic cavities were opened, and blood was collected with 20-gauge butterfly catheter via direct cardiac puncture. Anesthetized animals were immediately transferred to a carbon dioxide chamber for euthanasia. Hind limbs were removed at the coxofemoral joint. The left limb was placed into 10% neutral buffered formalin for 48 hours and then transferred to PBS for microcomputed tomography (microCT) analysis. Prior to microCT imaging, femur length was measured using calipers. After microCT, limbs were transferred to a 12.5% solution of ethylenediaminetetraacetic acid (EDTA) at pH 7 for decalcification. EDTA was replaced twice weekly for 6 weeks.

Microcomputed tomography of knee joints.

Knee joints were scanned in PBS using the Scanco microCT system (Scanco uCT80, Scanco Medical AG, Bruttisellen, Switzerland) with an isotropic voxel size of 18um. Built-in software (Scanco Medical AG IPL v4.05, Bruttisellen, Switzerland) was used to evaluate bone volume fraction (BV/TV), trabecular number, trabecular thickness, trabecular spacing, and mean tissue mineral density of bone. These parameters were measured in trabecular bone for the following regions of interest (ROI) in each animal: medial tibia, lateral tibia, medial femur, and

lateral tibia. Regions of interest were drawn with the cylinder tool. Fifty image slices were used to create the femoral and tibial ROIs. Clinical features of OA were scored by a veterinary radiologist using a whole joint grading scheme, as previously described[131].

Histologic grading of OA using OARSI recommendations.

After decalcification, three sagittal slices were made through each knee joint. Mid-sagittal slices were made for histologic evaluation of the IFP. Sagittal slices through the medial and lateral femoral condyles were made to assess OA changes in four sites: medial tibia, lateral tibia, medial femur, and lateral femur. Samples were paraffin embedded and a 5-micron section was stained with Toluidine Blue. Medial and lateral femoral condyles along with medial and lateral tibial plateaus, were scored using the recommended published guidelines[60]. This semiquantitative histopathologic grading scheme is based on articular cartilage structure, proteoglycan content, cellularity, tidemark integrity, and presence of osteophytes. Scores were performed in a blinded fashion by two independent pathologists (LBR and KSS). Scores from each of the four anatomic locations were assessed separately, and they were summed to obtain a total knee joint OA score for each guinea pig.

Complete blood count and serum biochemical profile.

At the time of harvest, a portion of whole blood collected via cardiac puncture was allocated to 0.5 mL EDTA microtubes for complete blood count (CBC). CBCs were performed at the Colorado State University (CSU) Clinical Pathology Laboratory using the Advia 120 hematology analyzer (Siemens, Munich, Germany) with instrument settings and software specifically designed for guinea pig samples. Blood films were manually reviewed, and a

leukocyte differential count was performed by a veterinary clinical pathologist (LR). Remaining blood was placed in red top glass tubes, allowed to clot for 30 minutes, and then centrifuged at 5,000 x g for 15 minutes for serum collection. Serum was aliquoted to cryovials and stored at -80°C for future analysis. One aliquot of serum was not frozen and submitted to the CSU Clinical Pathology Laboratory for serum biochemical analysis, including serum iron measurement, using the Roche Cobas 6000 (Basel, Switzerland).

Prussian blue staining of internal organs and liver iron quantitation.

Sections of liver and spleen were placed into 10% neutral buffered formalin at the time of harvest. After 48 hours, formalin was removed and replaced with 1X PBS solution. After left hind limbs were decalcified and knees were trimmed for histologic analysis, remaining femur and tibia long bones were cut longitudinally to obtain sections of bone marrow. These sections of liver, spleen, and bone marrow were paraffin-embedded and 5-micron sections were stained with Prussian blue to highlight tissue iron load. Iron quantitation was performed via atomic absorption spectroscopy (AAS) on 200-gram samples of formalin-fixed liver tissue by the CSU Toxicology Laboratory. Iron levels were reported as parts per million (ppm) dry weight.

Enhanced iron staining of knee joints.

To identify small amounts of iron in joint tissues, an enhanced staining protocol was used, as previously described[132]. Unstained sections of knee joints were heated at 60°C overnight. They were briefly deparaffinized by immersion into a gentle xylene substitute (SafeClear). After drying, slides were immersed in a solution of 1% potassium ferrocyanide, 0.05N hydrochloric acid, and 5% polyvinylpyrrolodione for 60 minutes. They were then

incubated in a 0.3% hydrogen peroxide and 0.01M sodium azide solution for 75 minutes. After rinsing in PBS, slides were transferred to a diaminobenzidine (DAB) solution. After rinsing and drying, slides were coverslipped using Permount. Negative control slides for each joint were made by following the described protocol without incubation in the potassium ferrocyanide solution. Four representative photographs of cartilage from each slide were used to make a single composite photograph for each animal. A single photo of the infrapatellar fat pad was taken for each animal. Nikon Elements software was used to quantify area of iron-positive areas on the cartilage composite and IFP photographs.

Immunohistochemistry of knee joints for 4-hydroxynonenal.

Immunohistochemistry (IHC) was performed on sections of knee joints using a polyclonal rabbit antibody to 4-hydroxynonenal (4HNE) (Abcam ab46545) at a dilution of 1:200. Prior to incubation with primary antibody, slides were incubated in citrate buffer overnight at 55°C for antigen retrieval, as recommended for skeletal tissues[133]. Slides were incubated in primary antibody overnight at 4°C, followed by a 30-minute incubation with a biotinylated goat anti-rabbit secondary antibody. Exposure to secondary antibody, alone, did not result in any positive immunostaining. Sections were counterstained with hematoxylin, coverslipped, and viewed by light microscopy. At least four sections from each joint were examined for immunostaining in chondrocytes, matrix, menisci, synovium, and within the IFP.

Statistical analyses.

Data for total body weights, femur length, histologic OA scores, whole joint microCT OA scores, bone morphometric measurements, CBC values, serum biochemical values, liver

AAS, and surface area of iron staining on knee joint photographs passed normality testing via the Kolmogorov-Smirnov test. These data were compared using parametric t tests. Statistical significance was set at $P < 0.05$. All statistical analyses were performed with GraphPad Prism (La Jolla, CA, USA).

4.3 Results.

General description of animals.

Total body weights for animals on the iron deficient diet and control diets were similar (Figure 4.1). Mean total body weight was 1058 grams for the control diet group and 1054 grams for the iron deficient diet group. Femur lengths were also similar between these two groups, with a mean of 42.89 mm in the control group and 42.72 mm in the deficient diet group (Figure 4.1).

Quantitative microCT measurements.

Mean values (and 95% confidence interval) for each of the quantitative microCT measurements are listed in Table 4.1. In this study, significant differences were found for: trabecular number in the lateral tibia, trabecular thickness in the medial femur, and bone tissue mineral density in all four regions of interest. No differences were found for BV/TV or trabecular spacing. Compared to animals on the control diet, animals on the iron deficient diet exhibited increased trabecular number in the lateral tibia and slightly decreased trabecular thickness in the medial femur. Interesting, bone tissue mineral density was uniformly decreased in all four regions of interest (medial tibia, lateral tibia, medial femur, lateral femur) in the iron deficient diet group compared to controls.

Whole joint microCT OA scores.

The whole joint microCT OA scores provides a global assessment of bony changes observed in the tibia, femur, and patella in each animal. There were no differences in whole joint microCT scores between animals on the iron deficient and control diets (Figure 4.2). Scores in both group groups ranged from 5 to 12. Mean score was 9 in the iron deficient diet group and 9.2 in the control diet group. In the control diet group, all 6 animals had small and large osteophytes present on both the tibia and femur. Two out of 6 animals in the control group also had osteophytes present on the patella. Four animals exhibited subchondral bone cystic changes and subchondral bone sclerosis. In the iron deficient diet group, 3 animals had large osteophytes on the tibia, femur, and patella while the remaining 3 animals lacked patellar osteophytes. Three animals had subchondral bone cysts and subchondral bone sclerosis.

OARSI histology score.

Histologic grading using published OARSI guidelines[60] demonstrated lower total joint scores for the iron deficient diet group compared to animals in the control diet (Figure 4.2). Mean total joint OARSI score was 10.67 (95% CI 3.909 – 17.42) in the deficient diet group and 24.0 (95% CI 18.18 – 29.82) in the control diet group ($P < 0.0039$). This same pattern was present when medial and lateral compartments (scores from tibia and femur added together) were considered separately (data not shown). Mean OARSI score for the medial compartment was 6.833 (95% CI 2.074 – 11.59) in the deficient diet group and 12.5 (95% CI 9.132 – 15.87) in the control diet group ($P < 0.0315$). Mean OARSI score for the lateral compartment was 3.833 (95% CI 1.591 – 6.076) in the deficient diet group and 12.2 (95% CI 9.812 – 14.59) in the control diet group ($P < 0.0001$). Representative photomicrographs demonstrating typical lesions seen in the

articular cartilage are shown in Figure 4.3. Figure 4.3A shows a fibrillated cartilage surface and an area of severe proteoglycan loss extending to the deep zone of the cartilage. Additionally, there is chondrocyte loss in this area. Figure 4.3B shows a relatively normal tibial surface with very mild proteoglycan loss in the superficial layer of cartilage and mild chondrocyte hypercellularity.

Complete blood count and serum biochemistry.

There were several findings indicating systemic iron deficiency in the iron deficient diet group. On CBC, the deficient diet group had lower hematocrit, lower mean red blood cell volume (MCV), and lower cellular hemoglobin concentration mean (CHCM), indicating a mild, microcytic, hypochromic anemia in these animals, consistent with iron deficiency (Figures 4.4). Mean hematocrit was 43.6% (95% CI 39.71 – 47.49) in the deficient diet group and 46.67% in the control diet group (95% CI 45.81 – 47.52) ($P = 0.0448$). Mean red blood cell volume was 60.0 fl (95% CI 52.3 – 67.7) in the deficient diet group and 82.33 fl (95% CI 79.79 – 84.88) in the control diet group ($P < 0.0001$). Mean CHCM was 28.8 g/dl (95% CI 27.76 – 29.84) in the deficient diet group while it was 31.83 g/dl (95% CI 31.40 – 32.26) in the control diet group ($P < 0.0001$). Other findings supportive of systemic iron deficiency in deficient diet group were an increased platelet count and decreased serum iron concentration (Figures 4.4). Mean platelet count was 585,200/µL (95% CI 485,400 – 685,000) in the deficient diet group and 410,200/µL (95% CI 340,500 – 479,900) in the control diet group.

There was no CBC or serum biochemical evidence to indicate a difference in systemic inflammation between the two groups. Total white blood cell counts, serum albumin, and serum globulins were similar in both diet groups (Figure 4.4). Mean WBC count was 5,280/µL (95% CI

3,850 – 6,710) in the deficient diet group and 4,667/μL (95% CI 2,746 – 6,588) in the control diet (P = 0.5338). Mean serum albumin was 3.0 g/dl (95% CI 2.726 – 3.274) in the deficient diet group and 2.933 g/dl (95% CI 2.775 – 3.091) in the control diet group (P = 0.5995). Mean serum globulin concentration was 2.3 g/dl (95% CI 2.124 – 2.476) in the deficient diet group and 2.233 g/dl (95% CI 2.125 – 2.342) in the control diet group (P = 0.4257).

Prussian blue staining of internal organs & liver iron quantitation.

In order to demonstrate tissue iron levels in the iron deficient and control diet animals, samples of liver, spleen, and bone marrow were stained with Prussian blue. This stain highlights iron, specifically that in the form of hemosiderin. The liver is the major organ dedicated to iron storage. The spleen and bone marrow are also iron-rich, due to the presence of macrophages that participate in red blood cell turnover and iron storage, respectively. Figures 4.5A and 4.5C demonstrate a lack of Prussian blue staining in the iron deficient diet liver and spleen, respectively. In contrast, normal amounts of blue iron deposits are noted in the liver and spleen of animals on the control diet (Figure 4.5B, D). Bone marrow exhibited similar trends as liver and spleen (not pictured). A sample of liver was used to quantitate iron levels in the two diet groups via AAS. Liver iron content was significantly higher in the control diet group compared to the iron deficient diet group (Figure 4.6). Mean liver iron content was 1,590 ppm dry weight (95% CI 853.9 – 2,326) in the control diet group, while it was 185.3 ppm (95% CI 53.59 – 316.9) in the deficient diet group (P = 0.0022).

Enhanced iron staining of knee joints.

An enhanced iron stain was used to detect small quantities of iron within joint tissues. No significant differences in iron staining were found in the cartilage or IFP between control and iron deficient diet groups (Figure 4.7). Surface area of iron staining in the cartilage was 143.4 square microns (95% CI 87.00 – 278.1) in the control group and 90.67 square microns (95% CI 68.13 – 113.2) in the iron deficient diet (P = 0.2699). In the IFP, surface area of iron staining was 36.00 square microns (95% CI 28.45 – 43.55) in the control group and 40.00 square microns (95% CI 31.63 – 48.37) in the iron deficient diet group (P = 0.3826).

IHC in knee joints for 4HNE.

Protein expression of 4HNE, a marker of lipid peroxidation, was strongly present within the meniscus of animals on the control diet. Likewise, mild to moderate expression was noted within chondrocytes in the superficial cartilage layer and within the synovium and IFP in control animals (Figure 4.8). In contrast, no staining was noted in the menisci, and slight positive staining was present in superficial chondrocytes, in animals in the iron deficient diet. Staining intensity was notably less in the synovium and IFP in the iron deficient diet group compared to controls, as well. No appreciable staining was noted within the extracellular cartilage matrix in either group.

4.4 Discussion.

Here, we demonstrated that histologic OA lesions were lessened in disease-prone Hartley guinea pigs fed an iron deficient diet for 19 weeks. To our knowledge, this is the first study examining effects of an iron deficient diet in a rodent model of spontaneous OA. In conjunction

with our work examining the OA-worsening effects of iron overload on disease-resistant Strain 13 guinea pigs, this work further solidifies that systemic iron status directly influences knee joint health. While an iron deficient diet is obviously not ideal for long-term wellbeing, this study offers proof-of-principle data that tempering ingestion of iron-rich foods may be beneficial in thwarting aging-related knee joint OA. In fact, some experts believe that it is better and healthier to be slightly iron deficient than to risk having too much iron, which can be toxic[89].

The most striking finding of the current work was a significantly decreased histologic OA score in the iron deficient diet group. As body weights were similar between the groups, this finding is attributed to the difference in iron content in the two diets. It is well-established that iron can induce chondrocyte apoptosis, although this is most readily apparent in the presence of heme iron, as seen with traumatic joint injury[169] and hemophilic arthropathy[170,171]. Apart from heme, reactive oxygen species also induce chondrocyte apoptosis[172]. Additionally, iron-loaded synoviocytes and macrophages release increased amounts of inflammatory cytokines such as TNF, IL-1, and IL-6 that subsequently stimulate MMP activity, resulting in degraded cartilage[92]. The decreased immunostaining for 4HNE across many tissue types in the iron deficient diet group suggests that these animals experienced less knee joint oxidant damage compared to control animals. Decreasing systemic iron levels may beneficially modulate local iron levels within the knee, resulting in less oxidant damage, apoptosis, and inflammation. Supporting this, an *in vitro* study found that human articular chondrocytes treated with lactoferrin, an endogenous iron-binding glycoprotein, exhibited decreased apoptosis in the presence of IL-1ß[173]. A similar study found that treatment with lactoferrin decreased chondrocyte expression of MMPs and inflammatory cytokines[174]. Together, these studies and our results suggest that reduction in iron may prevent cartilage deterioration.

Despite having significantly decreased cartilage lesions in the iron deficient diet group, we did not find any differences in bony changes associated with OA using the whole joint microCT scoring system. Animals in both the iron deficient and control diet groups exhibited osteophytes, subchondral bone sclerosis, and subchondral bone cysts at 31 weeks of age. However, there were differences in conventional microCT measurements between the groups, suggesting that influence of iron deficiency on bone may have been occurring but not radiographically achieved. Most notably was the decreased tissue mineral density of the subchondral trabecular bone in all anatomic regions examined. Human studies have found a positive association between bone mineral density and serum ferritin levels in men[175]. Another study similarly found an association with iron deficiency anemia and osteoporosis in the general population including men and women[176]. Dietary iron intake is also positively associated with bone mineral density in postmenopausal women[177]. Together, these studies offer evidence that systemic iron levels have a positive relationship with bone mineral density. Given these findings in people, it seems that a parallel trend exists in the Hartley guinea pig. However, the positive relationship between iron levels and bone mineral density clearly has limitations, as iron overload conditions, such as hereditary hemochromatosis, are commonly associated with osteoporosis[178]. This has been attributed to increased osteoclast activity in conditions of iron excess[178].

To examine the systemic effects of the iron deficient diet, and to ensure clinically relevant iron deficiency was achieved, blood and serum were collected for analysis. Guinea pigs on the iron deficient diet had many classical CBC and biochemistry results associated with iron deficiency. As expected, serum iron levels were significantly lower in the iron deficient diet group. Compared to control animals, iron deficient animals also had a lower hematocrit (estimate

of overall erythrocyte mass), decreased mean cell volume (MCV) of erythrocytes, and decreased erythrocyte cellular hemoglobin concentration mean (CHCM). In clinical terms, they exhibited a microcytic, hypochromic anemia, which is the classic pattern seen in iron deficiency in humans[179] as well as in dogs[180,181]. Our work demonstrates that this pattern holds true in a guinea pig model of nutritional iron deficiency as well, which has not been previously reported. In addition to the mild anemia present, guinea pigs on the iron deficient diet also had higher platelet counts. Thrombocytosis is another classic CBC finding associated with iron deficiency, but the mechanisms driving this change are not fully understood[182]. Thrombocytosis is also frequently noted in inflammatory conditions, as IL-6 stimulates thrombopoiesis[183]. However, in the current study, there were no changes present on CBC or serum biochemistry to suggest animals on the iron deficient diet had increased systemic inflammation.

To further characterize the extent of iron deficiency systemically and locally within the knee joint, we performed specialized histochemical stains in major organs involved with iron homeostasis and knee joints, respectively. Sections of liver, spleen, and bone marrow were stained with Perls' Prussian blue, which highlights iron deposits in tissues. As expected, the amount of iron present in all three of these organs was visibly less in the iron deficient animals compared to controls. Furthermore, quantitative iron levels in the liver measured by AAS confirmed these findings. Together, our blood and tissue results affirm that the diet used in this study achieved systemic iron deficiency.

As preliminary studies in our lab revealed that Perls' Prussian blue stain lacks sensitivity to detect the expected small amount of iron present in knee joints (data not shown), an enhanced stain was used. Despite use of this enhanced stain, no differences in iron in cartilage or the IFP were found. Although demonstrating increased sensitivity compared to Perls' Prussian blue, this

stain may still lack the required sensitivity to detect very low quantities of iron that may be present in these joints. It is also possible that turn-over of iron may take longer than the course of our study to influence joint tissue. Despite finding similar amounts of iron within the knee joints of both groups, there was visibly less 4HNE immunostaining in many tissues within the knee joint in the iron deficient diet group, indicating a lesser degree of oxidant damage in this group. More studies are needed to further characterize the changes that may be occurring locally within the knee joint in the face of systemic iron deficiency. In particular, studies examining iron import and export proteins within joint tissues may provide valuable insight into how systemic iron levels affect knee joint iron homeostasis.

This study provides data suggesting that systemic iron deficiency, achieved through an iron deficient diet, delays onset or progression of cartilage lesions in an OA-prone Hartley guinea pigs. Based on our results, this is most likely attributed to decreased levels of oxidant damage within knee joints in the face of iron deficiency. A limitation of the current work includes the use of male animals only. Future work will include female animals to assess for potential sex differences. Likewise, consumption of an iron deficient diet is likely not optimal for overall long-term health, nor is it a practical option. This proof-of-principle study aimed to determine if decreasing iron load, using an iron deficient diet, could lessen OA severity in disease-prone animals. This study was done in-parallel with another proof-of-principle study demonstrating iron overload induces OA lesion in disease-resistant Stain 13 guinea pigs. Based on the promising findings reported here, future work will investigate the ability of pharmacologic iron chelators to prevent or delay OA in Hartley guinea pigs. Systemic and/or local iron chelation is not currently considered in the treatment of spontaneous or post-traumatic OA, although it has been shown to be beneficial in a variety of conditions where oxidant damage secondary to excess

iron is implicated[184]. Additional studies examining iron trafficking pathways within joint tissues are also needed, as this is an unexplored niche. Such studies will improve our understanding of how iron contributes to development of spontaneous OA and may open the door to exploring novel treatments for this widespread and debilitating disease.

Table 4.1 – Conventional microCT values in control and iron deficient diet animals.

		Control Diet	Deficient Diet	P-value
Bone Volume/Total Volume	**MT**	0.4525 (0.3867,0.5183)	0.4606 (0.4094,0.5118)	0.8075
	LT	0.4269 (0.3811,0.4726)	0.4563 (0.4195,0.4930)	0.2266
	MF	0.4962 (0.4439,0.5485)	0.4560 (0.3982,0.5138)	0.2147
	LF	0.4513 (0.4112,0.4914)	0.4269 (0.3976,0.4561)	0.2343
Trabecular Number (1/mm)	**MT**	3.516 (3.190,3.843)	3.671 (3.421,3.922)	0.3563
	LT	3.498 (3,192,3.805)	3.834 (3.622,4.046)	**0.0346**
	MF	3.641 (3.300,3.982)	3.417 (3.008,3.825)	0.3049
	LF	3.514 (2.353,3.675)	3.406 (3.176,3.636)	0.3467
Trabecular Thickness (mm)	**MT**	0.1351 (0.1205,0.1497)	0.1346 (0.1261,0.1431)	0.9407
	LT	0.1255 (0.1141,0.1368)	0.1265 (0.1211,0.1319)	0.8291
	MF	0.1432 (0.1324,0.1539)	0.1331 (0.1289,0.1372)	**0.0299**
	LF	0.1359 (0.1179,0.1538)	0.1312 (0.1171,0.1454)	0.6143
Trabecular Spacing (mm)	**MT**	0.2624 (0.2289,0.2958	0.2464 (0.2068,0.2860)	0.4478
	LT	0.2617 (0.2339,0.2896)	0.2409 (0.2296,0.2521)	0.1042
	MF	0.2248 (0.1881,0.2615)	0.2491 (0.2131,0.2851)	0.2516
	LF	0.2425 (0.2269,0.2582)	0.2509 (0.2256,0.2763)	0.4847
Bone Tissue Mineral Density (g/cm^3)	**MT**	921.0 (904.4,937.7)	899.4 (883.5,915.3)	**0.0351**
	LT	918.6 (907.5,929.8)	897.5 (878.9,916.0)	**0.0304**
	MF	936.7 (912.1,961.2)	911.4 (898.2,924.6)	**0.0418**
	LF	949.5 (934.2,964.8)	922.3 (897.7,946.9)	**0.0367**

MT, medial tibia; LT, lateral tibia; MF, medial femur; LF, lateral femur

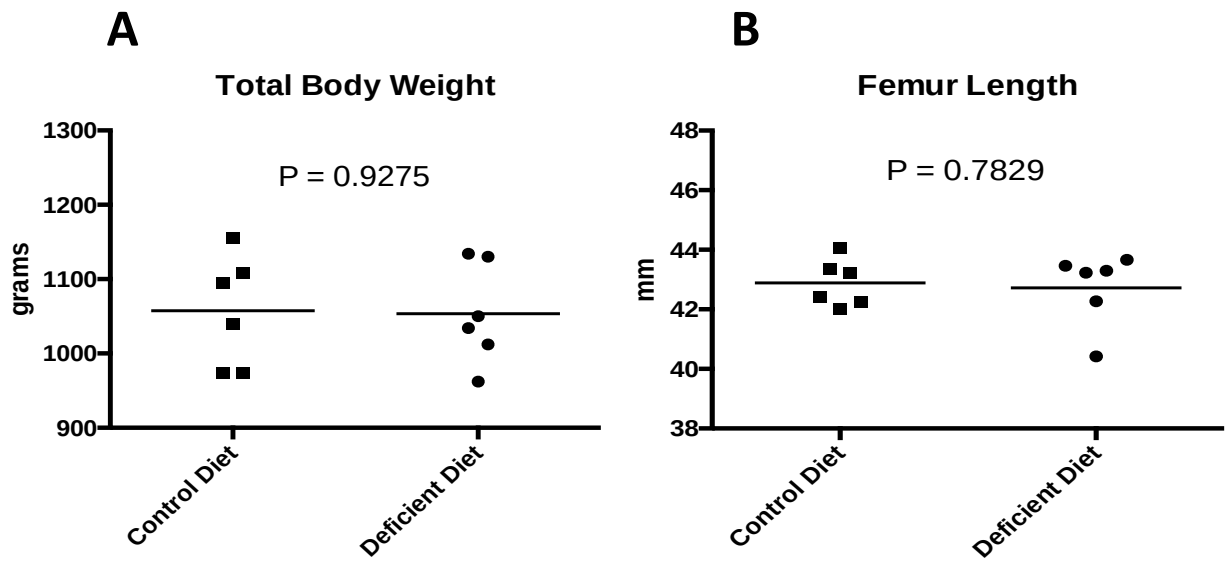

Figure 4.1 – Body weight and femur lengths in iron deficient diet study. Total body weight (A) and femur length (B) for control diet and iron deficient diet animals. Black line represents mean value.

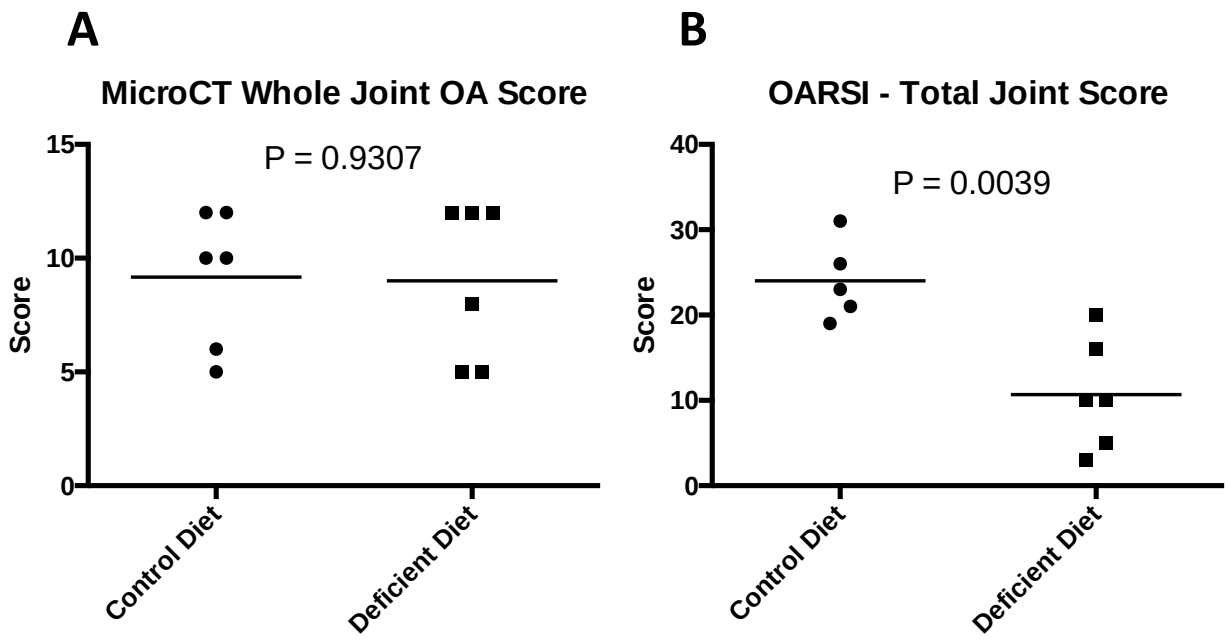

Figure 4.2 – MicroCT and OARSI histologic OA scores in the iron deficient diet study. MicroCT whole joint OA score (A) and histologic OA score (B) for control diet and iron deficient diet groups. Black line represents mean value.

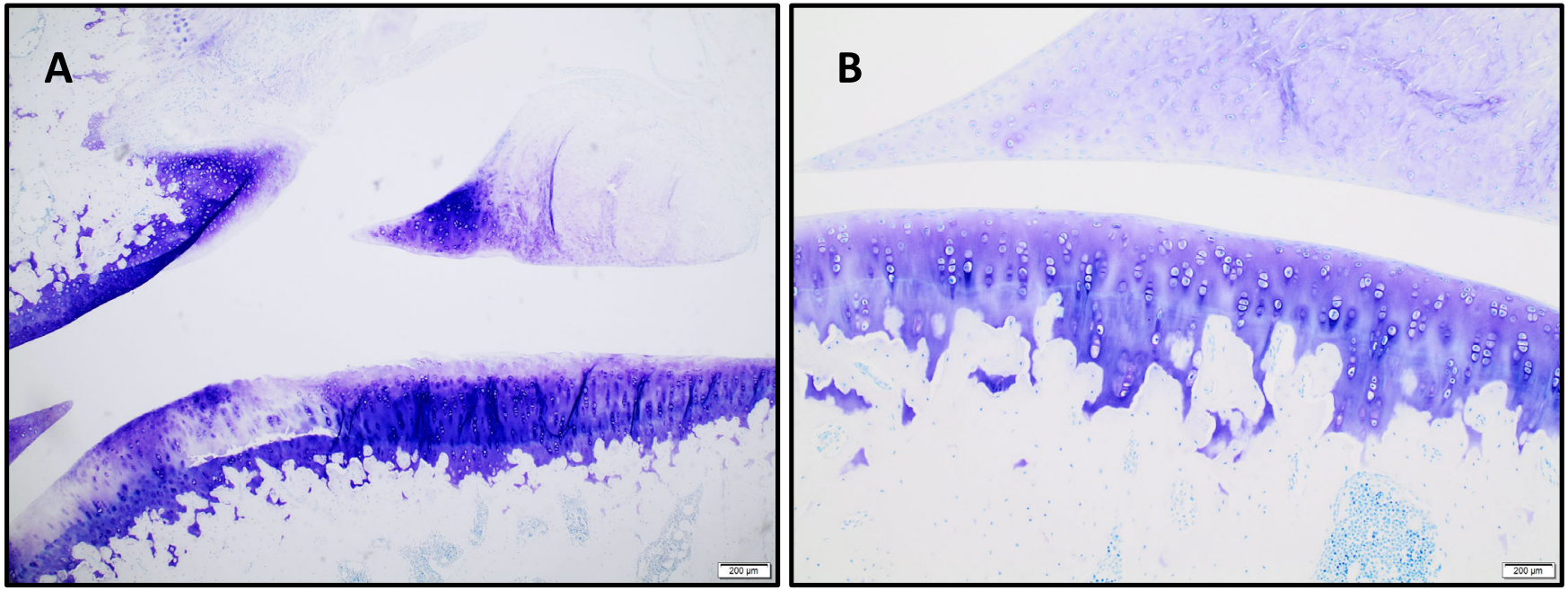

Figure 4.3 – Example photomicrographs of histologic OA lesion in the iron deficient diet study. Toluidine blue stained photomicrographs of medial compartment. A) Representative photomicrograph from an animal in the control diet group (Medial compartment OARSI score of 16). B) Representative photomicrograph from an animal in the iron deficient diet group (Medial compartment OARSI score of 6).

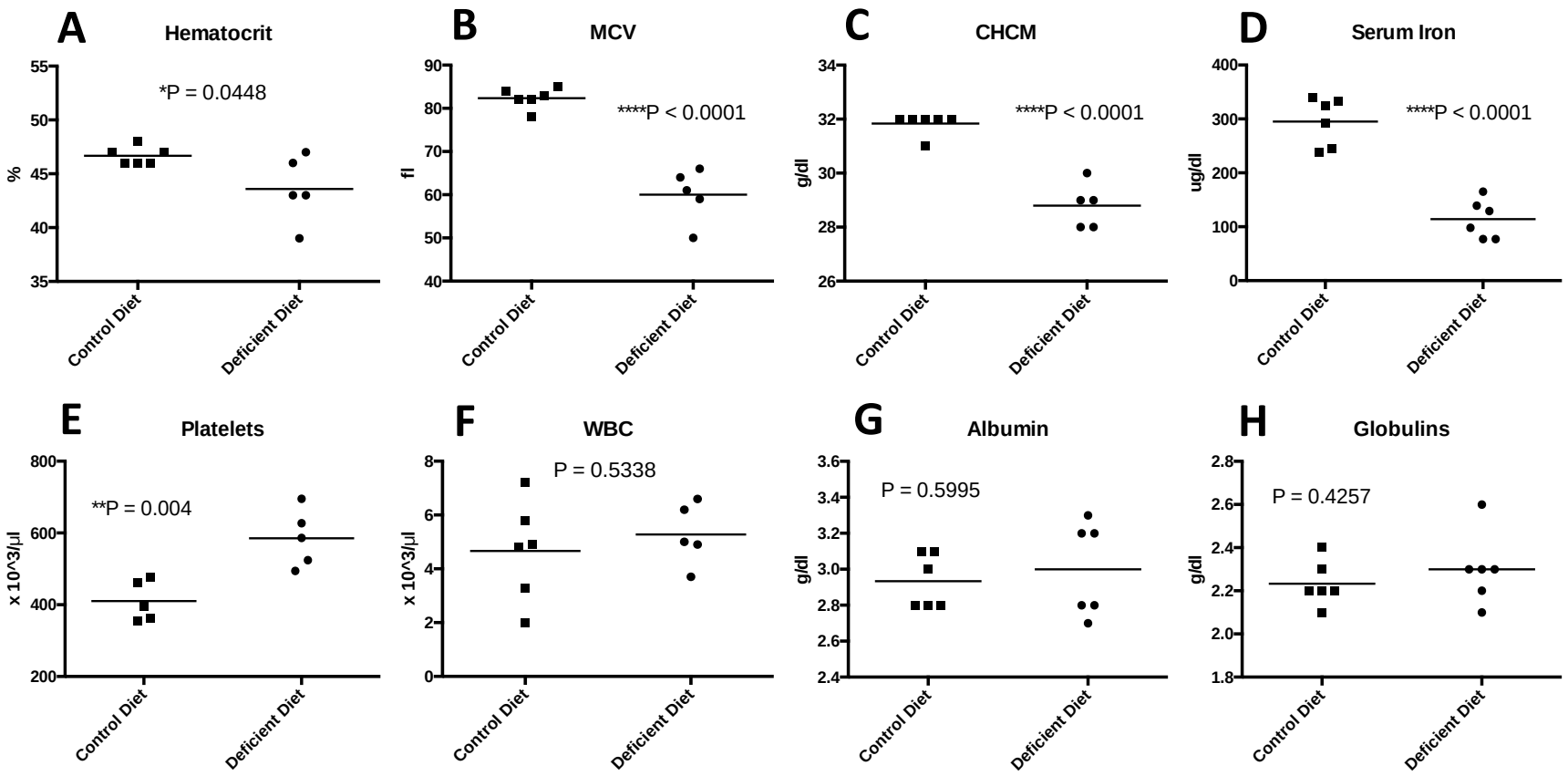

Figure 4.4 – CBC and biochemistry values from the iron deficient diet study. Select CBC and serum biochemical values from control diet and iron deficient diet groups. A) hematocrit, B) mean red blood cell volume, C) cellular hemoglobin concentration mean, D) serum iron, E) platelet count, F) white blood cell count, G) serum albumin, and H) serum globulins. Black line represents mean value.

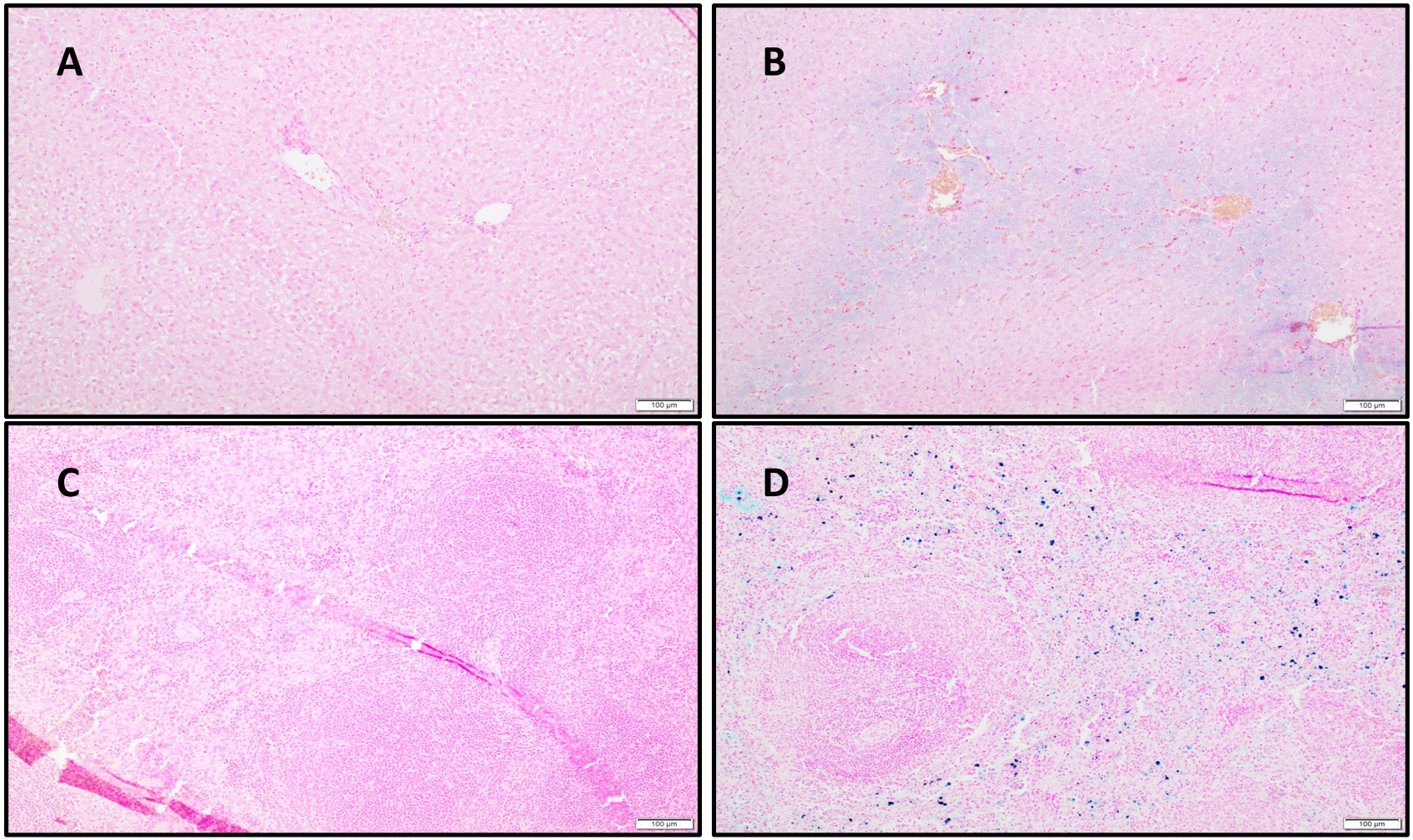

Figure 4.5 – Perl's Prussian blue photos from liver and spleen in iron deficient diet study. Representative Prussian blue photos from A) liver from an animal in the iron deficient diet group, B) liver from an animal in the control diet group, C) spleen from an animal in the iron deficient diet group, and D) spleen from an animal in the control diet group.

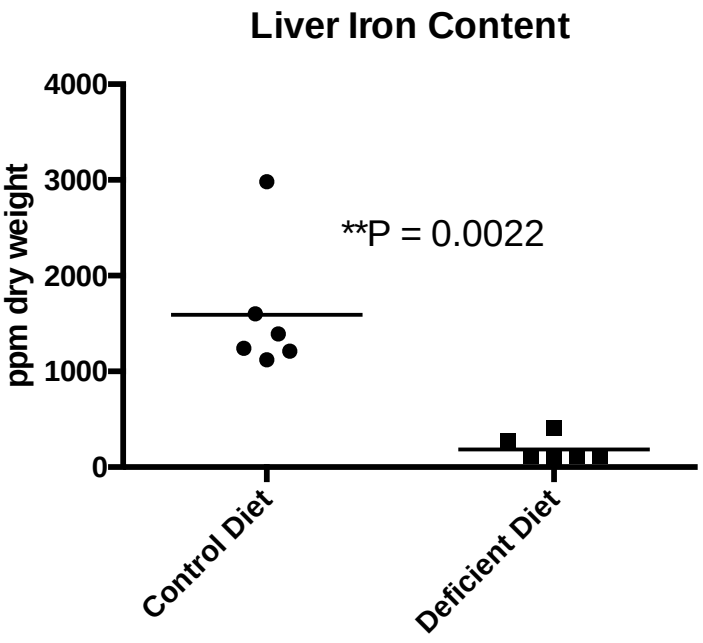

Figure 4.6 – Quantitative liver iron content in iron deficient diet study. Iron content reported as parts per million dry weight of liver in the A) control diet group, and B) iron deficient diet group. Black line represents mean value.

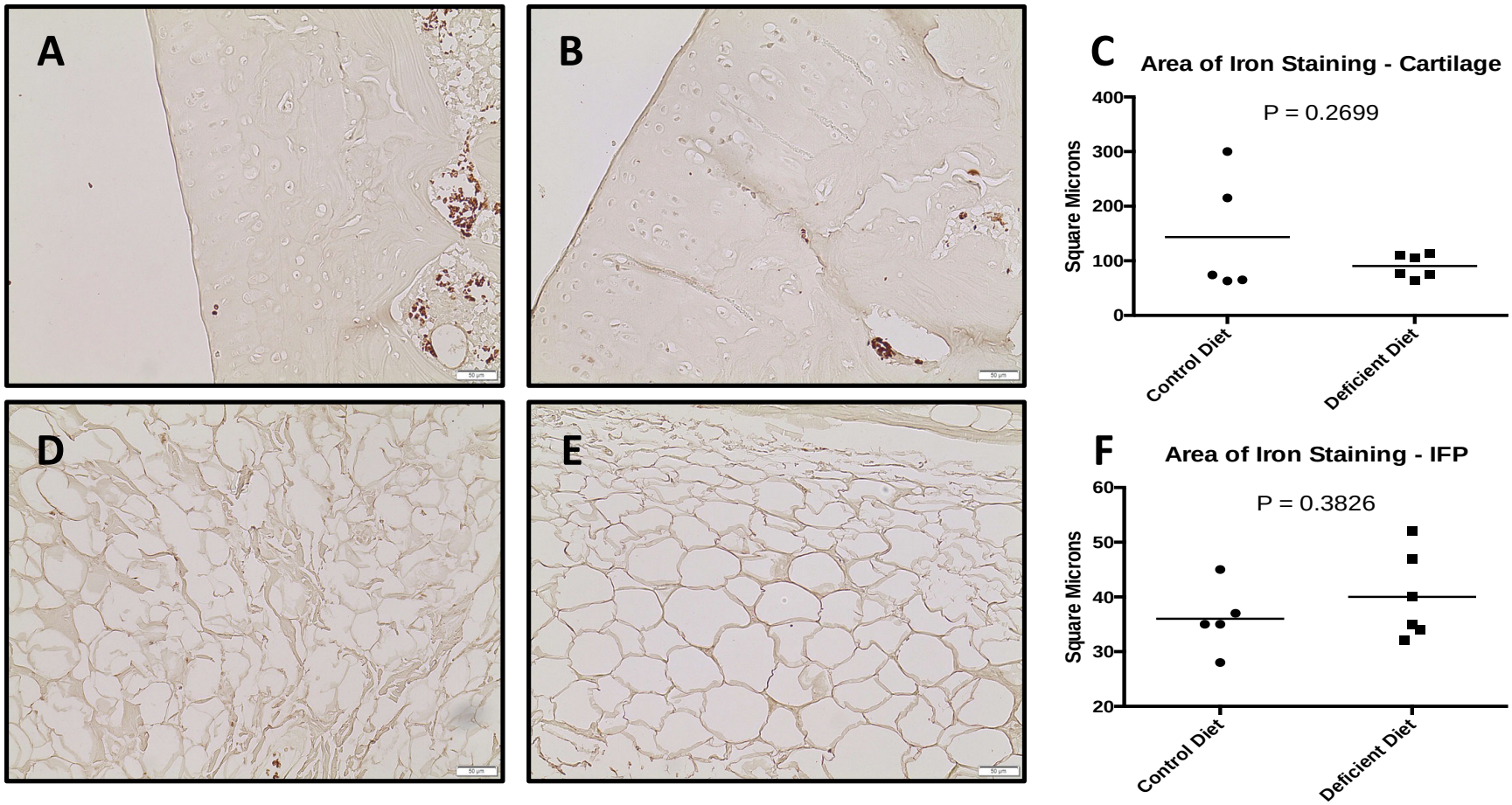

Figure 4.7 – Enhanced iron staining of knee joints in the iron deficient diet study. Iron staining in the cartilage of a control diet animal (A), cartilage of an iron deficient diet animal (B), IFP of a control diet animal (D), and IFP of an iron deficient diet animal (E). Area of iron staining in the cartilage (C) and IFP (D).

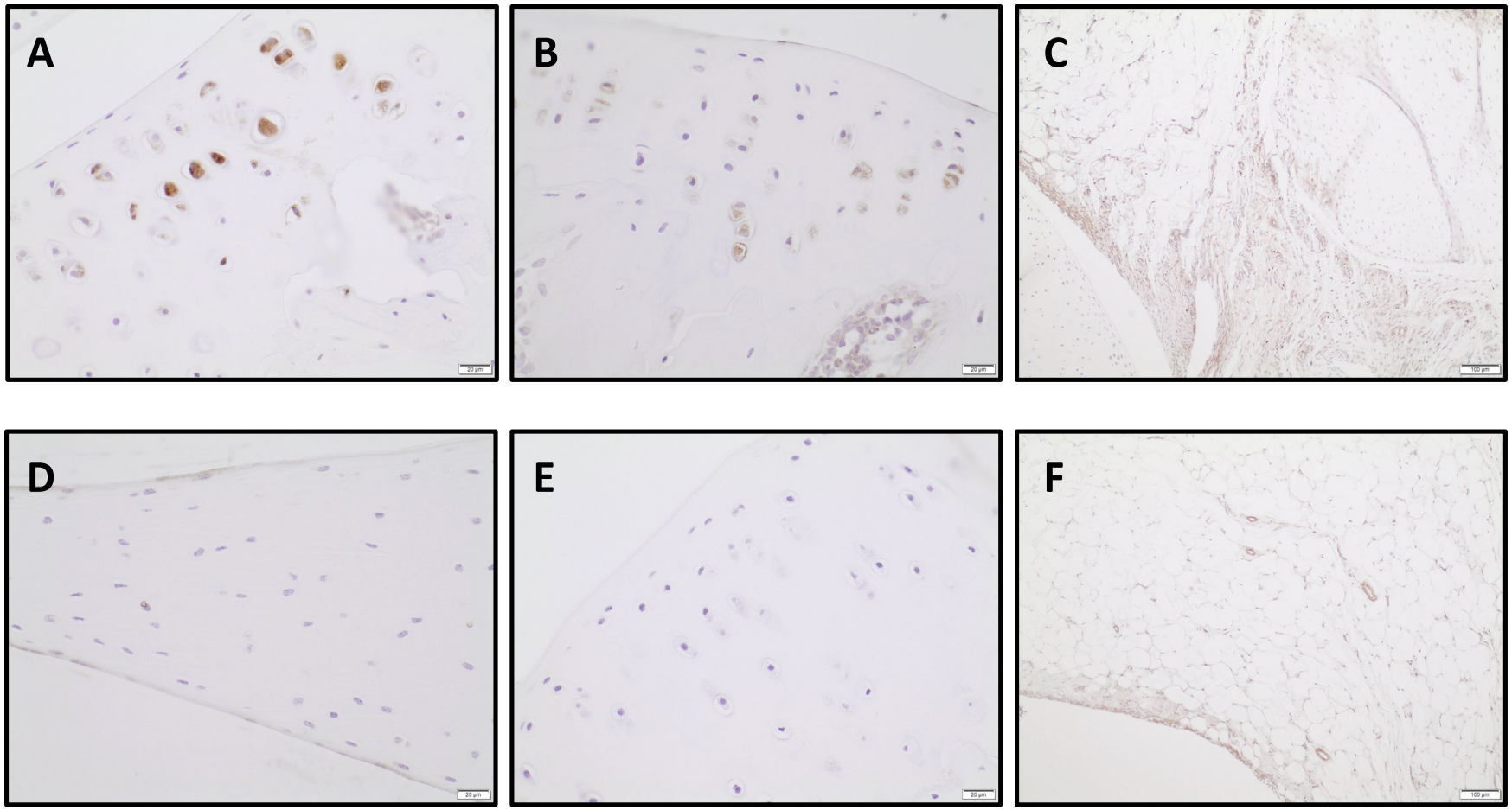

Figure 4.8 – 4-hydroxynonenal immunohistochemistry of knee joint in iron deficient diet study. 4HNE immunostaining in control diet meniscus (A), tibial cartilage (B), and IFP and synovium (C). 4HNE immunostaining in iron deficient diet meniscus (D), tibial cartilage (E), and IFP and synovium (F).

CHAPTER 5

THE INFRAPATELLAR FAT PAD MAY SERVE AS A LOCAL IRON DEPOT AND ITS REMOVAL IMPROVES OSTEOARTHRITIS LESIONS IN THE HARTLEY GUINEA PIG

5.1 Introduction.

Primary osteoarthritis (OA), especially that affecting the knee joint, afflicts over 273 million people across the globe[97]. Due to pain and negative effects on range of motion, knee joint OA contributes to decreased quality of life[98]. Although aging is the biggest factor associated with primary OA, specific mechanisms contributing to development of primary OA remain poorly elucidated, and there are no treatments available that can restore damaged cartilage[185]. Thus, over one million people in the U.S. undergo total knee replacement surgery each year[186], costing over $200 billion to Americans[13]. This reflects a void in the current understanding of this debilitating disease.

The knee joint is composed of many structures, including the distal femur, proximal tibia, the patella and its tendon, cartilage, synovium, menisci, synovial fluid, fat pads, blood vessels, and nerves. Adipose depots present in the knee joint include the infrapatellar fat pad (IFP), the posterior knee fat pad, the quadriceps fat pad, and the pre-femoral fat pad[47]. The IFP is the largest of these and is found in the anterior aspect of the joint in the space shaped by the patella, femoral condyles, and tibial plateau (Figure 5.1). In spite of its bulk, the exact functions of the IFP are not completely understood. The main role of the IFP is thought to be in facilitating distribution of synovial fluid across the knee joint, thereby providing lubrication[44–46]. It also likely provides shock absorbance from mechanical forces and knee joint stability[46]. Despite this

uncertainty, the IFP is considered a player in overall knee joint homeostasis and there is evidence to support its role in the pathogenesis of knee joint OA[41,44–47,157–161].

The IFP is comprised of a network of adipocytes, fibroblasts, leukocytes (primarily macrophages and lymphocytes), and collagen matrix[44,47]. As such, it is poised to be a source of inflammatory mediators that may contribute to OA[41,45–47,53,157–161]. A human study demonstrated that IFP-derived adipocyte conditioned media induced a pro-inflammatory response in T lymphocytes that resulted in increased proliferation and cytokine production[187]. In addition, Distal *et al.* have shown that interleukin (IL)-6 secretion from the IFP of women with knee OA was more than twice that of subcutaneous thigh fat[161].

Iron is emerging as a key player in numerous chronic disease processes associated with aging. This is due to a progressive and insidious accumulation of iron within tissues over time, promoting oxidant injury and subsequent tissue inflammation and damage[85]. While iron plays an established role in arthropathies associated with hereditary hemochromatosis[89], rheumatoid arthritis[88,89], and hemophilic arthropathy[90], its potential role in the pathogenesis of primary osteoarthritis is a relatively unexplored niche. One human study reported higher serum ferritin levels in men with knee joint OA than healthy controls. Additionally, the authors found a 4-fold increased risk of radiographic OA in men with high serum ferritin concentrations[168]. Another human study discovered increased levels of ferritin within the synovial fluid in patients with OA compared to controls[93]. These studies provide intriguing evidence that iron may be an important, yet overlooked, player in the pathogenesis of spontaneous OA.

While the source of iron within the knee joint is uncertain, adipose tissue can act as storage depots for iron. In the face of inflammation, macrophages within adipose tissue lose the ability to properly handle iron, and may consequently become iron overloaded[162]. Thus, we were

curious to determine if the IFP may serve as a local knee joint tissue depot that may store iron, thus contributing to development of disease. The aims of this study were three-fold: 1) determine if the IFP serves as an iron depot, and 2) investigate inflammatory and iron-related gene expression profiles of the IFP, and 3) assess disease outcome after surgical removal of the IFP. We employed the Hartley guinea pig for this study, as it is a valuable rodent model of spontaneous disease, with histopathologic lesions similar to those seen in people[60]. We hypothesize that the IFP does, indeed, act as a local iron depot within the knee joint and that, by surgically removing it, we may improve OA outcomes by eliminating a source of oxidant damage and inflammatory mediators.

5.2 Materials and Methods.

Animals.

All procedures were approved by the university's Institutional Animal Care and Use Committee and were performed in accordance with the NIH Guide for the Care and Use of Laboratory Animals. Two sets of male Dunkin-Hartley guinea pigs were purchased for this study. The first set of animals was comprised of thirty male Dunkin-Hartley guinea pigs (n=6 per age group) purchased from a commercial vendor (Charles River Laboratories, Wilmington, MA) at specified ages and maintained at Colorado State University's Laboratory Animal Resources housing facilities. Ages purchased were: 2 months (pre-OA), 3 months (OA onset), 5 months (early OA), 9 months (moderate OA), and 15 months (severe OA). These animals were used to determine cross-sectional changes in gene expression and histologic morphology within the IFP over time and during the development of OA.

The second part of the study investigated how surgical removal of the IFP influenced development of OA. For this study, seventeen male Dunkin-Hartley guinea pigs were purchased at 8 weeks of age. Surgery was performed at 12 weeks of age, as described below. All animals were monitored daily by a veterinarian. Guinea pigs were housed individually in solid bottom cages and fed *ad libitum* food and water.

Removal of the infrapatellar fat pad.

Removal of the IFP was performed on seventeen 12-week old animals. Both knees were prepared for sterile surgery. After medial parapatellar arthrotomy of the right knee, the patella was luxated laterally, permitting access to the femoral groove. A single incision was made in the joint capsule just medial to the patellar tendon, allowing access to, and full removal of, the IFP (Figure 5.1). The patella was repositioned and the skin incision closed. An identical sham procedure, without removal of the IFP, was performed on the left knee and served as an internal control for each animal.

Specimen collection.

Two, 3, 5, 9, and 15-month-old animals (age group animals) were harvested at these ages as they arrived to CSU. The IFP removal animals were harvested at 7 months of age. Body weights were recorded at time of harvest and animals were then anesthetized with a mixture of isoflurane and oxygen. Thoracic cavities were opened and blood was collected with 20-gauge butterfly catheter via direct cardiac puncture. Animals were immediately transferred to a carbon dioxide chamber for euthanasia. Hind limbs were removed at the coxofemoral joint. For the IFP removal animals, both limbs were placed into 10% neutral buffered formalin for 48 hours and

then transferred to PBS for microcomputed tomography (microCT) analysis. For the age group animals, only the left limb was placed into formalin. Prior to microCT imaging, femur length was measured using calipers. After microCT, limbs were transferred to a 12.5% solution of ethylenediaminetetraacetic acid (EDTA) at pH 7 for decalcification. EDTA was replaced twice weekly for 6 weeks.

For the age group animals, the right hind limb was also removed at time of harvest. On this limb, the knee joint was exposed by dissecting through the quadriceps muscles and reflecting the patella distally. The IFP was removed from the patellar tendon and placed in All Protect Tissue Reagent (Qiagen) for future gene expression analysis. Using a scalpel, cartilage was scraped from the patella, tibial plateau, femoral condyles, and femoral groove and placed into RNALater (Qiagen) for gene expression analysis. Menisci were also removed and placed into RNALater along with the cartilage.

Evaluation of OA via microCT and histologic grading of knee joints.

Knee joints were scanned in PBS using the Scanco microCT system (Scanco uCT80, Scanco Medical AG, Bruttisellen, Switzerland) with an isotropic voxel size of 18um. Clinical features of OA were scored by a veterinary radiologist using a whole joint grading scheme, as previously described[131]. After decalcification, three sagittal slices were made through each knee joint. Mid-sagittal slices were made for histologic evaluation of the IFP. Sagittal slices through the medial and lateral femoral condyles were made to assess OA changes in four sites: medial tibia, lateral tibia, medial femur, and lateral femur. Samples were paraffin embedded and a 5-micron section from each condyle was stained with Toluidine Blue for assessment of OA. Midsagittal sections were stained with H&E and Masson's trichrome stain. Medial and lateral

femoral condyles along with medial and lateral tibial plateaus, were scored using the recommended published guidelines[60]. This semiquantitative histopathologic grading scheme is based on articular cartilage structure, proteoglycan content, cellularity, and tidemark integrity. Scores were performed in a blinded fashion by two independent pathologists (LBR and KSS). Scores from each of the four anatomic locations were assessed separately. Scores for both the medial and lateral compartments were determined. In cases where proper sectioning allowed for scoring of all 4 sites, a total knee joint OA score was calculated for each guinea pig.

Complete blood count and serum biochemical profile.

At the time of harvest, a portion of blood collected via cardiac puncture was allocated to 0.5 mL EDTA microtubes for complete blood count (CBC). CBCs were performed at the Colorado State University (CSU) Clinical Pathology Laboratory using the Advia 120 hematology analyzer (Siemens, Munich, Germany) with instrument settings and software specifically designed for guinea pig samples. Blood films were manually reviewed, and a leukocyte differential count was performed by a veterinary clinical pathologist (LR). Remaining blood was placed in red top glass tubes, allowed to clot for 30 minutes, and then centrifuged at 5,000 x g for 15 minutes for serum collection. Serum was aliquoted to cryovials and stored at -80°C for serum protein C3 concentrations, which were measured using a commercially available ELISA kit (Abcam). One aliquot of serum was not frozen and submitted to the CSU Clinical Pathology Laboratory for serum biochemical analysis, including serum iron measurement, using the Roche Cobas 6000 (Basel, Switzerland).

Gene expression of the infrapatellar fat pad using NanoString technology.

Total RNA was extracted from IFP samples using an RNeasy Lipid Tissue Mini Kit (Qiagen) according to package instructions. RNA was quantified spectrophotometrically (Nanodrop ND-1000). A total of 250 ng of RNA, at a concentration of 20 ng/μl, was sent to NanoString Technologies. Probes were designed and synthesized by NanoString Technologies for the following genes of interest: monocyte chemotactic factor 1 (MCP-1), cyclooxygenase 2 (COX2), nuclear factor kappa B (NFkB), IL-6, ferritin heavy chain, superoxide dismutase 2 (SOD2), transferrin receptor 1 (TfR), divalent metal transporter 1 (DMT1), metal transporter ZIP14, and ferroportin. Housekeeping genes for data normalization included GAPDH and B-actin. Data analysis was performed using nSolver™ software provided by NanoString Technologies. Results, reported as absolute transcript counts, were normalized to positive controls and housekeeping genes.

Iron quantitation of the infrapatellar fat pad.

All IFPs were utilized for either gene expression or histologic analyses in the animals used in this study. Therefore, formalin-fixed IFP samples saved from previous, unrelated studies were used for iron quantitation. Samples from a group of young, 2-month-old animals (n=11) and from a group of 15-month-old animals (n = 18) were submitted to the CSU Toxicology Laboratory. Iron quantitation was performed via atomic absorption spectroscopy (AAS). Iron levels were reported as parts per million (ppm) dry weight.

Statistical analyses.

Data for total body weights, histologic OA scores, whole joint microCT OA scores, CBC and serum biochemical values, normalized NanoString mRNA absolute counts, and IFP iron AAS, were subjected to, and passed, normality testing via the Kolmogorov-Smirnov test. Data from the age group animals were compared using a one-way ANOVA with Tukey's post-hoc tests. Iron content in the IFP was compared using a t test. Histology and microCT OA scores from IFP removal and sham surgery limbs within each animal were compared using paired t tests. Statistical significance was set at $P < 0.05$. All statistical analyses were performed with GraphPad Prism (La Jolla, CA, USA).

5.3 Results.

General description of animals.

In the IFP aging aspect of this study, animals in each group gained weight as expected for males fed *ad libitum*, as previously reported[131]. In the IFP removal study, mean body weight at harvest was 952.6 grams (95% CI 846.4 – 1050). All animals in both studies appeared healthy throughout the duration of the study.

IFP iron content and Nanostring gene expression profile in aging guinea pigs.

To see if the IFP may serve as a local depot of iron within the knee joint, samples from two cohorts of guinea pigs were collected to measure iron content. IFPs were collected from 2-month-old animals, an age with minimal to no OA lesions, as well as from 15-month-old animals, an age with severe to end-stage disease. These animals were from work unrelated to the current project, but received no special treatments or interventions that may have altered iron

content within the joint. Iron content was significantly higher in the 15-month-old group. Mean iron content in this older group was 66.92 ppm (95% CI 55.64 – 78.19), while it was 47.01 (95% CI 30.31 – 63.71, P = 0.0355) in the younger group (Figure 5.2).

Within the aging groups, IFPs were collected for quantitative gene expression using Nanostring technology. Several genes for pro-inflammatory cytokines increased with age. Monocyte chemotactic protein-1 (MCP-1) was higher in the 9- and 15-month groups compared to the 2-month-old group (Figure 5.3, overall ANOVA P = 0.0120). Mean absolute mRNA count was 611.3 (95% CI 487.6 – 734.9) in the 9-month group, 567 (95% CI 419.2 – 714.8) in the 15-month group, and 286.7 (95% CI 186.5 – 387) in the 2-month group. Cyclooxygenase 2 (COX2) gene expression was higher in the 15-month-old group compared to the 2-month-old group (Figure 5.3, overall ANOVA P = 0.0232). Mean absolute mRNA count was 71.27 (95% CI 24.53 – 118) in the 15-month group and 25.35 (95% CI 16.65 – 34.04) in the 2-month group. Expression of the transcription factor nuclear factor kappa B (NFkB) was higher in the 15-month group compared to both 2- and 3-month-old animals (Figure 5.3, overall ANOVA P = 0.0252). Mean absolute mRNA count was 210.2 (95% CI 180.5 – 240) in the 15-month group, 161.4 (95% CI 123.7 – 199) in the 2-month group, and 161.9 (95% CI 141.2 – 182.5) in the 3-month group. Expression of interleukin-6 (IL-6) was higher in the 9-month-old group compared to 2- and 3-month-old animals (Figure 5.3, overall ANOVA P = 0.0080). Mean absolute mRNA count was 79.9 (95% CI 56.93 – 102.9) in the 9-month group and 15.04 (95% CI 8.549 – 21.54) and 27.39 (95% CI 3.439 – 51.33) in the 2- and 3-month groups, respectively.

In concert with these increases in inflammatory genes was increased expression of the iron storage protein ferritin. Ferritin expression was significantly higher in the 9-month-old group compared to the 2-month-old animals (Figure 5.4, overall ANOVA P = 0.0092). Mean

ferritin absolute mRNA count was 15,610 (95% CI 13,333 – 17,888) in the 2-month-old group and 22,771 (95% CI 18,150 – 27,393) in the 9-month-old group. Furthermore, expression of superoxide dismutase 2 (SOD2), an antioxidant that is upregulated in the presence of oxidant damage, was increased in the 9- and 15-month-old animals compared to the younger age groups (Figure 5.4, overall ANOVA P = 0.0016). Mean absolute mRNA count was 1,699 (95% CI 1,329 – 2,068), 3,451 (95% CI 1,846 – 5,056), 3,228 (95% CI 1,759 – 4,696), 4,268 (95% CI 2,552 – 5,985), and 5,557 (95%CI 3,947 – 7,167) in the 2-, 3-, 5-, 9-, and 15-month-old groups, respectively.

To examine iron trafficking within the IFP, as this is an unexplored topic, gene expression of several major iron import and export proteins was examined. While there was a significant decrease in TfR expression noted in the 9-month-old group compared to the 2-month-old group, this seems to be driven primarily by a single animal. (Figure 5.5, overall ANOVA P = 0.0184). Interestingly, expression of divalent metal transporter 1 (DMT1) was significantly increased in the 15-month-old group compared to 3-, 5-, and 9-month-old animals (Figure 5.5, overall ANOVA P = 0.0075). Mean absolute mRNA count was 291.5 (95% CI 212.9 – 370.1) in the 15-month group. Mean counts were 217.4 (95% CI 202.9 – 231.9), 212.7 (95% CI 192.6 – 232.9), and 196.4 (95% CI 157.7 – 235.1) in the 3-, 5-, and 9-month-old groups, respectively. Expression of Zip14 also increased steadily with age, with significant differences noted between 2- and 5-months, 2- and 15-months, and 3- and 15-months of age (Figure 5.5, overall ANOVA P = 0.0024). Mean absolute mRNA count was 214.4 (95% CI 128.5 – 300.3) in the 15-month group, 66.53 (95% CI 60.0 – 73.06) in the 2-month group, 109.2 (95% CI 37.61 – 180.8) in the 3-month group, and 183.0 (95% CI 115.5 – 250.4) in the 5-month group. Expression of ferroportin (FPN), the only known iron export protein, was significantly higher in the 15-month-

old group compared to all other age groups (Figure 5.5, overall ANOVA P = 0.0001). Mean absolute mRNA count was 668 (95% CI 511.5 – 824.6) in the 2-month group, 558.2 (95% CI 453.8 – 662.7) in the 3-month group, 574.8 (95% CI 436.3 – 713.3) in the 5-month group, 650 (95% CI 493.8 – 806.4) in the 9-month group, and 1,125 (95% CI 685.4 – 1,566) in the 15-month group.

Serum protein C3 levels in aging guinea pigs.

Routine CBC and serum biochemical profiles did not yield any significant differences among the age groups. Because increased levels of systemic inflammation were suspected in the older animals with more advanced OA, serum protein C3 levels were measured. Serum protein C3 is a more sensitive marker for inflammation than total white blood cell counts[188]. Serum protein C3 levels were higher in the 9- and 15-month-old groups compared to 2-, 3-, and 5-month-old animals (Figure 5.6). Mean serum C3 was 557.3 μg/ml (95% CI 412.1 – 702.4) in the 2-month group, 580.8 μg/ml (95% CI 483.5 – 678.2) in the 3-month group, 467.0 μg/ml (95% CI 385.6 – 548.3) in the 5-month group, 794.5 μg/ml (95% CI 692.3 – 896.8) in the 9-month group, and 738.2 μg/ml (95% CI 522.2 – 954.2) in the 15-month group.

MicroCT and histologic OA scores in IFP removal animals.

In the aging study, both microCT and histologic scores increased at each time point, as expected and previously reported[131]. For the IFP removal portion of the study, microCT and histologic OA scores were compared between the right limb with the IFP removed and the left limb that underwent sham surgery without IFP removal. In all 17 animals, microCT OA scores were improved in the IFP removal limbs compared to the contralateral sham limbs (Figure 5.7).

Ten of the animals had microCT OA scores of zero in the IFP removal limb at time of harvest. Mean microCT OA score in the IFP removal limbs was 1.4 (95% CI 0.4 – 2.5) while it was 6.5 (95% CI 5.1 – 7.9) in the sham limb ($P < 0.0001$). Histologic OA scores were primarily driven by pathology in the medial tibia (Figure 5.7). Mean OA score in the medial tibia was 1.3 (95% CI 0.69 – 1.9) in the IFP removal limb and 7.2 (95% CI 4.9 – 9.5) in the sham limb ($P < 0.0001$). Similar findings were noted in the medial compartment score (combining medial tibia and medial femur) and whole joint score (data not shown). Scores were not statistically different in the lateral compartment. Examples of histologic lesions are shown in Figure 5.8. Upon histologic examination using routine H&E staining, the area of the IFP appeared to have been replaced by a thick band of dense fibrous connective tissue (Figure 5.9). Masson's trichrome stain was used to confirm the collagenous nature of this tissue (Figure 5.9).

5.4 Discussion.

This is the first study to examine iron in the IFP in aging Hartley guinea pigs as they develop spontaneous OA. This study also firmly establishes the IFP's role in the development of OA, as its removal resulted in unprecedented delayed onset of disease in this animal model. This work highlights the need for continued exploration into unexplored mechanisms, such as progressive iron accumulation, as contributors to OA pathogenesis. The impetus for this study stemmed from our preliminary results showing a higher iron content within the IFP in aged Hartley guinea pigs with severe knee joint OA compared to young animals prior to the onset of disease. While the specific mechanisms behind this phenomenon are unclear, we pose that iron accrues within this adipose depot with age and, thus, contributes to local oxidant damage and inflammation within the knee joint.

Gene expression data collected for this study offer intriguing insights into how the IFP may contribute to development of knee joint OA. Several pro-inflammatory mediators (MCP-1, COX2, IL-6, and NFkB) exhibited increased gene expression in the IFP with increasing age. Most differences were noted in the 9- and 15-month age groups when compared to the 2-month group. A recent study examining IFPs removed from patients undergoing total knee replacement surgery compared to non-OA controls demonstrated increased protein expression of both MCP-1 and IL-6 via immunohistochemistry in the IFPs from OA patients[189]. Another study found increased gene expression of COX2 in IFPs removed from patients with radiographic knee OA[190].

Along with the increased IFP iron content in aged guinea pigs and inflammatory gene expression data, serum protein C3 levels also increased with age. Protein C3, a complement protein, is a sensitive acute phase protein in the guinea pig[188]. These results indicate that increasing IFP iron content corresponds to increasing levels of systemic inflammation as well as increased inflammation and oxidant damage locally in the knee joint.

Along with the higher mRNA transcript counts and systemic circulation of a pro-inflammatory mediator, there was also increased expression of ferritin and SOD2. Ferritin, an iron storage protein, is synthesized when cytoplasmic iron levels increase in an attempt to sequester iron in a non-labile form[191]. Likewise, SOD2, a mitochondrial antioxidant, is produced in response to high levels of intracellular oxidants[192]. Taken together, these results suggest that both iron and subsequent free radical species are present at increased levels in the IFP of older guinea pigs with severe OA.

As iron trafficking within the IFP has never been explored, we evaluated gene expression data for key iron transport proteins. Because of its ability to produce free radicals, iron is tightly

regulated at many levels, including how it is transported in the blood and into cells. Most iron in the circulation is bound to the serum protein transferrin. The transferrin-iron complex binds to TfR on the cell surface to enter the cell via endocytosis. Once inside the cell, iron is released from TfR and can enter the cell cytoplasm, while TfR is recycled to the cell surface[193]. This method of iron entry is well-described and occurs in many cell types in the body. Interestingly, there was no significant changes in gene expression of TfR in the IFP with age. This may suggest that TfR-mediated entry does not play a major role in IFP iron accumulation over time.

Despite the fact that most circulating iron is tightly bound to TfR, there is a small portion that circulates more freely. This fraction is often referred to as non-transferrin-bound iron (NTBI) and is readily taken up by many cell types[194]. In recent years, NTBI has been implicated in pathological iron uptake, contributing to neurodegenerative disorders[195,196], diabetes mellitus[197], and chronic renal failure[198]. Two major proteins have been identified that allow NTBI to enter cells: DMT1 and ZIP14. In the current study, gene expression of DMT1 sharply increased at 15 months of age while ZIP14 expression exhibited a steadier increase in expression over time. These results indicate that DMT1 and ZIP14 may be contributing to iron accumulation in the IFP with age, thus directly contributing to disease onset and/or progression. Expression of ferroportin, the only identified iron exporter, demonstrated increased expression at 15 months of age. This suggests a need for cellular iron removal, providing indirect evidence that IFP iron content is increased in this age group. Protein expression is needed to further characterize these changes in gene expression. Because ZIP14 expression starts increasing at an age before OA is severe, blockade of this receptor should be explored as a potential therapeutic target.

Data from the aging portion of this study provides tantalizing data to implicate that the IFP may serve as a local depot for both iron and inflammatory mediators. Given this, we then

hypothesized that removal of the IFP may be beneficial to OA by eradicating this source of detrimental iron and inflammation. Results of this study demonstrate that surgical removal of the IFP coincident with the onset of disease significantly decreased short-term progression of OA in the Hartley guinea pig. Based on clinical microCT OA scores, ten animals had no bony lesions associated with OA. This is remarkable given that scores are expected to be moderate at this age (7 months) in the OA-prone Hartley guinea pig based on previous work in our lab. Scores in the limb that received the sham surgery were often higher than expected for this age group, suggesting the surgery itself incited pathology, possibly due to presence of damage associated molecular patterns and heme iron in the joint following surgery. Benefits of IFP removal overcame these negative effects associated with surgery, alone.

Histologic examination of the knee joints revealed that this improvement in OA may be related to the development of a thick band of fibrous connective tissue in the space previously occupied by the IFP. There are two explanations that may explain these findings. First, the removal of the IFP abrogated a critical source of detrimental inflammatory mediators and iron in the knee not subsequently provided by the fibrous connective tissue. Secondly, the development of the fibrous connective tissue in place of a comparatively lax IFP provided enhanced biomechanical stability to the joint. *Ex vivo* work performed on cadavers revealed that resection of the IFP decreased tibial rotation of the knee[199]. From this, the authors extrapolated that the IFP may play a role in dictating the range of motion of the knee joint[199]. Future studies will incorporate extensive biomechanical testing to explore the possibility that the fibrous connective tissue offers increased joint stability compared to the IFP.

Considerations that should be noted in regards to the current study include assessment of only male animals and the short-term timeline in the course of OA development. Examining

effects of IFP removal at additional time points is needed to dissect the long-term benefit of IFP removal on knee health. Further, it is necessary to consider both sexes in continued work. It is not known if anti-inflammatory and increased stability benefits will hold true in a long-term scenario. In spite of this, we have still achieved an unprecedented delay of OA onset and progression in the Hartley guinea pig model. In conclusion, we have demonstrated that iron content in the IFP increases with age in the Hartley guinea pig and that this is associated with changes in gene expression that implicate the uptake of NTBI. Additionally, we have firmly established that the IFP plays a major role in onset and progression of primary OA, potentially by ridding the joint of an iron depot. Continued efforts into this area of research are needed and may alter treatment paradigms for patients predisposed to OA.

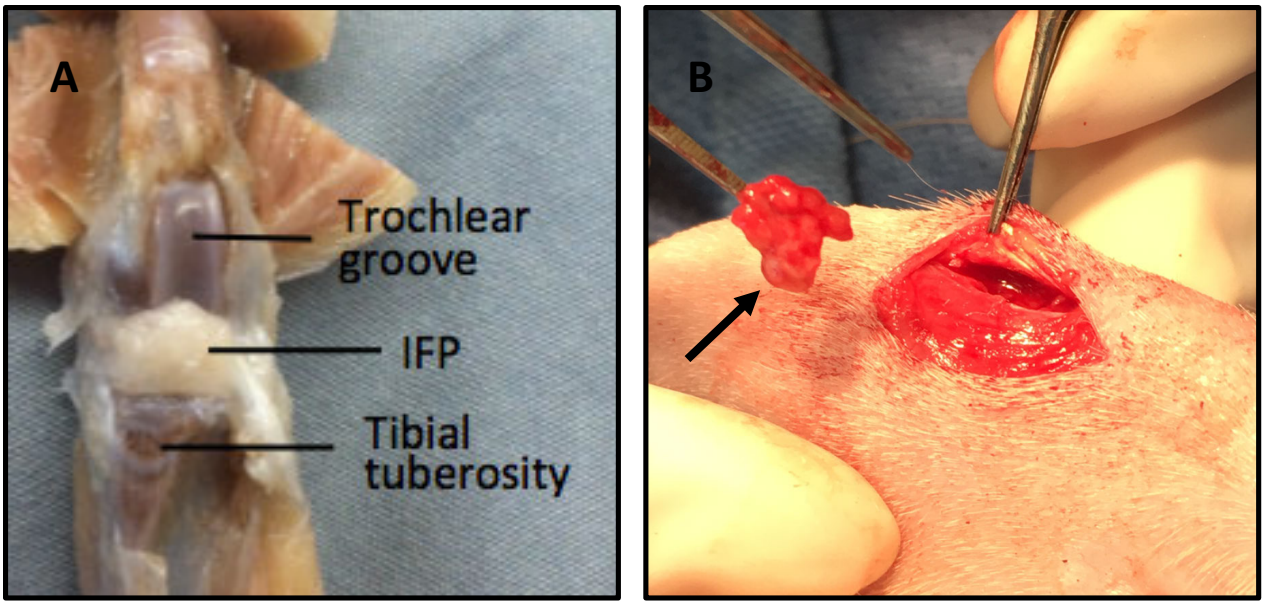

Figure 5.1 – Images of a guinea pig knee joint and IFP removal surgery. A) Photograph of a dissected guinea pig knee joint. The patella has been removed and reflected distally to showcase the IFP. B) Photo of IFP (arrow) after its removal during surgery.

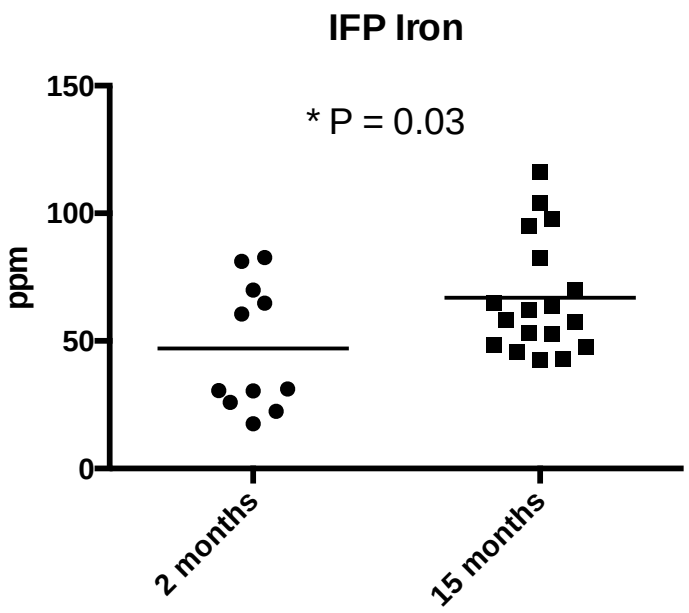

Figure 5.2 – Quantitative iron content in the IFP. Iron content, measured by atomic absorption spectroscopy, in the IFP in 2 month old guinea pigs compared to 15 month old animals.

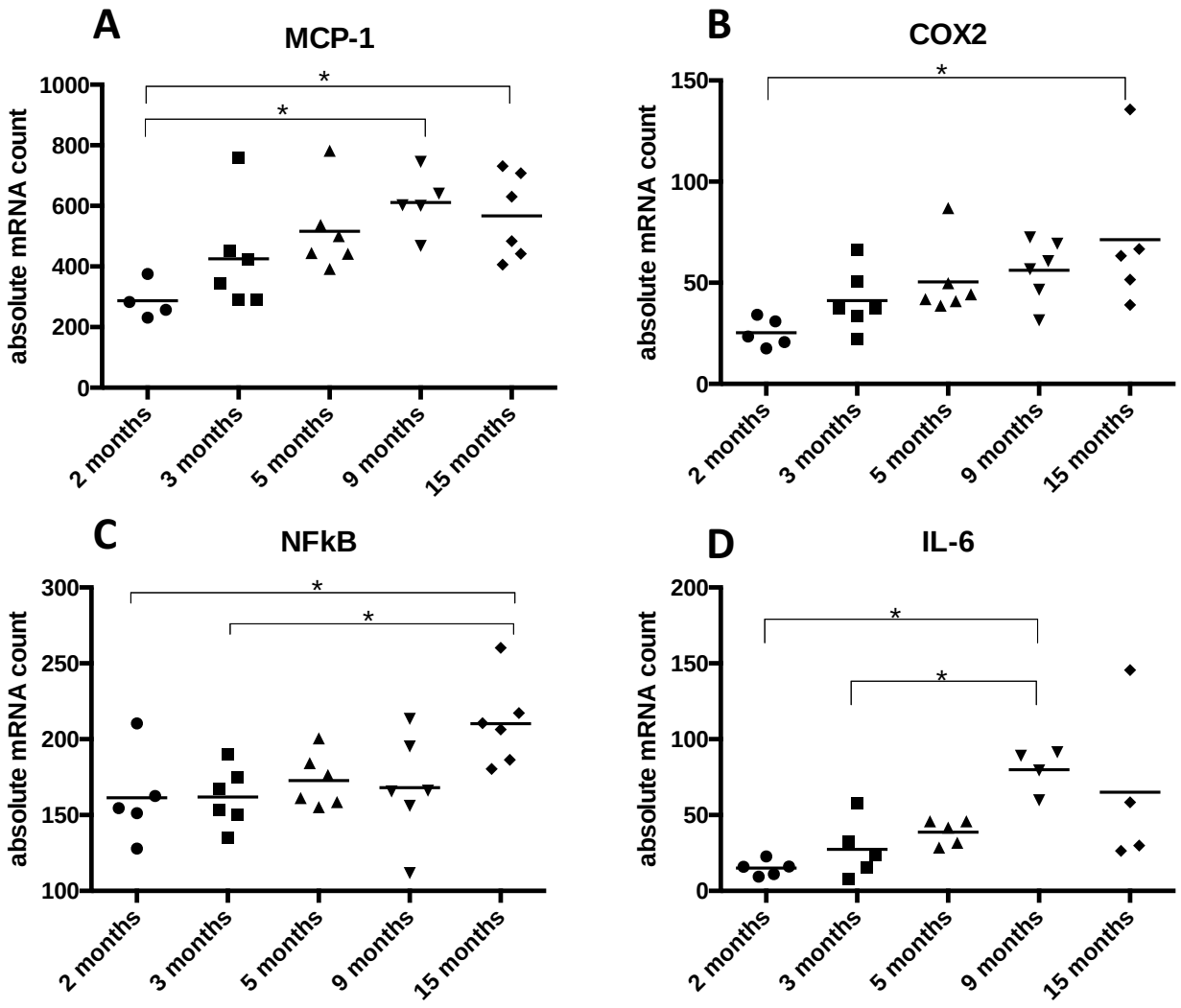

Figure 5.3 – Gene expression of pro-inflammatory mediators. Nanostring gene expression via absolute mRNA transcript count for MCP-1 (A), COX2 (B), NFkB (C), and IL-6 (D). Horizontal black line represents mean value. * $P \leq 0.05$.

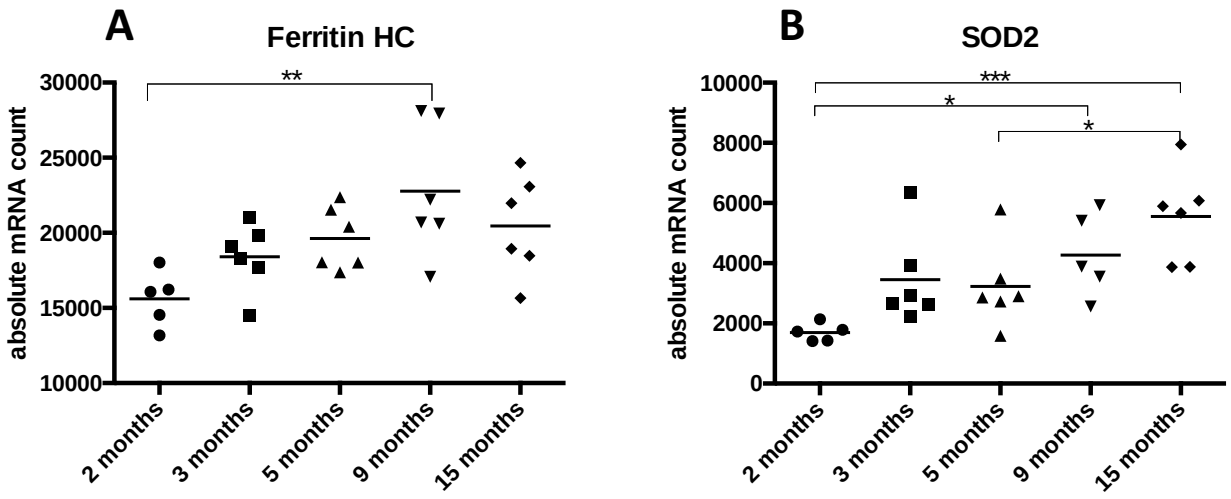

Figure 5.4 – Gene expression for iron storage and oxidant damage markers. Nanostring gene expression via absolute mRNA transcript count for ferritin heavy chain (A), and SOD2 (B). Horizontal black line represents mean value. * $P \leq 0.05$, ** $P \leq 0.01$, *** $P \leq 0.001$.

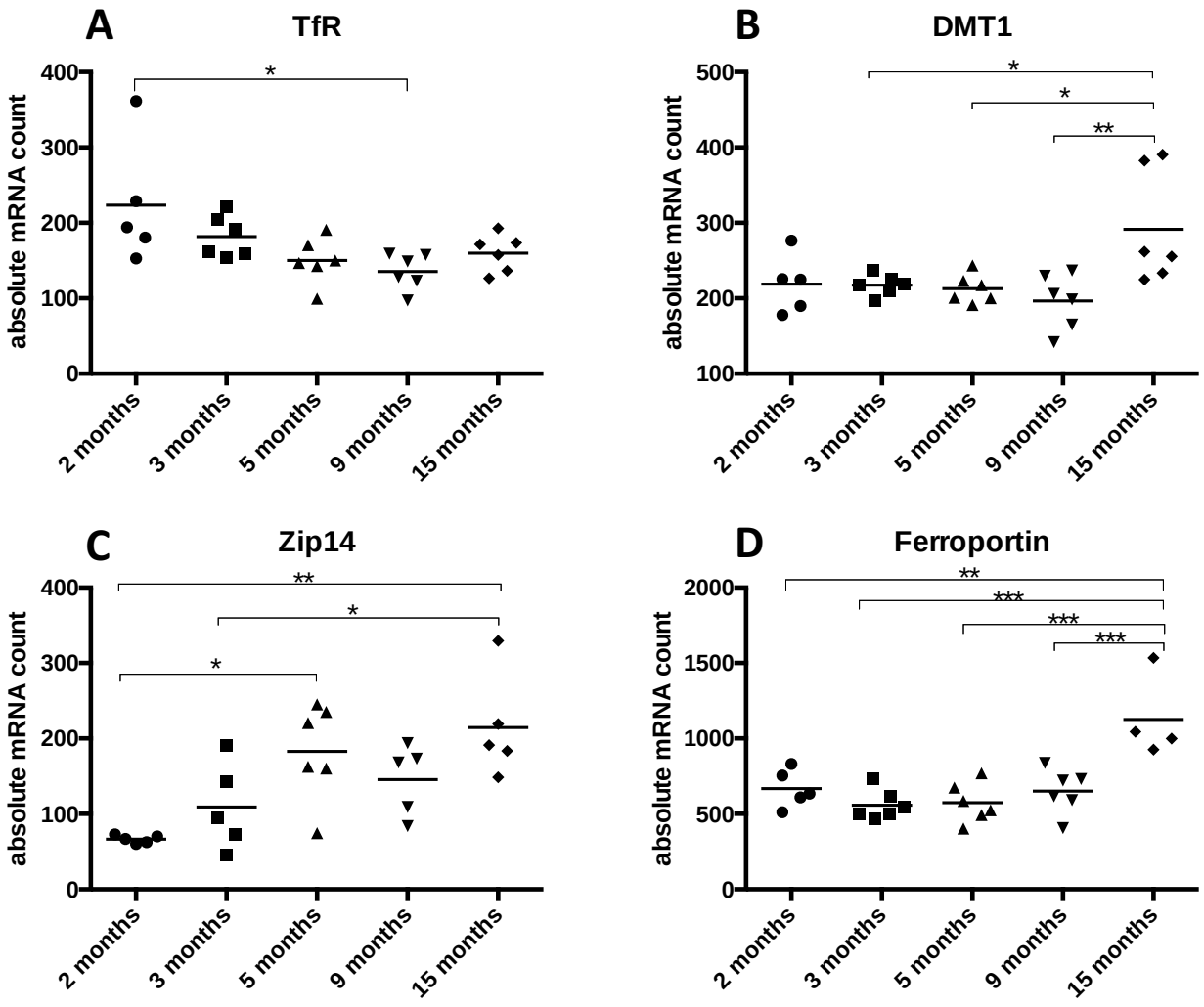

Figure 5.5 – Gene expression for iron trafficking proteins. Nanostring gene expression via absolute mRNA transcript count for TfR (A), DMT1 (B), Zip14 (C), and ferroportin (D). Horizontal black line represents mean value. * $P \leq 0.05$, ** $P \leq 0.01$, *** $P \leq 0.001$, **** $P \leq 0.0001$.

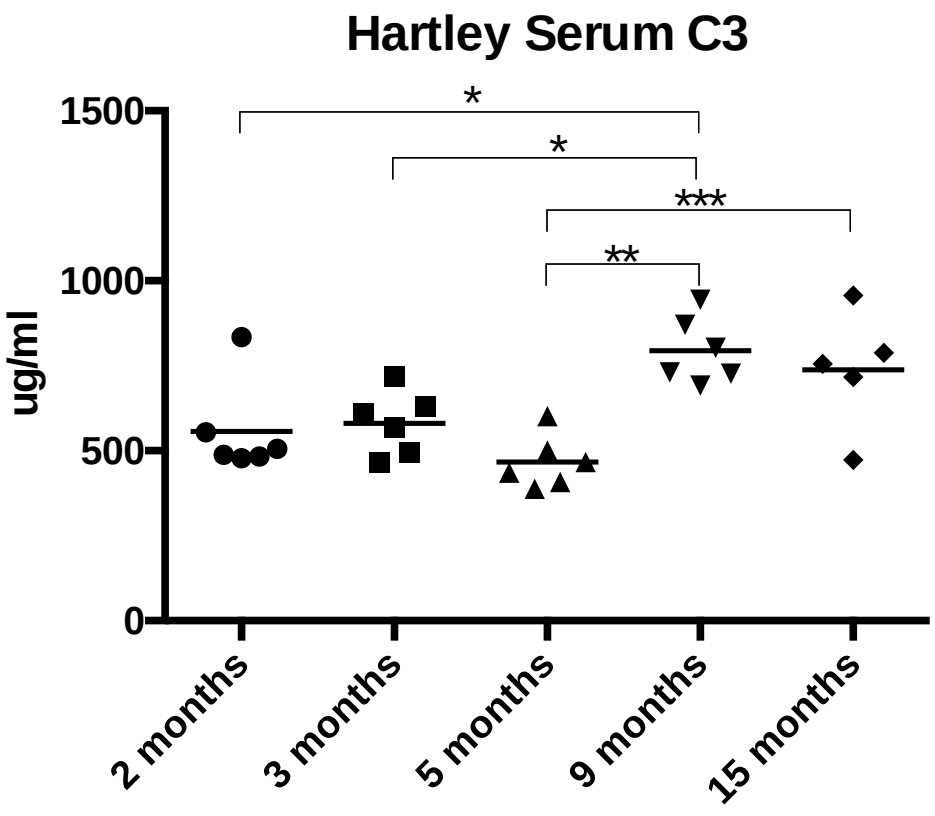

Figure 5.6 – Circulating levels of complement protein C3. Serum protein C3 levels in aging Hartley guinea pigs. Horizontal black line represents mean value. * $P \leq 0.05$, ** $P \leq 0.01$, *** $P \leq 0.001$.

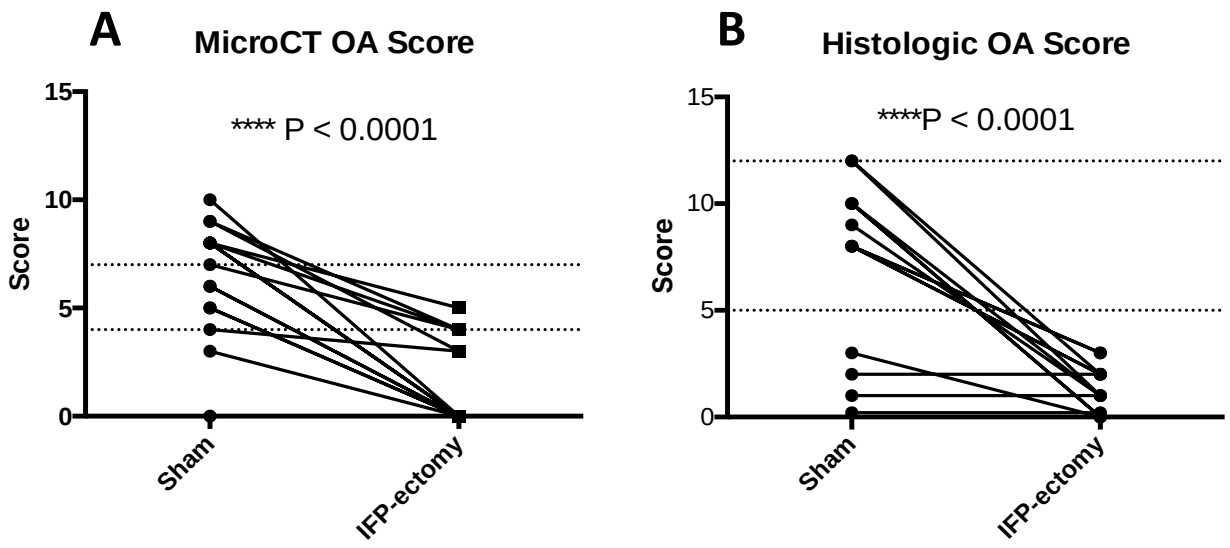

Figure 5.7 – Paired microCT and histologic OA scores in IFP removal study. MicroCT (A) and histologic (B) OA scores in the IFP removal study. Dotted lines represent typical OA scores expected for this age.

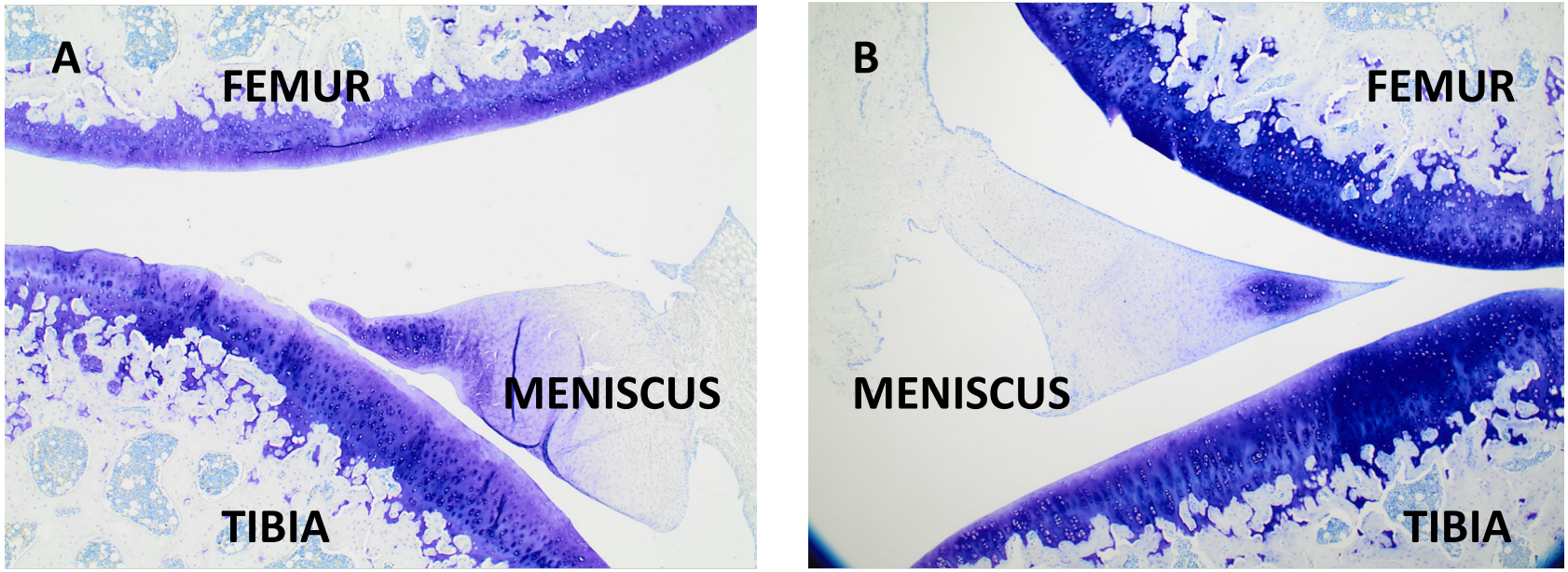

Figure 5.8 – Example photomicrographs of histologic lesions from IFP removal study. A) Irregular articular surface with mild fibrillation and proteoglycan loss in the superficial zone of the tibia from a limb that underwent sham surgery. B) IFP removal limb from the same animal exhibiting a smooth cartilage surface and very mild proteoglycan loss. 100X, Toluidine blue stain.

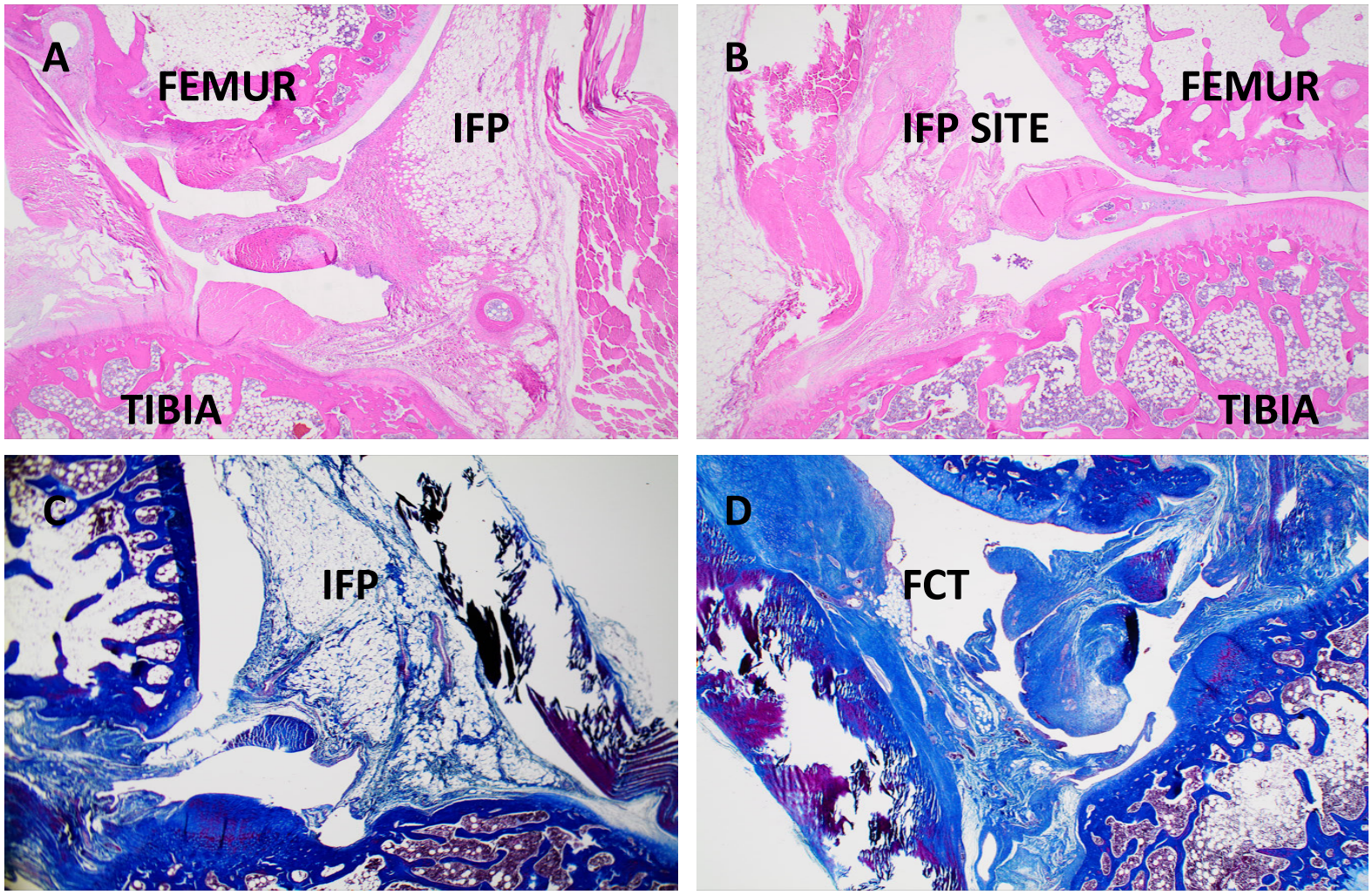

Figure 5.9 – Photomicrographs of IFP removal site. Mid-sagittal section showing IFP in a sham control limb (A) compared to an IFP removal leg where it appears to be replaced by pink connective tissue (B). H&E stains. Sections stained with Masson's trichrome to confirm collagenous nature of the connective tissue (C, D).

CHAPTER 6

CALORIE RESTRICTION WITH REGULAR CHOW, BUT NOT A HIGH FAT DIET, DELAYS ONSET OF SPONTANEOUS OSTEOARTHRITIS IN THE HARTLEY GUINEA PIG MODEL OF DISEASE

6.1 Introduction.

Osteoarthritis (OA), particularly knee OA, is a debilitating degenerative disorder affecting many people worldwide[97]. While OA secondary to a joint injury is typically associated with a defined onset, naturally-occurring OA occurs in the absence of specific trauma for reasons that are not yet understood. Advancing age has long been the primary risk factor for development of spontaneous OA[200]; however, obesity is encroaching on age as a leading OA hazard given the alarming rise in obesity rates across the globe[201,202]. The relationship between OA and obesity has been an area of increasing interest to researchers, but the mechanisms connecting these two conditions remain loosely defined. Early studies suggested that increased mechanical loading forces on joints contributed to worsened OA in obese patients[203]. However, higher incidence of OA in non-weight bearing joints, such as in the hands[28], indicates that increased joint load may not be the only factor at play. Thus, dietary factors, including food composition and total calorie intake, likely play a complex role in the development of primary OA.

Recent studies have placed emphasis on the role systemic metabolic disturbances may play in the development of OA[4,203–206]. Obesity is often associated with chronic, low-grade systemic inflammation[207–210]. For example, as the volume of adipose tissue expands, it outgrows its blood supply, leading to tissue hypoxia and stimulation of pro-inflammatory cytokines[33].

Enhanced lipopolysaccharide translocation from the gut to the bloodstream is another contributor to a chronic inflammatory state in obese individuals, particularly in response to high dietary fat content[32]. Similarly, high levels of circulating saturated fatty acids stimulate innate immune receptors such as toll-like receptor 4, resulting in a heightened pro-inflammatory state[33]. Increased circulating leptin concentration in obese individuals can also promote inflammation via stimulation of cytokines such as interleukin (IL) -1 beta (IL-1β), tumor necrosis factor (TNF), and IL-6[34]. Additionally, high leptin levels have been shown to promote OA via increased activity of cartilage-degrading matrix metalloproteinases (MMPs) and aggrecanases[33,35].

Previous work examining the role of obesity in promoting OA has concentrated on utilizing high fat diets (HFDs) in mouse[37–40,211], rat[32,42], and, more rarely, rabbit[43] animal models. Many of these studies have focused on post-traumatic OA secondary to surgical injury with a lesser number centered on naturally-occurring OA. Collectively, these studies provide convincing evidence that high fat diet-induced obesity leads to worsened OA severity. Many have demonstrated that it is the increased fat mass, not overall body weight, associated with high fat diets that is correlated with OA severity[32,37,38,40,43]. This is likely attributed to the metabolically active, inflammatory cytokine-producing nature of this adipose tissue. Diets used in these rodent studies vary in the amount of fat present, although 40-60% fat (derived from animal-based saturated fats) is typical. While such a high percentage of fat is effective in inducing obesity in mice and rats, it does not accurately reflect human diets, which are closer to 30% fat in a standard Western diet[212].

While HFDs have a detrimental effect on health, calorie restriction has emerged as a lifestyle factor that can prolong life and decrease the likelihood of developing chronic diseases

such as atherosclerosis, type II diabetes and neurodegenerative disease[213]. These positive effects are due to decreased oxidant damage, increased DNA repair, and decreased production of inflammatory cytokines secondary to less adipose tissue mass[214–217]. Very few studies, however, have examined the effects of calorie restriction on development of OA. In dogs, calorie restriction appeared to delay onset of OA[218,219]. A long-term study in mice did not demonstrate in any differences in histologic OA severity between *ad libitum* and calorie-restricted mice, although it should be noted that fat mass was not different between the groups at the end of the study[213]. There is also one study examining calorie restriction in the Hartley guinea pig model of spontaneous OA. This work demonstrated that calorie restriction resulted in lessened OA severity at both 9 and 18 months of age[220], time points that correspond to late and end-stage disease, respectively. Given this, we were interested in pursuing the influence of calorie restriction at earlier ages in the time course of disease.

Guinea pigs are perhaps an underutilized rodent model of OA. In particular, the Hartley strain is a useful model of spontaneous knee joint OA, as it develops disease in a condensed time frame and demonstrates pathologic lesions that are nearly identical to those seen in humans with aging-related OA[60,221]. Guinea pigs have also emerged as being suitable models for a variety of metabolic diseases, including cardiovascular disease, atherosclerosis, and type II diabetes[222–224]. Furthermore, guinea pig lipid metabolism is more comparable to human lipid metabolism than any other rodent[222,225–227]. High fat diets have been successfully used in guinea pigs to drive metabolic diseases, such as type II diabetes[222] and non-alcoholic fatty liver disease[228]. In contrast to mouse and rat studies using a high fat diet, the diets used in these guinea pig studies tend to range from 20-30% fat, which is more typical of a Westernized human diet. High fat diets used in guinea pig studies also have a mixture of saturated animal-based fats and unsaturated plant-

based fats. As guinea pigs tend to be more fastidious about diet than mice and rats, they do not tend to develop overt obesity in concert with metabolic derangements when fed high fat diets[222,228]. This may allow for evaluation of the metabolic effects of HFDs without the potential confounding influence of mechanical factors associated with overt obesity. To date, there are no studies exploring the potential role a high fat diet may play in the development of spontaneous OA in a guinea pig model.

Collectively, the aims of the current study were to compare and contrast the effects of overconsumption and calorie restriction using standard rodent chow to that of a HFD on the onset of spontaneous OA in a guinea pig model. We hypothesized that animals on a HFD would exhibit worsened OA scores compared to both *ad libitum* and calorie-restricted animals on a regular chow diet. Likewise, we expected calorie restriction to result in improved OA scores at this early time point.

6.2 Materials and Methods.

Animals.

All procedures were approved by the university's Institutional Animal Care and Use Committee and were performed in accordance with the NIH Guide for the Care and Use of Laboratory Animals. Twenty-four 6- to 7-week-old male Dunkin-Hartley guinea pigs were purchased from a commercial vendor (Charles River Laboratories, Wilmington, MA). Animals were maintained at Colorado State University's Laboratory Animal Resources housing facilities and were monitored daily by a veterinarian. All guinea pigs were singly-housed in solid bottom cages and provided *ad libitum* access to water daily.

After one week of acclimation, animals were randomly allocated to one of four feeding groups: 1) *ad libitum* regular chow (obese), 2) calorie restricted regular chow (lean), 3) *ad libitum* HFD, and 4) calorie restricted HFD. As laboratory-raised guinea pigs fed *ad libitum* often become obese with age[229], this first group was referred to as such in the current study. Further, as animals in group 3 were noted to self-restrict consumption of the HFD to the same amount as those in group 4 (25 grams), this group was condensed to a single HFD group. All animals were harvested at 5 months of age, a time when this strain of guinea pig has recognized signs of early OA[60].

Diet composition.

The regular chow diet (Teklad Global Guinea Pig Diet #2040, Madison, WI) provided 31% calories from protein, 12% from fat, and 57% from carbohydrate. This diet was supplemented with vitamin C (1050 mg/kg). Fat was derived from linseed meal. Protein and carbohydrates were derived from a mixture of alfalfa, wheat, oats, and fish meal. Animals on the restricted regular chow diet received 30 grams of food daily for the duration of the study[213]. The HFD (#151006, Dyets Inc, Bethlehem, PA) provided 18% calories from protein, 30% from fat, and 52% from carbohydrates. Fat was sourced from a mixture of Primex vegetable shortening and beef tallow. The source of protein was isolated soy protein, and carbohydrates were derived from sucrose and fructose. All animals receiving the HFD consumed 25 grams of food each day.

Tissue Collection.

At the time of harvest, animals were anesthetized with a mixture of isoflurane and oxygen. Body weights were recorded at this time. Thoracic cavities were opened, and blood was

collected with 20-gauge butterfly catheter via direct cardiac puncture. After blood collection, anesthetized animals were immediately transferred to a carbon dioxide chamber for euthanasia. Hind limbs were removed at the coxofemoral joint. The left limb was placed into 10% neutral buffered formalin for 48 hours and then transferred to PBS for microCT analysis. After microCT imaging was complete, tibial length was measured using calipers. Limbs were then transferred to a 12.5% solution of ethylenediaminetetraacetic acid (EDTA) at pH 7 for decalcification. EDTA was replaced twice weekly for 6 weeks.

After the right hind limb was removed, the knee joint was exposed by dissecting through the quadriceps muscles and reflecting the patella distally. The infrapatellar fat pad (IFP) was removed from the patellar tendon, weighed, and then placed in All Protect Tissue Reagent (Qiagen) for gene expression analysis. Fat from the left epididymis (hence forth referred to as gonad fat), was removed and weighed. A section of masseter muscle was collected from each animal and its width was measured.

MicroCT.

Knee joints were scanned using the Inveon microPET/CT system (Siemens Medical Solutions, Malvern PA), with a voxel size of 18 micrometers, a voltage of 100 kV, and an exposure time of 2356 ms. Clinical features of OA were scored on reconstructed microCT images using a whole joint grading scheme developed by our lab in conjunction with a veterinary radiologist[131]. Features graded include: presence/size and location of osteophytes, subchondral bone cystic changes, subchondral bone sclerosis, articular bone lysis, and intraarticular soft tissue mineralization. Images were scored in duplicate in a random order, blinded to diet group. An intraclass correlation coefficient of 1.0 for intra-reviewer consistency was calculated.

Histologic Grading of OA.

After decalcification, coronal slices of the knees at the level of the medial tibial plateau were sectioned, as previously described[60]. Samples were paraffin embedded and a 5-micron intact central section was stained with toluidine blue. Medial and lateral femoral condyles, along with medial and lateral tibial plateaus, were scored using the recommended published guidelines[60]. This semiquantitative histopathologic grading scheme is based on articular cartilage structure, proteoglycan content, cellularity, tidemark integrity, and presence of osteophytes. Scores were performed in a blinded fashion by two independent pathologists (LBR and KSS). Scores from each of the four anatomic locations were summed to obtain a total knee joint OA score for each guinea pig.

Immunohistochemistry for MCP-1 on knee joints.

Immunohistochemistry (IHC) was performed on sections of knee joints using a polyclonal rabbit antibody to MCP-1 (Abcam ab9669) at a dilution of 1:100. Prior to incubation with primary antibody, slides were incubated in citrate buffer overnight at 55°C for antigen retrieval, as recommended for skeletal tissues[133]. Slides were incubated in primary antibody overnight at 4°C, followed by a 30-minute incubation with a biotinylated goat anti-rabbit secondary antibody. Bone marrow hematopoietic cells and macrophages frequently exhibited MCP-1 staining, serving as internal positive controls for each section. Exposure to secondary antibody, alone, did not result in any positive immunostaining. Sections were counterstained with hematoxylin, coverslipped, and viewed by light microscopy. At least four sections from each joint were examined for immunostaining in chondrocytes, matrix, and within the IFP.

Complete blood count, serum biochemical profile and serum protein C3 measurement.

At the time of harvest, blood collected via cardiac puncture was allocated to 0.5 mL EDTA microtubes for complete blood count (CBC). CBCs were performed at the CSU Clinical Pathology Laboratory using the Advia 120 hematology analyzer (Siemens, Munich, Germany) with instrument settings and software specifically designed for guinea pig samples. Blood films were manually reviewed, and a leukocyte differential count was performed by a veterinary clinical pathologist (LR). Remaining blood taken at euthanasia was placed in red top glass tubes to incite clotting. After 30 minutes, red top tubes were adequately clotted and placed into a centrifuge at 5,000 x g for 10 minutes for serum collection. One aliquot of serum was submitted to the Colorado State University (CSU) Clinical Pathology Laboratory for serum biochemical analysis using the Roche Cobas 6000 (Basel, Switzerland). Remaining serum was aliquoted to cryovials, snap frozen in liquid nitrogen, and then stored at -80°C for C3 analysis. Serum protein C3 levels were measured on snap frozen serum using a guinea pig-specific ELISA (Abcam ab157705) according to the manufacturer's protocol.

Gene expression of IFP using NanoString technology.

Total RNA was extracted from IFP samples using an RNeasy Lipid Tissue Mini Kit (Qiagen, Hilden, Germany). RNA was quantified spectrophotometrically with a NanoDrop™ 2000 (ThermoFisher Scientific, Waltham, MA). A total of 250 ng of RNA, at a concentration of 20 ng/µl, was sent to the University of Arizona Genetics Core for analysis. Custom, guinea pig-specific probes were designed and synthesized by NanoString Technologies (see Table 6.1 for genes analyzed). Data analysis was performed using nSolver™ software provided by NanoString

Technologies. Results, reported as absolute transcript counts, were normalized to positive controls and housekeeping genes.

Statistical analyses.

Data for total body weights, tibial length, gonad fat weight, IFP weight, masseter muscle width, histologic OA scores, clinical microCT OA scores, CBC values, serum biochemical values, serum protein C3 values, and NanoString mRNA normalized absolute counts were subjected to, and passed, normality testing via the Kolmogorov-Smirnov test. Data were compared using parametric ordinary one-way ANOVA analyses followed by Tukey's multiple comparisons tests to allow for adjusted P values. Statistical significance was set at $P < 0.05$. All statistical analyses were performed with GraphPad Prism (La Jolla, CA, USA).

6.3 Results.

General description of guinea pigs in each diet group.

All animals in each group survived the duration of the study. Final body weights for the obese group were significantly higher than both the lean and HFD groups. There was no difference in body weights between the lean and HFD groups (Figure 6.1). To ensure that differences in body weight were not attributable to variations in skeletal properties, tibial lengths from all animals were measured. There was no statistical difference in tibial length between any of the three diet groups (Figure 6.1). To determine if muscle mass may be different between the three groups, the width of the masseter muscle was measured and compared. Muscle width was significantly smaller in HFD group compared to the obese *ad libitum* regular chow group. Mean

muscle width in the obese group was 5.8 mm (95% CI 4.4 – 7.2), 4.7 mm (95% CI 3.8 – 5.5) in the lean calorie restricted group, and 3.6 mm (95% CI 3.1 – 4.1) in the HFD group (P = 0.0029).

In addition to body weights, two adipose depots were also weighed and contrasted among the groups. Gonad fat (collected from the epididymis) was chosen to represent an abdominal adipose store, while the IFP was selected to represent a depot local to the knee joint. Despite differences in total body weights, gonad fat weights in the obese and HFD groups were similar. Gonad fat weight in both of these groups was significantly higher than that of the lean group (Figure 6.2). Interestingly, this pattern was not seen for IFP weight. IFP weights for all 3 groups were similar, with no statistical differences found (Figure 6.2).

MicroCT and histologic assessment of OA.

Osteoarthritis was assessed via two methodologies. MicroCT was utilized to examine bony changes associated with OA, while histologic assessment of joints via the OARSI grading scheme was used to evaluate articular cartilage abnormalities. Using the clinical OA microCT scoring system, both obese and HFD groups had similar OA scores. Scores for these groups were statistically higher than those reported in the lean group (Figure 6.3). Of note, in the lean group, many of the animals had no microCT evidence of OA at 5 months of age, a time when early bony changes are consistently present in Hartley guinea pigs[60]. All animals in both the obese and HFD group had visible small osteophytes present on the patella and/or the tibia (Figure 6.4). In contrast, only one animal in the lean group had a small osteophyte present on the patella. All remaining lean animals were radiographically normal, with no bony changes associated with OA.

The OARSI grading scheme resulted in a similar trend to that seen with the clinical microCT score. Again, both obese and HFD groups had similar OARSI OA scores that were

significantly higher those present in the lean group. Interestingly, although the total OA scores were similar in the obese and HFD groups, specific cartilage lesions appeared to differ. Articular cartilage surface fibrillation and superficial fissures were noted within the obese group (Figure 6.5). Superficial proteoglycan loss, with both focal and diffuse distributions, occasional chondrocyte clustering, and focal cell loss were noted in the HFD group (Figure 6.5). In the lean group, some animals exhibited mild superficial proteoglycan loss, but articular surface integrity was often maintained (Figure 6.5).

CBC, serum biochemistry, and protein C3 data.

Complete blood count, serum biochemistry data, and serum protein C3 were assessed for evidence of systemic inflammation and other metabolic effects the diet conditions had on normal physiology. On CBC, platelet counts, which have been associated with increased levels of IL-6 in guinea pigs[153], were higher in the HFD group compared to both the lean and obese group. Additionally, platelet counts in the obese group were higher than those of the lean group, but not as high as the HFD group (Figure 6.6).

While increased platelet count can indicate a higher level of inflammation[230], it is non-specific and other indicators of inflammation, such as an increased white blood cell count, were not noted in this study. To more conclusively determine if a higher level of inflammation was present in the obese and HFD groups, a guinea-pig specific ELISA for protein C3, an acute phase reactant, was used to analyze serum. Serum protein C3 levels were similar among the obese and HFD groups and were significantly higher than levels present in the lean group (Figure 6.6).

In addition to the higher platelet and protein C3 levels, two other significant differences were noted on serum biochemical profiles. Total cholesterol levels were higher in both the obese

and HFD groups compared to lean animals (Figure 6.6). Interestingly, there was a wide spread of cholesterol values for the HFD group, with some animals having values similar to those of the lean group and others having much higher serum concentrations. In addition, blood urea nitrogen (BUN), a protein breakdown product excreted by the kidneys, was similar in the obese and lean groups. BUN in these groups was significantly higher than levels seen in the HFD group (Figure 6.6).

Gene expression data from the infrapatellar fat pad.

As the goal of this study was to determine how HFD and calorie restriction affect knee OA, we were particularly interested to see how these dietary manipulations might affect the IFP. Using NanoString technology, absolute mRNA counts for many pro- and anti-inflammatory cytokines, chemokines, and matrix metalloproteinase (MMP) genes were evaluated (Table 6.1). Numerous pro-inflammatory genes were upregulated in the HFD group. Compared to the lean group, the HFD animals had higher expression of several pro-inflammatory genes including IL-4, IL-5, nuclear factor kappa beta (NFkB), cyclooxygenase 2 (COX2), transforming growth factor-β (TGF-β), and TNF. Compared to the obese group, HFD-fed animals exhibited higher expression of IL-6, MCP-1, NFkB, COX2, and TNF. Additionally, the HFD group had higher expression of matrix metalloproteinase-13 (MMP13), which cleaves type II collagen, than both the obese and lean groups. Expression of MMP2, which cleaves type IV collagen, and tissue inhibitor of metalloproteinases 2 (Timp2), an inhibitor of MMP activity, was also higher in the HFD group than the obese group.

When examining adipokines and other genes related to lipid metabolism, there were also several notable differences in gene expression among the groups. Leptin, an adipokine that

normally inhibits hunger but exhibits resistance in obesity, was significantly increased in the HFD group compared to the lean group. It also trended towards being higher in the obese regular chow group compared to lean animals, but this did not reach statistical significance. Adiponectin, an adipokine that is traditionally decreased systemically in obesity, had higher gene expression in the IFP of the HFD group compared to the obese regular chow group. Lipoprotein lipase, which hydrolyzes triglycerides for cellular use, was increased in the lean regular chow group compared to both the obese regular chow and HFD groups. It was also higher in the HFD group compared to obese regular chow animals. Finally, peroxisome proliferator-activator gamma (PPARγ), was increased in the lean regular chow group compared to both the obese regular chow and HFD groups.

Immunohistochemistry for MCP-1.

Protein expression of MCP-1 was prominent within chondrocytes in the obese regular chow group and the HFD group. No visible differences in staining intensity or percentage of positive cells were noted between these two groups. In contrast, there was little to no MCP-1 staining within chondrocytes in the lean group (Figure 6.7). Staining within the extracellular matrix was minimal in all three groups.

6.4 Discussion.

This study demonstrates that calorie-restriction using a low-fat, regular chow diet lessens OA severity early in disease onset in a guinea pig model of spontaneous disease. An interesting, yet unintended, outcome of the study was that animals fed the HFD essentially self-imposed calorie restriction, despite being fed *ad libitum*. Due to their fastidious nature, guinea pigs in this

group ate less food than expected, resulting in body weights that were similar to those seen in the purposefully calorie-restricted, regular chow group. Despite similar body weights among the HFD and calorie-restricted groups, microCT and histologic OA scores were worse in the HFD group. Thus, the benefits of calorie-restriction appear to be diminished by the pro-inflammatory nature of the HFD. Our findings lend support to the growing body of evidence that the link between OA and adiposity may be attributable to systemic and local knee joint inflammation. Total body weight ranged from 645-816 grams in the HFD group. Interestingly, heavier animals in this group had worse microCT OA scores based ($r = 0.62$, $P = 0.0313$). Thus, increased weight-bearing on joints cannot be excluded as a factor in the development of knee joint OA. Rather, it seems likely that both loading forces and inflammation contribute to disease development.

In the current study, obese regular chow-fed animals had similar OA scores as leaner animals fed a HFD. Despite the difference in total body weight, an abdominal fat depot was similarly sized between these two groups. These findings suggest that the HFD animals, although lean, had reduced lean muscle mass. This was corroborated by the decreased size of the masseter muscle in the HFD group compared to the obese regular chow group. The lower BUN in the HFD animals is another indication of lower muscle mass, but may also be attributed to decreased protein consumption in this group. When comparing the macronutrient composition of the regular chow and high fat diets, the proportion of carbohydrates was similar; however, the HFD contained 30% fat and 18% protein, while the regular chow contained 12% fat and 31% protein. It is possible that either the lesser amount of protein and/or higher amount of fat content in the diet contributed to reduced muscle mass in the HFD group.

Regardless of body weight differences between the obese and HFD groups, they exhibited similar OA scores. This indicates that diet composition, and not simply body weight or calorie-restriction, alone, may play a key role in the development of primary OA. Abdominal fat depots were similarly sized in the obese regular chow and lean HFD groups; however, this fat depot was significantly smaller in the calorie-restricted regular chow group. This finding suggests that animals fed the HFD maintained higher levels of adiposity, with smaller muscle mass, despite having body weights comparable to the calorie-restricted regular chow group.

In contrast to the variably sized abdominal fat depot among the three diet groups, the local knee joint adipose tissue, the IFP, was similarly sized amongst all three diet groups. Thus, it appears that the IFP is well-preserved, even in the face of calorie restriction. While more exploration is required to define the specific role of the IFP in OA, the current findings suggest preservation of this tissue depot may be essential to joint health. Indeed, while there is still debate as to whether the IFP is more akin to subcutaneous[231] or visceral fat[159], the current study indicates that it may be a unique adipose depot that is not under the same metabolic influences as other fat tissues found in the body. A few studies employing HFD-induced mouse models of OA found that IFP volume or area increased after being fed a HFD[39,41]. In one of these studies, IFP area was also positively correlated to osteophyte area, as determined by histology[41]. Human studies examining relationships between body mass index (BMI) and IFP size have yielded conflicting results. At least two studies have found no association between body mass index and IFP size in both lean and overweight/obese individuals[54,158]. Results of the current study mimic what has been reported in these human studies, with no differences in IFP weight found despite differing total body weights in guinea pigs. However, another human study has reported a moderately positive correlation ($r = 0.50$ in females, $P < 0.001$; $r = 0.34$ in males, $P = 0.03$)[232].

This is parallel to findings in a study of predominantly women that found a higher IFP volume in obese individuals[233]. More work is needed to further clarify the role of IFP in both healthy and obese individuals.

While overall mass of the IFP was similar among the three groups, gene expression profiles of the IFP differed. In general, expression of pro-inflammatory genes was higher in the HFD group compared to both obese and calorie-restricted regular chow groups. Specifically, NFkB, a transcription factor, and downstream targets IL-6 and TNF exhibited increased expression in the HFD group. It is well-established that both HFDs and obesity incite a chronic, low-grade inflammatory state due to upregulated NFkB and subsequent secretion of inflammatory cytokines such as IL-1, IL-6, and TNF[156,234]. Here, we demonstrate that upregulation of these genes occurs locally in the knee joint in the IFP, potentially directly contributing to inflammation and subsequent OA in guinea pigs fed a HFD. Other pro-inflammatory pathways that were upregulated in the HFD group include the COX2 pathway, as well as the chemotactic factor MCP-1. Many of these pro-inflammatory cytokines and adipokines are known to increase activity of cartilage-degrading MMPs[235].

The current study also demonstrated increased gene expression of MMP13 in the HFD group compared to both the obese *ad libitum* and lean calorie-restricted groups. MMP13 primarily degrades type II collagen, a major constituent of the extracellular cartilage matrix. Additionally, MMP2 gene expression was higher in the HFD group compared to the obese *ad libitum* group. MMP2 cleaves type IV collagen. Type IV collagen is found in the pericellular matrix directly adjacent to chondrocytes and has anti-angiogenic properties that may play a role in maintaining an avascular and hypoxic environment in normal, healthy cartilage[236]. In damaged cartilage, the relative abundance of type IV collagen drops precipitously[237]. Our data suggest that

MMP activity originating from the IFP in obese and HFD-fed animals may contribute to degradation of types II and IV collagen in cartilage.

Given the abundance of gene expression data indicating increased inflammation within knee joints of the HFD and obese regular chow groups, IHC probing for MCP-1 protein expression was performed. Expression of this protein in chondrocytes and the IFP were similar between the obese regular chow and HFD groups, while expression was not present in the lean calorie restricted group. These findings confirm that there is increased inflammation within the knee joint in the obese and HFD groups compared to the lean group. Likewise, this data supports the premise that calorie-restriction with a low-fat diet results in low levels of knee joint inflammation. MCP-1 is a pro-inflammatory chemokine that plays a key role in OA pathogenesis and neuropathic pain[238]. Synovial fluid MCP-1 levels have been associated with radiographic knee OA and clinical symptoms in humans[239,240]. Human articular chondrocytes express MCP-1, which increases expression of MMPs resulting in proteoglycan loss *in vitro*[241,242]. Additionally, administration of an MCP-1 signaling inhibitor protected cartilage after joint injury in a rat model[243].

In addition to evidence of local inflammation in the knee joint of the guinea pigs on the HFD, animals also had signs of increased systemic inflammation. While perhaps not at a level able to incite an increased white blood cell count on routine CBCs, the increased platelet count in both the HFD and obese regular chow groups compared to calorie restricted regular chow animals may indicate a higher level of systemic inflammation. Cytokines, particularly IL-6, stimulate thrombopoiesis in the bone marrow[244], which results in a reactive thrombocytosis in a variety of inflammatory conditions, including obesity[245]. An increased platelet count, alone, however, is not specific for inflammation. Lack of differences in white blood cell numbers may

be due to the low-grade or relatively short-term nature of the inflammation typically described with obesity. As such, we measured a more sensitive and specific biomarker of inflammation, serum protein C3, an acute phase reactant in guinea pigs[188]. This assay confirmed that both the HFD and obese regular chow groups had greater levels of circulating inflammatory proteins than calorie restricted regular chow animals. In humans, the major acute phase reactant, C-reactive protein, has been correlated to severity of radiographic OA[246]. Similar to these human studies, serum C3 levels were positively correlated to radiographic microCT OA score ($r = 0.45$, $P = 0.0395$) in the current study.

An intriguing finding of the current study was the variability in the types of cartilage lesions noted between the obese *ad libitum* group and the HFD group. Overall OARSI OA scores for these two groups were similar; however, the types of lesions observed differed. In the obese *ad libitum* group, there were more fibrillations and fissures in the articular cartilage surface. In the HFD group, proteoglycan loss was more prominent. The reason for these differences should be pursued, although we speculate it may be due to differences in total body weight. Increased loading on joints in the obese group may more directly cause surface damage via formation of fissures. Loss of proteoglycan in the HFD group may be due to increased systemic inflammation or due to decreased protein content in the diet. Of note, types of lesions noted on microCT were did not differ between these groups. More differences in bony changes may emerge if this study extended beyond 5 months of age.

This study provides several important conclusions regarding effects of diet on development of spontaneous OA. Firstly, calorie restriction was able to delay the onset of OA in disease-prone Hartley guinea pigs. Secondly, the benefit of calorie-restriction was diminished in animals eating a high fat diet. This is likely due to the higher levels of systemic and local

inflammation seen in these animals. Thus, diet composition, and not calorie content alone, must be considered a key player in development of OA. High fat diets may not be optimal for knee joint health.

Of note, the current study utilized only saturated fats in the HFD. This was necessitated in order to make a shelf-stable pellet at room temperature. However, it is well-established that saturated fats induce inflammation. Future studies will alter fat composition of the diet to include unsaturated fats to determine if overall percentage of fat in the diet or fatty acid composition is more important in driving development of OA. It is also important to repeat this study using female animals to determine if there may be any sex differences in response to diet. Extending this study beyond 5 months of age is also important to determine long-term effects of these diets. To the authors' knowledge, this is the first study to examine the IFP in the guinea pig. Our results suggest the IFP plays a role in disease development and that inflammatory profiles of the IFP are altered by changes in diet. More work is needed to further define the role of the IFP in development of spontaneous OA.

Table 6.1 Normalized absolute mRNA counts present in the IFP. Data is represented as the mean (range).

Gene	Function	Obese	Lean	HFD	P-value
IFNγ	Pro-inflammatory cytokine	7.222 (4.360-11.440)	15.64 (7.060-20.44)	16.31 (2.490-37.06)	0.1204
IL-10	Anti-inflammatory cytokine	11.95 (9.680-14.87)	8.283 (2.350-13.74)	13.94 (3.660-23.90)	0.1372
IL-1β	Pro-inflammatory cytokine	30.41 (15.75-71.81)	29.45 (24.01-39.37)	42.97 (22.21-53.90)	0.0944
IL-4	Th2 response, tissue repair/fibrosis	15.54 (13.73-20.83)	13.60 (7.060-17.58)	22.63 (13.13-37.33)	**0.0112***
IL-5	Promotes Ig production and eosinophil activation	18.13 (12.91-22.65)	13.12 (9.750-18.09)	25.97 (16.04-41.05)	**0.0029***
IL-6	Pro-inflammatory cytokine	25.01 (20.12-29.16)	29.60 (18.68-45.15)	58.82 (21.73-76.84)	**0.0151**$^{+}$
LIF	Anti-inflammatory cytokine	23.78 (18.37-32.85)	28.21 (16.52-38.43)	28.71 (12.02-42.72)	0.5087
MCP-1	Pro-inflammatory cytokine	333.3 (265.4-487.0)	439.4 (361.0-510.5)	564.9 (398.7-812.7)	**0.0005**$^{+}$
NFκB	Pro-inflammatory transcription factor	112.1 (95.20-132.7)	119.7 (102.8-145.1)	161.0 (107.8-231.4)	**0.0015**$^{*,+}$
COX2	Pro-inflammatory enzyme	32.61 (23.52-54.11)	34.99 (29.61-48.63)	52.55 (35.37-69.86)	**0.0010**$^{*,+}$
Tacr1	Binds Substance P, pro-inflammatory, causes pain	205.3 (142.0-276.1)	167.8 (121.6-254.9)	211.3 (107.4-340.4)	0.3172
TGF-β1	Tissue repair, both pro and anti-inflammatory	275.2 (195.1-403.5)	254.9 (206.1-330.4)	375.3 (210.6-591.1)	**0.0173***
TNF	Pro-inflammatory cytokine	10.92 (8.710-13.53)	8.082 (7.060-9.000)	15.07 (7.290-22.49)	**0.0009**$^{*,+}$
HIF1α	Responds to hypoxia	1640 (1116-2020)	1552 (893.8-2654)	1899 (1170-3089)	0.4487
MMP13	Cleaves type II collagen	19.74 (13.12-31.65)	11.88 (8.790-14.26)	35.43 (15.31-59.03)	**0.0059**$^{*,+}$
MMP2	Cleaves type IV collagen	8192 (6133-10346)	9722 (7571-12566)	11514 (8944-14686)	**0.0157**$^{+}$
MMP9	Cleaves type IV and V collagen, activates neutrophils	14.46 (2.610-46.53)	17.47 (8.250-23.08)	26.23 (2.250-64.05)	0.2951
Timp1	Inhibits MMPs	1310 (956.1-1709)	1076 (768.8-1563)	1145 (761.4-1826)	0.4103
Timp2	Inhibits MMPs	6270 (4494-7529)	7654 (6354-9109)	8014 (6089-10405)	**0.0248**$^{+}$
Adiponectin	Glucose sensitivity and FA oxidation	10530 (8885-11904)	20830 (12666-24246)	23818 (9818-38769)	**0.0093**$^{+}$
Leptin	Inhibits hunger, resistance seen in obesity	6379 (3975-9012)	2296 (1191-3651)	9471 (3921-26498)	**0.0348***
LPL	Hydrolyzes TGs into FAs and glycerol	2843 (1188-3988)	16118 (7900-22842)	7536 (3271-16678)	**<0.0001**$^{*,+,\dagger}$
PPARγ	Lipid uptake and adipogenesis, insulin sensitization, anti-inflammatory	185.4 (105.7-249.1)	466.2 (275.3-736)	254.6 (139.2-426.2)	**0.001***,†

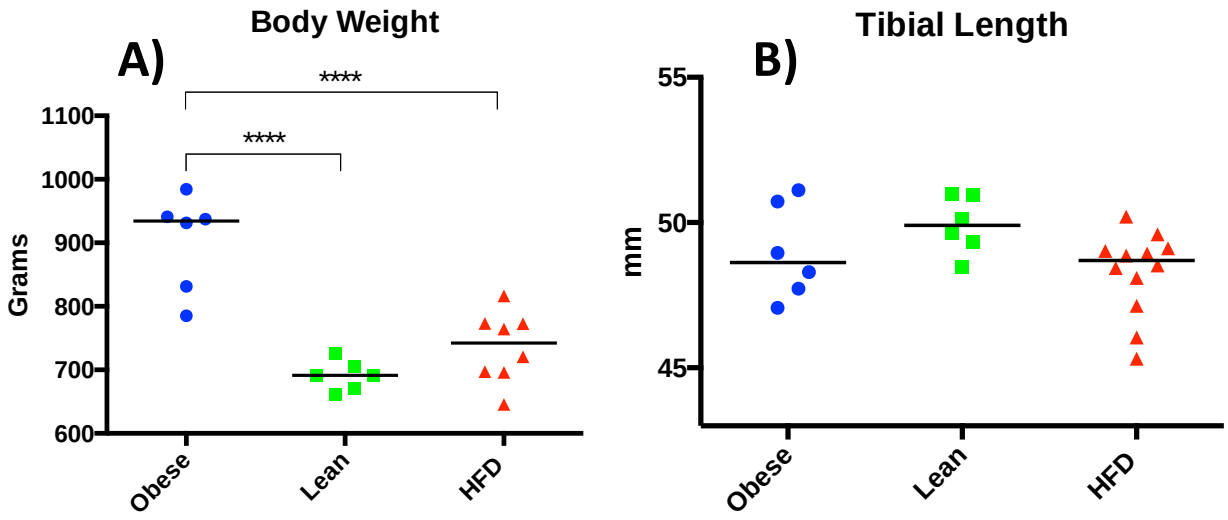

Figure 6.1 Body weights and tibial lengths in the HFD study. Total body weight (A) and tibial length (B) obese, lean, and HFD groups. Black line represents mean value. **** P < 0.0001.

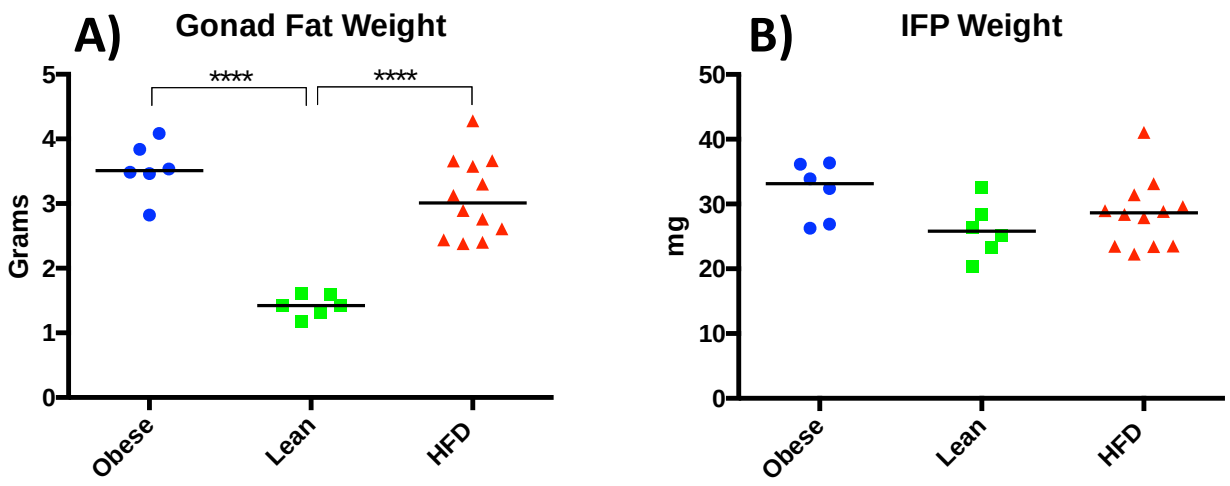

Figure 6.2 – Fat depot weights. Weight of gonad fat (A) and IFP (B) in obese, lean, and HFD groups. Black line represents mean value **** $P < 0.0001$.

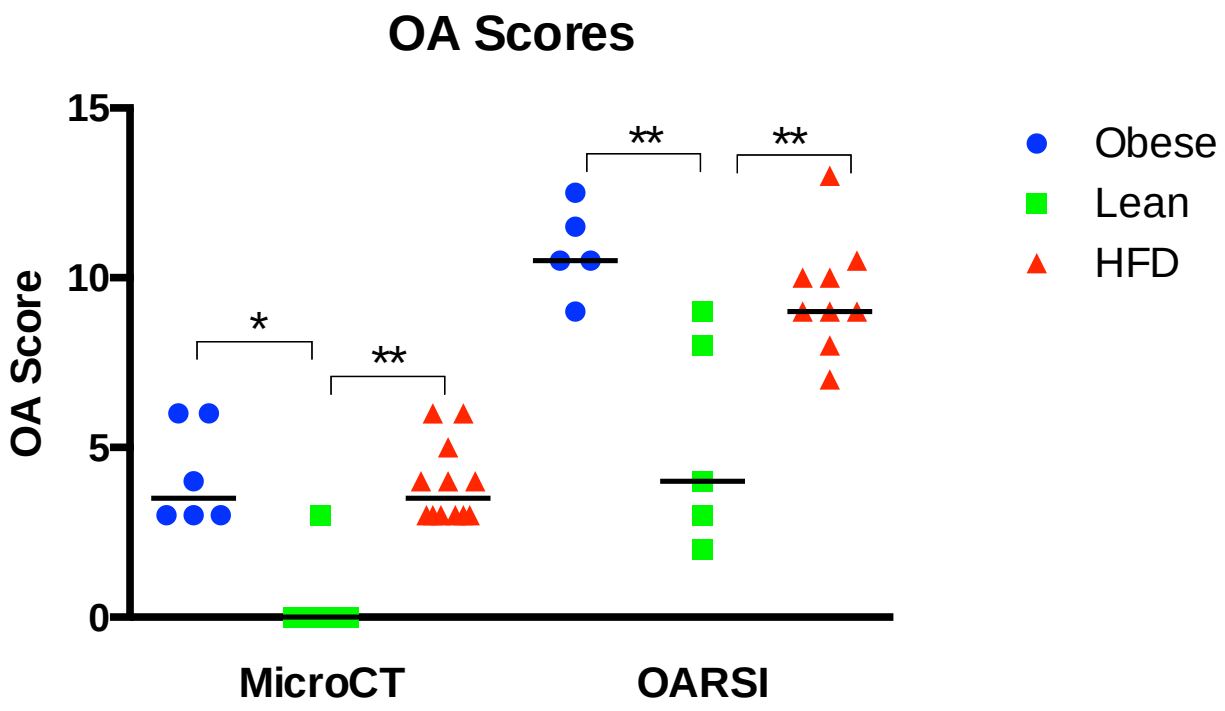

Figure 6.3 – Whole joint OA scores. MicroCT and OARSI histologic scores in obese, lean, and HFD groups. * $P < 0.05$, ** $P < 0.01$.


Calorie Restricted/Lean
Ad Libitum/Obese
HFD
Coronal
Sagittal
A
B
C
D
E
F

Figure 6.4 – Example images of microCT lesions in the three diet groups. (A) Dorsal and (B) sagittal reconstructions from a calorie-restricted animal with no OA lesions. MicroCT OA score of 0. (C) Dorsal reconstruction from an obese animal. There is sclerosis and small osteophytes on the medial femoral condyle (red arrows) and mild sclerosis of the central tibial plateau (blue arrows). (D) Sagittal reconstruction from same animal. Mild sclerosis of the cranial patella and caudal tibial condyle is present. MicroCT OA score of 6. (E) HFD coronal lateral osteophyte tibia (green arrow). (F) HFD sagittal mild irregularity proximal patella (green arrow). MicroCT OA score of 4.

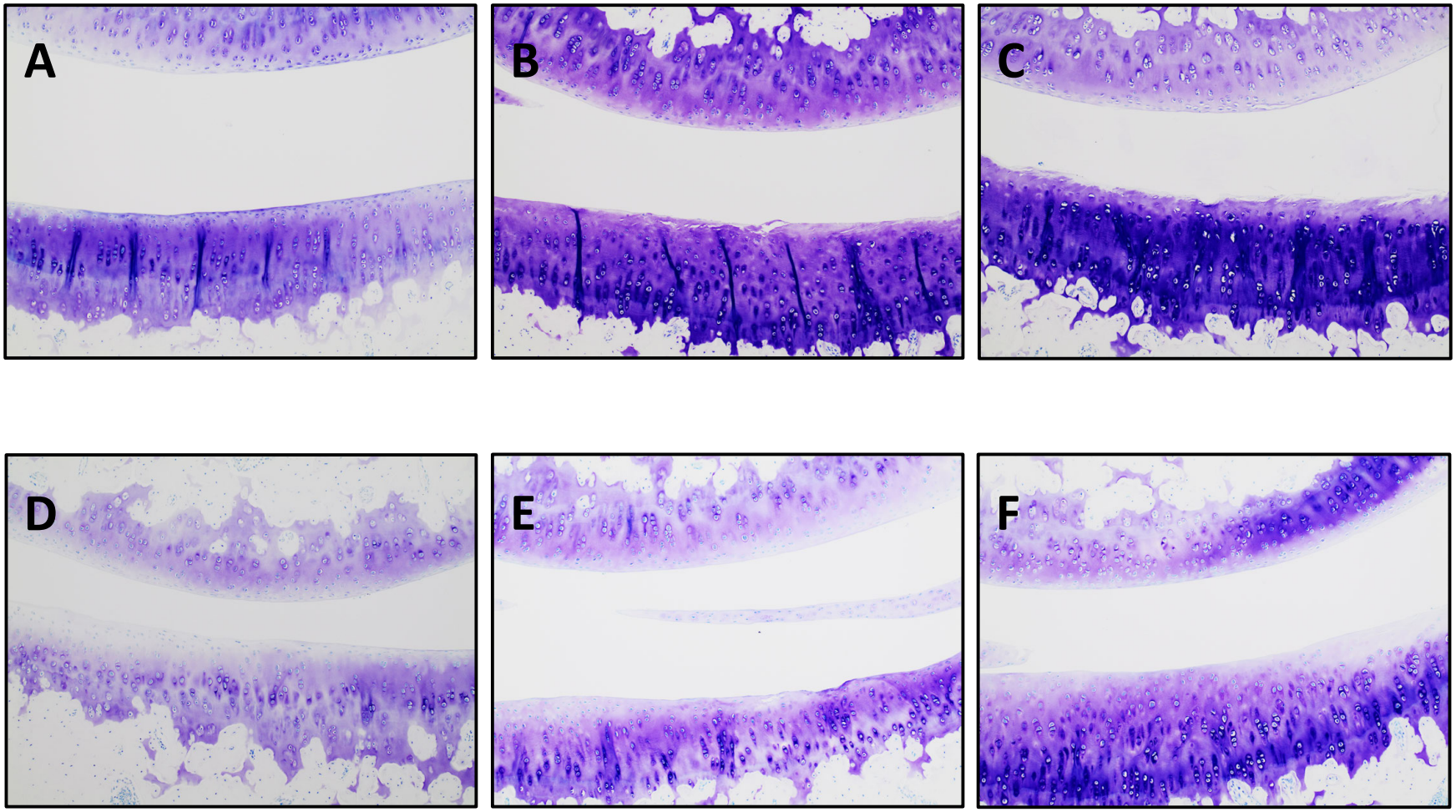

Figure 6.5 – Photomicrographs of histologic lesions in the obese, lean, and HFD groups. (A) T blue photomicrograph of the medial compartment from a calorie-restricted/lean animal. The articular surface is smooth with only mild superficial proteoglycan loss. (B & C) T blue photomicrographs from *ad libitum*/obese animals. The articular surfaces are fibrillated, there is proteoglycan loss in the superficial and middle zones, and there is cell clustering. (D-F) T blue photomicrographs from HFD-fed animals. There is regional to diffuse proteoglycan loss in the superficial and middle zones, mild articular surface irregularity, occasional cell clustering, and focal cell loss within the superficial zone.

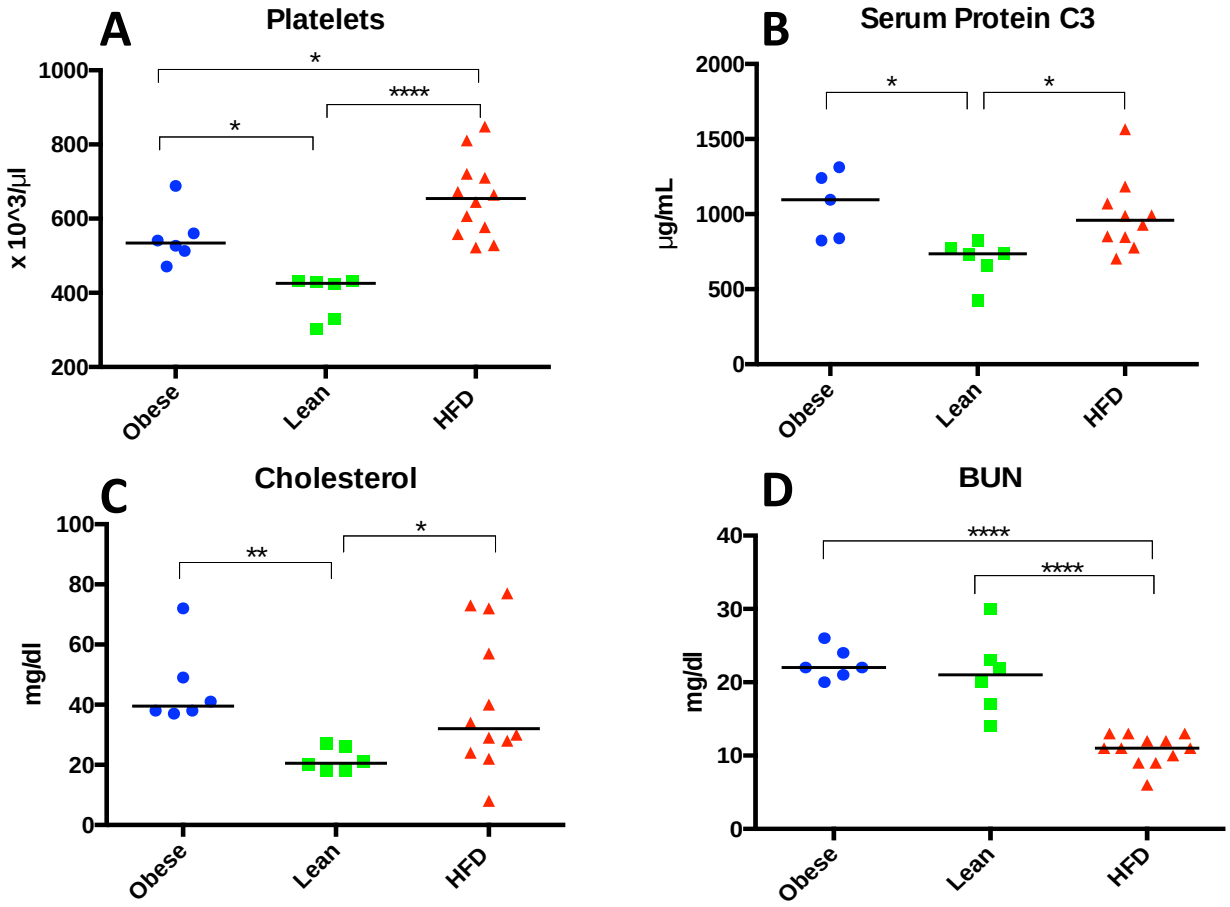

Figure 6.6 – CBC and biochemistry findings in obese, lean, and HFD groups. Total platelet counts (A), protein C3 levels (B), serum cholesterol (C), and serum BUN (D) in obese, lean, and HFD groups. Black line represents mean values. * $P < 0.05$, ** $P < 0.01$, **** $P < 0.0001$.

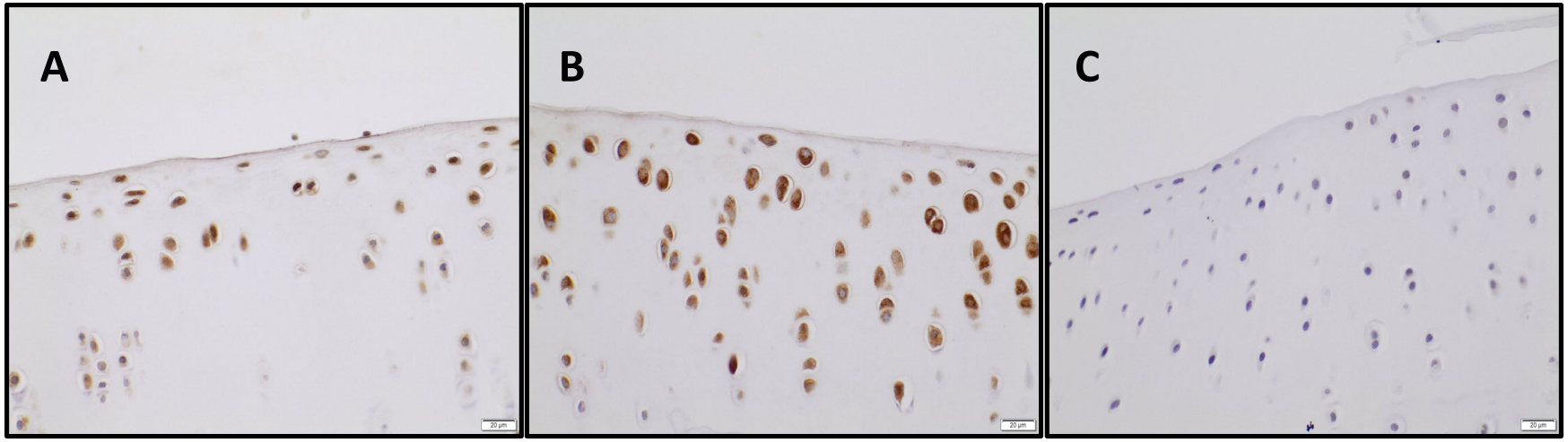

Figure 6.7 – Monocyte chemoattractant protein-1 immunohistochemistry in obese, HFD, and lean animals. Representative images of immunostaining for MCP-1 on the medial tibial plateau for the ad libitum regular chow group (A), the HFD group (B), and calorie-restricted group (C). 400X.

REFERENCES

1. Hunter DJ, Felson DT. Osteoarthritis. *BMJ*. 2006;332(7542):639-642. doi:10.1136/bmj.332.7542.639.
2. Bellamy N, Buchanan WW. A preliminary evaluation of the dimensionality and clinical importance of pain and disability in osteoarthritis of the hip and knee. *Clin Rheumatol*. 1986;5(2):231-241. doi:10.1007/BF02032362.
3. Felson DT. The epidemiology of knee osteoarthritis: Results from the framingham osteoarthritis study. *Semin Arthritis Rheum*. 1990;20(3):42-50. doi:10.1016/0049-0172(90)90046-I.
4. Kulkarni K, Karssiens T, Kumar V, et al. Obesity and osteoarthritis. *Maturitas*. 2016;89:22-28. doi:10.1016/j.maturitas.2016.04.006.
5. ANDERSON JJ, FELSON DT. FACTORS ASSOCIATED WITH OSTEOARTHRITIS OF THE KNEE IN THE FIRST NATIONAL HEALTH AND NUTRITION EXAMINATION SURVEY (HANES I). *Am J Epidemiol*. 1988;128(1):179-189. doi:10.1093/oxfordjournals.aje.a114939.
6. Hart DJ, Doyle D V., Spector TD. Incidence and risk factors for radiographic knee osteoarthritis in middle-aged women: The Chingford Study. *Arthritis Rheum*. 1999;42(1):17-24. doi:10.1002/1529-0131(199901)42:1<17::AID-ANR2>3.0.CO;2-E.
7. Blagojevic M, Jinks C, Jeffery A, Jordan KP. Risk factors for onset of osteoarthritis of the knee in older adults: a systematic review and meta-analysis. *Osteoarthr Cartil*. 2010;18(1):24-33. doi:10.1016/J.JOCA.2009.08.010.
8. Punzi L, Galozzi P, Luisetto R, et al. Post-traumatic arthritis: overview on pathogenic mechanisms and role of inflammation. *RMD open*. 2016;2(2):e000279. doi:10.1136/rmdopen-2016-000279.
9. Brown TD, Johnston RC, Saltzman CL, Marsh JL, Buckwalter JA. Posttraumatic osteoarthritis: a first estimate of incidence, prevalence, and burden of disease. *J Orthop Trauma*. 2006;20(10):739-744. doi:10.1097/01.bot.0000246468.80635.ef.
10. Lluch Girbés E, Nijs J, Torres-Cueco R, López Cubas C. Pain Treatment for Patients With Osteoarthritis and Central Sensitization. *Phys Ther*. 2013;93(6):842-851. doi:10.2522/ptj.20120253.
11. Mason JM, Breitbart AS, Barcia M, Porti D, Pergolizzi RG, Grande DA. Cartilage and bone regeneration using gene-enhanced tissue engineering. *Clin Orthop Relat Res*. 2000;(379 Suppl):S171-8. http://www.ncbi.nlm.nih.gov/pubmed/11039767. Accessed August 18, 2018.
12. Kessler MW, Grande DA. Tissue engineering and cartilage. *Organogenesis*. 2008;4(1):28-32. http://www.ncbi.nlm.nih.gov/pubmed/19279712. Accessed August 18, 2018.
13. Kotlarz H, Gunnarsson CL, Fang H, Rizzo JA. Insurer and out-of-pocket costs of osteoarthritis in the US: evidence from national survey data. *Arthritis Rheum*. 2009;60(12):3546-3553. doi:10.1002/art.24984.
14. Crofford LJ. Use of NSAIDs in treating patients with arthritis. *Arthritis Res Ther*. 2013;15 Suppl 3(Suppl 3):S2. doi:10.1186/ar4174.
15. Kuyinu EL, Narayanan G, Nair LS, Laurencin CT. Animal models of osteoarthritis: classification, update, and measurement of outcomes. *J Orthop Surg Res*. 2016;11:19.

doi:10.1186/s13018-016-0346-5.
16. Man GS, Mologhianu G. Osteoarthritis pathogenesis - a complex process that involves the entire joint. *J Med Life*. 2014;7(1):37-41. http://www.ncbi.nlm.nih.gov/pubmed/24653755. Accessed August 21, 2018.
17. Sulzbacher I. Osteoarthritis: histology and pathogenesis. *Wiener Medizinische Wochenschrift*. 2013;163(9-10):212-219. doi:10.1007/s10354-012-0168-y.
18. Glyn-Jones S, Palmer AJR, Agricola R, et al. Osteoarthritis. *Lancet*. 2015;386(9991):376-387. doi:10.1016/S0140-6736(14)60802-3.
19. Pufe T, Lemke A, Kurz B, et al. Mechanical overload induces VEGF in cartilage discs via hypoxia-inducible factor. *Am J Pathol*. 2004;164(1):185-192. doi:10.1016/S0002-9440(10)63109-4.
20. Beckmann R, Houben A, Tohidnezhad M, et al. Mechanical forces induce changes in VEGF and VEGFR-1/sFlt-1 expression in human chondrocytes. *Int J Mol Sci*. 2014;15(9):15456-15474. doi:10.3390/ijms150915456.
21. Chen Y-J, Chan D-C, Chiang C-K, et al. Advanced glycation end-products induced VEGF production and inflammatory responses in human synoviocytes via RAGE-NF-κB pathway activation. *J Orthop Res*. 2016;34(5):791-800. doi:10.1002/jor.23083.
22. DeGroot J, Verzijl N, Wenting-Van Wijk MJG, et al. Accumulation of advanced glycation end products as a molecular mechanism for aging as a risk factor in osteoarthritis. *Arthritis Rheum*. 2004;50(4):1207-1215. doi:10.1002/art.20170.
23. Rasheed Z, Akhtar N, Haqqi TM. Advanced glycation end products induce the expression of interleukin-6 and interleukin-8 by receptor for advanced glycation end product-mediated activation of mitogen-activated protein kinases and nuclear factor- B in human osteoarthritis chondrocytes. *Rheumatology*. 2011;50(5):838-851. doi:10.1093/rheumatology/keq380.
24. Greene MA, Loeser RF. Aging-related inflammation in osteoarthritis. *Osteoarthr Cartil*. 2015;23(11):1966-1971. doi:10.1016/j.joca.2015.01.008.
25. Xia S, Zhang X, Zheng S, et al. An Update on Inflamm-Aging: Mechanisms, Prevention, and Treatment. *J Immunol Res*. 2016;2016:8426874. doi:10.1155/2016/8426874.
26. Singh T, Newman AB. Inflammatory markers in population studies of aging. *Ageing Res Rev*. 2011;10(3):319-329. doi:10.1016/j.arr.2010.11.002.
27. Livshits G, Zhai G, Hart DJ, et al. Interleukin-6 is a significant predictor of radiographic knee osteoarthritis: The Chingford study. *Arthritis Rheum*. 2009;60(7):2037-2045. doi:10.1002/art.24598.
28. Carman WJ, Sowers M, Hawthorne VM, Weissfeld LA. Obesity as a risk factor for osteoarthritis of the hand and wrist: a prospective study. *Am J Epidemiol*. 1994;139(2):119-129. http://www.ncbi.nlm.nih.gov/pubmed/8296779. Accessed June 28, 2017.
29. Greene MA, Loeser RF. Aging-related inflammation in osteoarthritis. *Osteoarthr Cartil*. 2015;23(11):1966-1971. doi:10.1016/j.joca.2015.01.008.
30. Delmonico MJ, Harris TB, Visser M, et al. Longitudinal study of muscle strength, quality, and adipose tissue infiltration. *Am J Clin Nutr*. 2009;90(6):1579-1585. doi:10.3945/ajcn.2009.28047.
31. Tchkonia T, Morbeck DE, Von Zglinicki T, et al. Fat tissue, aging, and cellular senescence. *Aging Cell*. 2010;9(5):667-684. doi:10.1111/j.1474-9726.2010.00608.x.
32. Collins KH, Paul HA, Reimer RA, Seerattan RA, Hart DA, Herzog W. Relationship

between inflammation, the gut microbiota, and metabolic osteoarthritis development: studies in a rat model. *Osteoarthr Cartil*. 2015;23(11):1989-1998. doi:10.1016/j.joca.2015.03.014.
33. Sartori-Cintra AR, Aikawa P, Cintra DEC. Obesity versus osteoarthritis: beyond the mechanical overload. *Einstein (Sao Paulo)*. 2014;12(3):374-379. http://www.ncbi.nlm.nih.gov/pubmed/25184806. Accessed June 28, 2017.
34. Pou KM, Massaro JM, Hoffmann U, et al. Visceral and Subcutaneous Adipose Tissue Volumes Are Cross-Sectionally Related to Markers of Inflammation and Oxidative Stress. *Circulation*. 2007;116(11). http://circ.ahajournals.org/content/116/11/1234. Accessed July 18, 2017.
35. Fernandes JC, Martel-Pelletier J, Pelletier J-P. The role of cytokines in osteoarthritis pathophysiology. *Biorheology*. 2002;39(1-2):237-246. http://www.ncbi.nlm.nih.gov/pubmed/12082286. Accessed July 18, 2017.
36. Messier SP, Mihalko SL, Legault C, et al. Effects of Intensive Diet and Exercise on Knee Joint Loads, Inflammation, and Clinical Outcomes Among Overweight and Obese Adults With Knee Osteoarthritis. *JAMA*. 2013;310(12):1263. doi:10.1001/jama.2013.277669.
37. Wu C-L, Jain D, McNeill JN, et al. Dietary fatty acid content regulates wound repair and the pathogenesis of osteoarthritis following joint injury. *Ann Rheum Dis*. 2015;74(11):2076-2083. doi:10.1136/annrheumdis-2014-205601.
38. Mooney RA, Sampson ER, Lerea J, Rosier RN, Zuscik MJ. High-fat diet accelerates progression of osteoarthritis after meniscal/ligamentous injury. *Arthritis Res Ther*. 2011;13(6):R198. doi:10.1186/ar3529.
39. Chang W, Demoe J, Kent C, et al. INFRAPATELLAR FAT PAD HYPERTROPHY WITHOUT INFLAMMATION IN A DIET-INDUCED MOUSE MODEL OF OBESITY AND OSTEOARTHRITIS. *Osteoarthr Cartil*. 2011;19(1):S66. doi:10.1016/S1063-4584(11)60157-X.
40. Griffin TM, Fermor B, Huebner JL, et al. Diet-induced obesity differentially regulates behavioral, biomechanical, and molecular risk factors for osteoarthritis in mice. *Arthritis Res Ther*. 2010;12(4):R130. doi:10.1186/ar3068.
41. Iwata M, Ochi H, Hara Y, et al. Initial responses of articular tissues in a murine high-fat diet-induced osteoarthritis model: pivotal role of the IPFP as a cytokine fountain. Fritz JH, ed. *PLoS One*. 2013;8(4):e60706. doi:10.1371/journal.pone.0060706.
42. Collins KH, Hart DA, Seerattan RA, Reimer RA, Herzog W. High-fat/high-sucrose diet-induced obesity results in joint-specific development of osteoarthritis-like degeneration in a rat model. *Bone Joint Res*. 2018;7(4):274-281. doi:10.1302/2046-3758.74.BJR-2017-0201.R2.
43. Brunner AM, Henn CM, Drewniak EI, et al. High dietary fat and the development of osteoarthritis in a rabbit model. *Osteoarthr Cartil*. 2012;20(6):584-592. doi:10.1016/j.joca.2012.02.007.
44. Mace J, Bhatti W, Anand S. Infrapatellar fat pad syndrome: a review of anatomy, function, treatment and dynamics. *Acta Orthop Belg*. 2016;82(1):94-101. http://www.ncbi.nlm.nih.gov/pubmed/26984660. Accessed June 27, 2018.
45. Bastiaansen-Jenniskens YM, Wei W, Feijt C, et al. Stimulation of fibrotic processes by the infrapatellar fat pad in cultured synoviocytes from patients with osteoarthritis: a possible role for prostaglandin f2α. *Arthritis Rheum*. 2013;65(8):2070-2080. doi:10.1002/art.37996.

46. Van Beeck A, Clockaerts S, Somville J, et al. Does infrapatellar fat pad resection in total knee arthroplasty impair clinical outcome? A systematic review. *Knee*. 2013;20(4):226-231. doi:10.1016/j.knee.2013.01.005.
47. Clockaerts S, Bastiaansen-Jenniskens YM, Runhaar J, et al. The infrapatellar fat pad should be considered as an active osteoarthritic joint tissue: a narrative review. *Osteoarthr Cartil*. 2010;18(7):876-882. doi:10.1016/j.joca.2010.03.014.
48. Gierman LM, Wopereis S, van El B, et al. Metabolic profiling reveals differences in concentrations of oxylipins and fatty acids secreted by the infrapatellar fat pad of donors with end-stage osteoarthritis and normal donors. *Arthritis Rheum*. 2013;65(10):2606-2614. doi:10.1002/art.38081.
49. Han W, Cai S, Liu Z, et al. Infrapatellar fat pad in the knee: is local fat good or bad for knee osteoarthritis? *Arthritis Res Ther*. 2014;16(4):R145. doi:10.1186/ar4607.
50. Ioan-Facsinay A, Kloppenburg M. An emerging player in knee osteoarthritis: the infrapatellar fat pad. *Arthritis Res Ther*. 2013;15(6):225. doi:10.1186/ar4422.
51. Fu Y, Huebner JL, Kraus VB, Griffin TM. Effect of Aging on Adipose Tissue Inflammation in the Knee Joints of F344BN Rats. *J Gerontol A Biol Sci Med Sci*. 2016;71(9):1131-1140. doi:10.1093/gerona/glv151.
52. Distel E, Cadoudal T, Durant S, Poignard A, Chevalier X, Benelli C. The infrapatellar fat pad in knee osteoarthritis: an important source of interleukin-6 and its soluble receptor. *Arthritis Rheum*. 2009;60(11):3374-3377. doi:10.1002/art.24881.
53. Ushiyama T, Chano T, Inoue K, Matsusue Y. Cytokine production in the infrapatellar fat pad: another source of cytokines in knee synovial fluids. *Ann Rheum Dis*. 2003;62(2):108-112. http://www.ncbi.nlm.nih.gov/pubmed/12525378. Accessed June 27, 2018.
54. Chuckpaiwong B, Charles HC, Kraus VB, Guilak F, Nunley JA. Age-associated increases in the size of the infrapatellar fat pad in knee osteoarthritis as measured by 3T MRI. *J Orthop Res*. 2010;28(9):1149-1154. doi:10.1002/jor.21125.
55. Hui W, Litherland GJ, Elias MS, et al. Leptin produced by joint white adipose tissue induces cartilage degradation via upregulation and activation of matrix metalloproteinases. *Ann Rheum Dis*. 2012;71(3):455-462. doi:10.1136/annrheumdis-2011-200372.
56. Haviv B, Bronak S, Thein R. The complexity of pain around the knee in patients with osteoarthritis. *Isr Med Assoc J*. 2013;15(4):178-181. http://www.ncbi.nlm.nih.gov/pubmed/23781753. Accessed August 18, 2018.
57. Yusuf E, Kortekaas MC, Watt I, Huizinga TWJ, Kloppenburg M. Do knee abnormalities visualised on MRI explain knee pain in knee osteoarthritis? A systematic review. *Ann Rheum Dis*. 2011;70(1):60-67. doi:10.1136/ard.2010.131904.
58. McCoy AM. Animal Models of Osteoarthritis: Comparisons and Key Considerations. *Vet Pathol*. 2015;52(5):803-818. doi:10.1177/0300985815588611.
59. Staines KA, Poulet B, Wentworth DN, Pitsillides AA. The STR/ort mouse model of spontaneous osteoarthritis – an update. *Osteoarthr Cartil*. 2017;25(6):802-808. doi:10.1016/j.joca.2016.12.014.
60. Kraus VB, Huebner JL, DeGroot J, Bendele A. The OARSI histopathology initiative - recommendations for histological assessments of osteoarthritis in the guinea pig. *Osteoarthritis Cartilage*. 2010;18 Suppl 3(Suppl 3):S35-52. doi:10.1016/j.joca.2010.04.015.
61. Huebner JL, Kraus VB. Assessment of the utility of biomarkers of osteoarthritis in the guinea pig. *Osteoarthr Cartil*. 2006;14(9):923-930. doi:10.1016/j.joca.2006.03.007.

62. Santangelo KS, Pieczarka EM, Nuovo GJ, Weisbrode SE, Bertone AL. Temporal expression and tissue distribution of interleukin-1β in two strains of guinea pigs with varying propensity for spontaneous knee osteoarthritis. *Osteoarthr Cartil*. 2011;19(4):439-448. doi:10.1016/j.joca.2011.01.004.
63. Schwarz P, Strnad P, Singer N, et al. Identification, sequencing, and cellular localization of hepcidin in guinea pig (Cavia porcellus). *J Endocrinol*. 2009;202(3):389-396. doi:10.1677/JOE-09-0191.
64. BURNS JJ. Missing Step in Man, Monkey and Guinea Pig required for the Biosynthesis of L-Ascorbic Acid. *Nature*. 1957;180(4585):553-553. doi:10.1038/180553a0.
65. Rutgers M, van Pelt MJP, Dhert WJA, Creemers LB, Saris DBF. Evaluation of histological scoring systems for tissue-engineered, repaired and osteoarthritic cartilage. *Osteoarthr Cartil*. 2010;18(1):12-23. doi:10.1016/j.joca.2009.08.009.
66. Pritzker KPH, Gay S, Jimenez SA, et al. Osteoarthritis cartilage histopathology: grading and staging. *Osteoarthr Cartil*. 2006;14(1):13-29. doi:10.1016/j.joca.2005.07.014.
67. Aigner T, Cook JL, Gerwin N, et al. Histopathology atlas of animal model systems – overview of guiding principles. *Osteoarthr Cartil*. 2010;18:S2-S6. doi:10.1016/j.joca.2010.07.013.
68. Braun HJ, Gold GE. Diagnosis of osteoarthritis: Imaging. *Bone*. 2012;51(2):278-288. doi:10.1016/j.bone.2011.11.019.
69. Roemer FW, Eckstein F, Hayashi D, Guermazi A. The role of imaging in osteoarthritis. *Best Pract Res Clin Rheumatol*. 2014;28(1):31-60. doi:10.1016/j.berh.2014.02.002.
70. Piscaer TM, Waarsing JH, Kops N, et al. In vivo imaging of cartilage degeneration using μCT-arthrography. *Osteoarthr Cartil*. 2008;16(9):1011-1017. doi:10.1016/j.joca.2008.01.012.
71. Roemer FW, Crema MD, Trattnig S, Guermazi A. Advances in Imaging of Osteoarthritis and Cartilage. *Radiology*. 2011;260(2):332-354. doi:10.1148/radiol.11101359.
72. Conaghan PG, Hunter DJ, Maillefert JF, Reichmann WM, Losina E. Summary and recommendations of the OARSI FDA osteoarthritis Assessment of Structural Change Working Group. *Osteoarthr Cartil*. 2011;19(5):606-610. doi:10.1016/j.joca.2011.02.018.
73. Borthakur A, Reddy R. Imaging Cartilage Physiology. *Top Magn Reson Imaging*. 2010;21(5):291-296. doi:10.1097/RMR.0b013e31823dfe2e.
74. Pantopoulos K, Porwal SK, Tartakoff A, Devireddy L. Mechanisms of mammalian iron homeostasis. *Biochemistry*. 2012;51(29):5705-5724. doi:10.1021/bi300752r.
75. RIGG T, TAYLOR W, WEISS J. The rate constant of the bimolecular reaction between hydrogen peroxide and ferrous ion. *Experientia*. 1954;10(5):202-203.
76. Walling C. Fenton's reagent revisited. *Acc Chem Res*. 1975;8(4):125-131. doi:10.1021/ar50088a003.
77. Drakesmith H, Nemeth E, Ganz T. Ironing out Ferroportin. *Cell Metab*. 2015;22(5):777-787. doi:10.1016/j.cmet.2015.09.006.
78. Crichton RR, Charloteaux-Wauters M. Iron transport and storage. *Eur J Biochem*. 1987;164(3):485-506. http://www.ncbi.nlm.nih.gov/pubmed/3032619. Accessed June 1, 2016.
79. Ponka P, Lok CN. The transferrin receptor: role in health and disease. *Int J Biochem Cell Biol*. 1999;31(10):1111-1137. http://www.ncbi.nlm.nih.gov/pubmed/10582342. Accessed June 1, 2016.
80. Ganz T. Macrophages and systemic iron homeostasis. *J Innate Immun*. 2012;4(5-6):446-

453. doi:10.1159/000336423.
81. Finazzi D, Arosio P. Biology of ferritin in mammals: an update on iron storage, oxidative damage and neurodegeneration. *Arch Toxicol*. 2014;88(10):1787-1802. doi:10.1007/s00204-014-1329-0.
82. Theil EC. Ferritin: the protein nanocage and iron biomineral in health and in disease. *Inorg Chem*. 2013;52(21):12223-12233. doi:10.1021/ic400484n.
83. Steinbicker AU, Muckenthaler MU. Out of balance--systemic iron homeostasis in iron-related disorders. *Nutrients*. 2013;5(8):3034-3061. doi:10.3390/nu5083034.
84. Grimes CN, Giori L, Fry MM. Role of hepcidin in iron metabolism and potential clinical applications. *Vet Clin North Am Small Anim Pract*. 2012;42(1):85-96. doi:10.1016/j.cvsm.2011.10.002.
85. Xu J, Marzetti E, Seo AY, Kim J-S, Prolla TA, Leeuwenburgh C. The emerging role of iron dyshomeostasis in the mitochondrial decay of aging. *Mech Ageing Dev*. 2010;131(7-8):487-493. doi:10.1016/j.mad.2010.04.007.
86. Liu J, Sun B, Yin H, Liu S. Hepcidin: A Promising Therapeutic Target for Iron Disorders. *Med (United States)*. 2016;95(14):e3150. doi:10.1097/MD.0000000000003150.
87. Camacho A, Simão M, Ea H-K, et al. Iron overload in a murine model of hereditary hemochromatosis is associated with accelerated progression of osteoarthritis under mechanical stress. *Osteoarthr Cartil*. 2016;24(3):494-502. doi:10.1016/j.joca.2015.09.007.
88. Biemond P, Swaak AJ, van Eijk HG, Koster JF. Intraarticular ferritin-bound iron in rheumatoid arthritis. A factor that increases oxygen free radical-induced tissue destruction. *Arthritis Rheum*. 1986;29(10):1187-1193. http://www.ncbi.nlm.nih.gov/pubmed/3768055. Accessed June 21, 2018.
89. Weinberg ED. The hazards of iron loading. *Metallomics*. 2010;2(11):732. doi:10.1039/c0mt00023j.
90. Nieuwenhuizen L, Schutgens REG, van Asbeck BS, et al. Identification and expression of iron regulators in human synovium: evidence for upregulation in haemophilic arthropathy compared to rheumatoid arthritis, osteoarthritis, and healthy controls. *Haemophilia*. 2013;19(4):e218-27. doi:10.1111/hae.12208.
91. Abbott DF, Gresham GA. Arthropathy in transfusional siderosis. *Br Med J*. 1972;1(5797):418-419. http://www.ncbi.nlm.nih.gov/pubmed/5058161. Accessed June 21, 2018.
92. Senator GB, Muirden KD. Concentration of iron in synovial membrane, synovial fluid, and serum in rheumatoid arthritis and other joint diseases. *Ann Rheum Dis*. 1968;27(1):49-54. http://www.ncbi.nlm.nih.gov/pubmed/5640842. Accessed June 21, 2018.
93. Carroll GJ, Sharma G, Upadhyay A, Jazayeri JA. Ferritin concentrations in synovial fluid are higher in osteoarthritis patients with HFE gene mutations (C282Y or H63D). *Scand J Rheumatol*. 2010;39(5):413-420. doi:10.3109/03009741003677449.
94. Askari AD, Muir WA, Rosner IA, Moskowitz RW, McLaren GD, Braun WE. Arthritis of hemochromatosis. Clinical spectrum, relation to histocompatibility antigens, and effectiveness of early phlebotomy. *Am J Med*. 1983;75(6):957-965. http://www.ncbi.nlm.nih.gov/pubmed/6650551. Accessed June 21, 2018.
95. Kennish L, Attur M, Oh C, et al. Age-dependent ferritin elevations and HFE C282Y mutation as risk factors for symptomatic knee osteoarthritis in males: a longitudinal cohort study. *BMC Musculoskelet Disord*. 2014;15(1):8. doi:10.1186/1471-2474-15-8.

96. Wittenauer R, Smith L, Aden K. *Priority Medicines for Europe and the World " A Public Health Approach to Innovation " Update on 2004 Background Paper Background Paper 6.12 Osteoarthritis.*; 2013.
97. Cross M, Smith E, Hoy D, et al. The global burden of hip and knee osteoarthritis: estimates from the global burden of disease 2010 study. *Ann Rheum Dis*. 2014;73(7):1323-1330. doi:10.1136/annrheumdis-2013-204763.
98. Sowers MR, Karvonen-Gutierrez CA. The evolving role of obesity in knee osteoarthritis. *Curr Opin Rheumatol*. 2010;22(5):533-537. doi:10.1097/BOR.0b013e32833b4682.
99. JAKOBSSON U, HALLBERG IR. Pain and quality of life among older people with rheumatoid arthritis and/or osteoarthritis: a literature review. *J Clin Nurs*. 2002;11(4):430-443. doi:10.1046/j.1365-2702.2002.00624.x.
100. Doros G, Lavin PT, Daley M, Miller LE. A method for establishing class III medical device equivalence: sodium hyaluronate (GenVisc 850) for the treatment of knee osteoarthritis. *Med Devices (Auckl)*. 2016;9:205-211. doi:10.2147/MDER.S104327.
101. Phillips S, Silvia Li C, Phillips M, et al. Treatment of Osteoarthritis of the Knee with Bracing: A Scoping Review. *Orthop Rev (Pavia)*. 2016;8(2):6256. doi:10.4081/or.2016.6256.
102. Freitag J, Bates D, Boyd R, et al. Mesenchymal stem cell therapy in the treatment of osteoarthritis: reparative pathways, safety and efficacy - a review. *BMC Musculoskelet Disord*. 2016;17(1):230. doi:10.1186/s12891-016-1085-9.
103. Gregory MH, Capito N, Kuroki K, et al. A review of translational animal models for knee osteoarthritis. *Arthritis*. 2012;2012:764621. doi:10.1155/2012/764621.
104. Bendele AM, Hulman JF. Spontaneous cartilage degeneration in guinea pigs. *Arthritis Rheum*. 1988;31(4):561-565. doi:10.1002/art.1780310416.
105. Kohn MD, Sassoon AA, Fernando ND. Classifications in Brief: Kellgren-Lawrence Classification of Osteoarthritis. *Clin Orthop Relat Res*. 2016;474(8):1886-1893. doi:10.1007/s11999-016-4732-4.
106. Das Neves Borges P, Forte AE, Vincent TL, Dini D, Marenzana M. Rapid, automated imaging of mouse articular cartilage by microCT for early detection of osteoarthritis and finite element modelling of joint mechanics. *Osteoarthritis Cartilage*. 2014;22(10):1419-1428. doi:10.1016/j.joca.2014.07.014.
107. Wang T, Wen C-Y, Yan C-H, Lu W-W, Chiu K-Y. Spatial and temporal changes of subchondral bone proceed to microscopic articular cartilage degeneration in guinea pigs with spontaneous osteoarthritis. *Osteoarthr Cartil*. 2013;21(4):574-581. doi:10.1016/j.joca.2013.01.002.
108. Yan J -y., Tian F -m., Wang W-Y, et al. Parathyroid hormone (1-34) prevents cartilage degradation and preserves subchondral bone micro-architecture in guinea pigs with spontaneous osteoarthritis. *Osteoarthr Cartil*. 2014;22(11):1869-1877. doi:10.1016/j.joca.2014.07.013.
109. Willett TL, Kandel R, De Croos JNA, Avery NC, Grynpas MD. Enhanced levels of non-enzymatic glycation and pentosidine crosslinking in spontaneous osteoarthritis progression. *Osteoarthr Cartil*. 2012;20(7):736-744. doi:10.1016/j.joca.2012.03.012.
110. Waarsing J., Day J., van der Linden J., et al. Detecting and tracking local changes in the tibiae of individual rats: a novel method to analyse longitudinal in vivo micro-CT data. *Bone*. 2004;34(1):163-169. doi:10.1016/j.bone.2003.08.012.
111. Palacio-Mancheno PE, Larriera AI, Doty SB, Cardoso L, Fritton SP. 3D Assessment of

Cortical Bone Porosity and Tissue Mineral Density Using High-Resolution μCT: Effects of Resolution and Threshold Method. *J Bone Miner Res*. 2014;29(1):142-150. doi:10.1002/jbmr.2012.
112. Wang SX, Arsenault L, Hunziker EB. Stereologic analysis of tibial-plateau cartilage and femoral cancellous bone in guinea pigs with spontaneous osteoarthritis. *Clin Orthop Relat Res*. 2011;469(10):2796-2805. doi:10.1007/s11999-011-1899-6.
113. Felson DT, Zhang Y. An update on the epidemiology of knee and hip osteoarthritis with a view to prevention. *Arthritis Rheum*. 1998;41(8):1343-1355. doi:10.1002/1529-0131(199808)41:8<1343::AID-ART3>3.0.CO;2-9.
114. Kohn MD, Sassoon AA, Fernando ND. Classifications in Brief: Kellgren-Lawrence Classification of Osteoarthritis. *Clin Orthop Relat Res*. 2016;474(8):1886-1893. doi:10.1007/s11999-016-4732-4.
115. Li G, Yin J, Gao J, et al. Subchondral bone in osteoarthritis: insight into risk factors and microstructural changes. *Arthritis Res Ther*. 2013;15(6):223. doi:10.1186/ar4405.
116. Zamli Z, Robson Brown K, Tarlton JF, et al. Subchondral bone plate thickening precedes chondrocyte apoptosis and cartilage degradation in spontaneous animal models of osteoarthritis. *Biomed Res Int*. 2014;2014:606870. doi:10.1155/2014/606870.
117. Kim Y-M, Joo Y-B. Patellofemoral osteoarthritis. *Knee Surg Relat Res*. 2012;24(4):193-200. doi:10.5792/ksrr.2012.24.4.193.
118. Yan J-Y, Tian F-M, Wang W-Y, et al. Age dependent changes in cartilage matrix, subchondral bone mass, and estradiol levels in blood serum, in naturally occurring osteoarthritis in Guinea pigs. *Int J Mol Sci*. 2014;15(8):13578-13595. doi:10.3390/ijms150813578.
119. Santangelo KS, Pieczarka EM, Nuovo GJ, Weisbrode SE, Bertone AL. Temporal expression and tissue distribution of interleukin-1β in two strains of guinea pigs with varying propensity for spontaneous knee osteoarthritis. *Osteoarthritis Cartilage*. 2011;19(4):439-448. doi:10.1016/j.joca.2011.01.004.
120. Santangelo KS, Nuovo GJ, Bertone AL. In vivo reduction or blockade of interleukin-1β in primary osteoarthritis influences expression of mediators implicated in pathogenesis. *Osteoarthritis Cartilage*. 2012;20(12):1610-1618. doi:10.1016/j.joca.2012.08.011.
121. Malfait A-M, Little CB. On the predictive utility of animal models of osteoarthritis. *Arthritis Res Ther*. 2015;17(1):225. doi:10.1186/s13075-015-0747-6.
122. Bagi CM, Zakur DE, Berryman E, Andresen CJ, Wilkie D. Correlation between μCT imaging, histology and functional capacity of the osteoarthritic knee in the rat model of osteoarthritis. *J Transl Med*. 2015;13:276. doi:10.1186/s12967-015-0641-7.
123. Pauly HM, Larson BE, Coatney GA, et al. Assessment of cortical and trabecular bone changes in two models of post-traumatic osteoarthritis. *J Orthop Res*. 2015;33(12):1835-1845. doi:10.1002/jor.22975.
124. Finnilä MAJ, Thevenot J, Aho O-M, et al. Association between subchondral bone structure and osteoarthritis histopathological grade. *J Orthop Res*. May 2016. doi:10.1002/jor.23312.
125. Sun Y, Scannell BP, Honeycutt PR, Mauerhan DR, H JN, Hanley EN. Cartilage Degeneration, Subchondral Mineral and Meniscal Mineral Densities in Hartley and Strain 13 Guinea Pigs. *Open Rheumatol J*. 2015;9:65-70. doi:10.2174/1874312901409010065.
126. Piscaer TM, van Osch GJVM, Verhaar JAN, Weinans H. Imaging of experimental osteoarthritis in small animal models. *Biorheology*. 2008;45(3-4):355-364.

http://www.ncbi.nlm.nih.gov/pubmed/18836236. Accessed September 19, 2016.
127. Palmer AW, Guldberg RE, Levenston ME. Analysis of cartilage matrix fixed charge density and three-dimensional morphology via contrast-enhanced microcomputed tomography. *Proc Natl Acad Sci U S A*. 2006;103(51):19255-19260. doi:10.1073/pnas.0606406103.
128. Xie L, Lin ASP, Levenston ME, Guldberg RE. Quantitative assessment of articular cartilage morphology via EPIC-μCT. *Osteoarthr Cartil*. 2009;17(3):313-320. doi:10.1016/j.joca.2008.07.015.
129. Walling C. Fenton's reagent revisited. *Acc Chem Res*. 1975;8(4):125-131. doi:10.1021/ar50088a003.
130. Schwartz KA, Fisher J, Adams~ ET. Morphologic Investigations of the Guinea Pig Model of Iron Overload*. 1993;21(3). http://journals.sagepub.com/doi/pdf/10.1177/019262339302100307. Accessed June 20, 2018.
131. Radakovich LB, Marolf AJ, Shannon JP, Pannone SC, Sherk VD, Santangelo KS. Development of a microcomputed tomography scoring system to characterize disease progression in the Hartley guinea pig model of spontaneous osteoarthritis. *Connect Tissue Res*. December 2017:1-11. doi:10.1080/03008207.2017.1409218.
132. Sands SA, Leung-Toung R, Wang Y, Connelly J, LeVine SM. Enhanced Histochemical Detection of Iron in Paraffin Sections of Mouse Central Nervous System Tissue: Application in the APP/PS1 Mouse Model of Alzheimers Disease. *ASN Neuro*. 2016;8(5). doi:10.1177/1759091416670978.
133. Idleburg C, DeLassus EN, Novack D V. Immunohistochemistry of Skeletal Tissues. In: *Methods in Molecular Biology (Clifton, N.J.)*. Vol 1226. ; 2015:87-95. doi:10.1007/978-1-4939-1619-1_8.
134. Rushton DH, Dover R, Sainsbury AW, Norris MJ, Gilkes JJ, Ramsay ID. Why should women have lower reference limits for haemoglobin and ferritin concentrations than men? *BMJ*. 2001;322(7298):1355-1357. http://www.ncbi.nlm.nih.gov/pubmed/11387188. Accessed August 10, 2018.
135. Huebner JL, Hanes MA, Beekman B, TeKoppele JM, Kraus VB. A comparative analysis of bone and cartilage metabolism in two strains of guinea-pig with varying degrees of naturally occurring osteoarthritis. *Osteoarthr Cartil*. 2002;10(10):758-767. http://www.ncbi.nlm.nih.gov/pubmed/12359161. Accessed August 10, 2018.
136. Menkes CJ, Lane NE. Are osteophytes good or bad? *Osteoarthr Cartil*. 2004;12 Suppl A:S53-4. http://www.ncbi.nlm.nih.gov/pubmed/14698643. Accessed August 10, 2018.
137. van der Kraan PM, van den Berg WB. Osteophytes: relevance and biology. *Osteoarthr Cartil*. 2007;15(3):237-244. doi:10.1016/J.JOCA.2006.11.006.
138. Boegård T, Rudling O, Petersson IF, Jonsson K. Correlation between radiographically diagnosed osteophytes and magnetic resonance detected cartilage defects in the patellofemoral joint. *Ann Rheum Dis*. 1998;57(7):395-400. http://www.ncbi.nlm.nih.gov/pubmed/9797565. Accessed August 10, 2018.
139. Felson DT, Gale DR, Elon Gale M, et al. Osteophytes and progression of knee osteoarthritis. *Rheumatology*. 2005;44(1):100-104. doi:10.1093/rheumatology/keh411.
140. Carroll GJ, Breidahl WH, Bulsara MK, Olynyk JK. Hereditary hemochromatosis is characterized by a clinically definable arthropathy that correlates with iron load. *Arthritis Rheum*. 2011;63(1):286-294. doi:10.1002/art.30094.

141. Chen S, Feng T, Vujić Spasić M, et al. Transforming Growth Factor β1 (TGF-β1) Activates Hepcidin mRNA Expression in Hepatocytes. *J Biol Chem*. 2016;291(25):13160-13174. doi:10.1074/jbc.M115.691543.
142. Wang R-H, Li C, Xu X, et al. A role of SMAD4 in iron metabolism through the positive regulation of hepcidin expression. *Cell Metab*. 2005;2(6):399-409. doi:10.1016/j.cmet.2005.10.010.
143. Sinigaglia L, Fargion S, Fracanzani AL, et al. Bone and joint involvement in genetic hemochromatosis: role of cirrhosis and iron overload. *J Rheumatol*. 1997;24(9):1809-1813. http://www.ncbi.nlm.nih.gov/pubmed/9292808. Accessed August 15, 2018.
144. Guggenbuhl P, Deugnier Y, Boisdet JF, et al. Bone mineral density in men with genetic hemochromatosis and HFE gene mutation. *Osteoporos Int*. 2005;16(12):1809-1814. doi:10.1007/s00198-005-1934-0.
145. Valenti L, Varenna M, Fracanzani AL, Rossi V, Fargion S, Sinigaglia L. Association between iron overload and osteoporosis in patients with hereditary hemochromatosis. *Osteoporos Int*. 2009;20(4):549-555. doi:10.1007/s00198-008-0701-4.
146. Diamond T, Pojer R, Stiel D, Alfrey A, Posen S. Does iron affect osteoblast function? Studies in vitro and in patients with chronic liver disease. *Calcif Tissue Int*. 1991;48(6):373-379. http://www.ncbi.nlm.nih.gov/pubmed/2070271. Accessed August 15, 2018.
147. de Vernejoul MC, Pointillart A, Golenzer CC, et al. Effects of iron overload on bone remodeling in pigs. *Am J Pathol*. 1984;116(3):377-384. http://www.ncbi.nlm.nih.gov/pubmed/6476075. Accessed August 15, 2018.
148. Tsay J, Yang Z, Ross FP, et al. Bone loss caused by iron overload in a murine model: importance of oxidative stress. *Blood*. 2010;116(14):2582-2589. doi:10.1182/blood-2009-12-260083.
149. Jagger CJ, Lean JM, Davies JT, Chambers TJ. Tumor Necrosis Factor-α Mediates Osteopenia Caused by Depletion of Antioxidants. *Endocrinology*. 2005;146(1):113-118. doi:10.1210/en.2004-1058.
150. Ha J-H, Doguer C, Wang X, Flores SR, Collins JF. High-Iron Consumption Impairs Growth and Causes Copper-Deficiency Anemia in Weanling Sprague-Dawley Rats. *PLoS One*. 2016;11(8):e0161033. doi:10.1371/journal.pone.0161033.
151. Gyorffy EJ, Chan H. Copper deficiency and microcytic anemia resulting from prolonged ingestion of over-the-counter zinc. *Am J Gastroenterol*. 1992;87(8):1054-1055. http://www.ncbi.nlm.nih.gov/pubmed/1642210. Accessed August 14, 2018.
152. Kaser A, Brandacher G, Steurer W, et al. Interleukin-6 stimulates thrombopoiesis through thrombopoietin: role in inflammatory thrombocytosis. *Blood*. 2001;98(9):2720-2725.
153. Leven RM, Clark B, Tablin F. Effect of Recombinant Interleukin-6 and Thrombopoietin on Isolated Guinea Pig Bone Marrow Megakaryocyte Protein Phosphorylation and Proplatelet Formation. *Blood Cells, Mol Dis*. 1997;23(2):252-268. doi:10.1006/bcmd.1997.0142.
154. Gruys E, Toussaint MJM, Niewold TA, Koopmans SJ. Acute phase reaction and acute phase proteins. *J Zhejiang Univ Sci B*. 2005;6(11):1045-1056. doi:10.1631/jzus.2005.B1045.
155. Bacon BR, Britton RS. The pathology of hepatic iron overload: A free radical-Mediated Process? *Hepatology*. 1990;11(1):127-137. doi:10.1002/hep.1840110122.
156. Santangelo KS, Radakovich LB, Fouts J, Foster MT. Pathophysiology of obesity on knee

joint homeostasis: contributions of the infrapatellar fat pad. *Horm Mol Biol Clin Investig*. 2016;26(2):97-108. doi:10.1515/hmbci-2015-0067.
157. Gierman LM, Wopereis S, van El B, et al. Metabolic profiling reveals differences in concentrations of oxylipins and fatty acids secreted by the infrapatellar fat pad of end-stage osteoarthritis and normal donors. *Arthritis Rheum*. July 2013:n/a-n/a. doi:10.1002/art.38081.
158. Han W, Cai S, Liu Z, et al. Infrapatellar fat pad in the knee: is local fat good or bad for knee osteoarthritis? *Arthritis Res Ther*. 2014;16(4):R145. doi:10.1186/ar4607.
159. Ioan-Facsinay A, Kloppenburg M. An emerging player in knee osteoarthritis: the infrapatellar fat pad. *Arthritis Res Ther*. 2013;15(6):225. doi:10.1186/ar4422.
160. Fu Y, Huebner JL, Kraus VB, Griffin TM. Effect of Aging on Adipose Tissue Inflammation in the Knee Joints of F344BN Rats. *Journals Gerontol Ser A Biol Sci Med Sci*. 2016;71(9):1131-1140. doi:10.1093/gerona/glv151.
161. Distel E, Cadoudal T, Durant S, Poignard A, Chevalier X, Benelli C. The infrapatellar fat pad in knee osteoarthritis: An important source of interleukin-6 and its soluble receptor. *Arthritis Rheum*. 2009;60(11):3374-3377. doi:10.1002/art.24881.
162. Hubler MJ, Peterson KR, Hasty AH. Iron homeostasis: a new job for macrophages in adipose tissue? *Trends Endocrinol Metab*. 2015;26(2):101-109. doi:10.1016/j.tem.2014.12.005.
163. Kohgo Y, Ikuta K, Ohtake T, Torimoto Y, Kato J. Body iron metabolism and pathophysiology of iron overload. *Int J Hematol*. 2008;88(1):7-15. doi:10.1007/s12185-008-0120-5.
164. Green R, Charlton R, Seftel H, et al. Body iron excretion in man. *Am J Med*. 1968;45(3):336-353. doi:10.1016/0002-9343(68)90069-7.
165. Ganz T, Enns CA. Hepcidin, a key regulator of iron metabolism and mediator of anemia of inflammation. *Blood*. 2003;102(3):783-788. doi:10.1182/blood-2003-03-0672.
166. Vela D. Hepcidin, an emerging and important player in brain iron homeostasis. *J Transl Med*. 2018;16(1):25. doi:10.1186/s12967-018-1399-5.
167. Gnana-Prakasam JP, Martin PM, Mysona BA, Roon P, Smith SB, Ganapathy V. Hepcidin expression in mouse retina and its regulation via lipopolysaccharide/Toll-like receptor-4 pathway independent of Hfe. *Biochem J*. 2008;411(1):79-88. doi:10.1042/BJ20071377.
168. Kennish L, Attur M, Oh C, et al. Age-dependent ferritin elevations and HFE C282Y mutation as risk factors for symptomatic knee osteoarthritis in males: a longitudinal cohort study. *BMC Musculoskelet Disord*. 2014;15(1):8. doi:10.1186/1471-2474-15-8.
169. Hooiveld M, Roosendaal G, Wenting M, van den Berg M, Bijlsma J, Lafeber F. Short-Term Exposure of Cartilage to Blood Results in Chondrocyte Apoptosis. *Am J Pathol*. 2003;162(3):943-951. doi:10.1016/S0002-9440(10)63889-8.
170. Pulles AE, Mastbergen SC, Schutgens REG, Lafeber FPJG, van Vulpen LFD. Pathophysiology of hemophilic arthropathy and potential targets for therapy. *Pharmacol Res*. 2017;115:192-199. doi:10.1016/j.phrs.2016.11.032.
171. LAFEBER FPJG, MIOSSEC P, VALENTINO LA. Physiopathology of haemophilic arthropathy. *Haemophilia*. 2008;14(s4):3-9. doi:10.1111/j.1365-2516.2008.01732.x.
172. Henrotin Y., Bruckner P, Pujol J-P. The role of reactive oxygen species in homeostasis and degradation of cartilage. *Osteoarthr Cartil*. 2003;11(10):747-755. doi:10.1016/S1063-4584(03)00150-X.
173. Xue H, Tu Y, Ma T, et al. Lactoferrin Inhibits IL-1β-Induced Chondrocyte Apoptosis

Through AKT1-Induced CREB1 Activation. *Cell Physiol Biochem*. 2015;36(6):2456-2465. doi:10.1159/000430206.
174. Yan D, Chen D, Shen J, Xiao G, van Wijnen AJ, Im H-J. Bovine lactoferricin is anti-inflammatory and anti-catabolic in human articular cartilage and synovium. *J Cell Physiol*. 2013;228(2):447-456. doi:10.1002/jcp.24151.
175. Lee KS, Jang JS, Lee DR, et al. Serum ferritin levels are positively associated with bone mineral density in elderly Korean men: the 2008–2010 Korea National Health and Nutrition Examination Surveys. *J Bone Miner Metab*. 2014;32(6):683-690. doi:10.1007/s00774-013-0540-z.
176. Pan M-L, Chen L-R, Tsao H-M, et al. Iron Deficiency Anemia as a Risk Factor for Osteoporosis in Taiwan: A Nationwide Population-Based Study. *Nutrients*. 2017;9(6):616. doi:10.3390/nu9060616.
177. Harris MM, Houtkooper LB, Stanford VA, et al. Dietary Iron Is Associated with Bone Mineral Density in Healthy Postmenopausal Women. *J Nutr*. 2003;133(11):3598-3602. doi:10.1093/jn/133.11.3598.
178. Wawer AA, Jennings A, Fairweather-Tait SJ. Iron status in the elderly: A review of recent evidence. *Mech Ageing Dev*. 2018;175:55-73. doi:10.1016/J.MAD.2018.07.003.
179. Bainton DF, Finch CA. The diagnosis of iron deficiency anemia. *Am J Med*. 1964;37(1):62-70. doi:10.1016/0002-9343(64)90212-8.
180. Weiser G, O'Grady M. Erythrocyte Volume Distribution Analysis and Hematologic Changes in Dogs with Iron Deficiency Anemia. *Vet Pathol*. 1983;20(2):230-241. doi:10.1177/030098588302000211.
181. Naigamwalla DZ, Webb JA, Giger U. Iron deficiency anemia. *Can Vet J = La Rev Vet Can*. 2012;53(3):250-256. http://www.ncbi.nlm.nih.gov/pubmed/22942439. Accessed August 9, 2018.
182. Schloesser LL, Kipp MA, Wenzel FJ. Thrombocytosis in iron-deficiency anemia. *J Lab Clin Med*. 1965;66(1):107-114. doi:10.5555/URI:PII:0022214365900831.
183. Kaser A, Brandacher G, Steurer W, et al. Interleukin-6 stimulates thrombopoiesis through thrombopoietin: role in inflammatory thrombocytosis. *Blood*. 2001;98(9):2720-2725. doi:10.1182/BLOOD.V98.9.2720.
184. Poggiali E, Cassinerio E, Zanaboni L, Cappellini MD. An update on iron chelation therapy. *Blood Transfus*. 2012;10(4):411-422. doi:10.2450/2012.0008-12.
185. Trippel S, Ghivizzani S, Nixon A. Gene-based approaches for the repair of articular cartilage. *Gene Ther*. 2004;11(4):351-359. doi:10.1038/sj.gt.3302201.
186. Katz JN, Brownlee SA, Jones MH. The role of arthroscopy in the management of knee osteoarthritis. *Best Pract Res Clin Rheumatol*. 2014;28(1):143-156. doi:10.1016/j.berh.2014.01.008.
187. Klein-Wieringa IR, Andersen SN, Kwekkeboom JC, et al. Adipocytes modulate the phenotype of human macrophages through secreted lipids. *J Immunol*. 2013;191(3):1356-1363. doi:10.4049/jimmunol.1203074.
188. Sjunnesson H, Sturegard E, Grubb A, Willen R, Wadstrom T. Comparative study of Helicobacter pylori infection in guinea pigs and mice -- elevation of acute-phase protein C3 in infected guinea pigs. *FEMS Immunol Med Microbiol*. 2001;30(2):167-172. doi:10.1111/j.1574-695X.2001.tb01566.x.
189. Favero M, El-Hadi H, Belluzzi E, et al. Infrapatellar fat pad features in osteoarthritis: a histopathological and molecular study. *Rheumatology*. 2017;56(10):1784-1793.

doi:10.1093/rheumatology/kex287.
190. Aikawa J, Uchida K, Takano S, et al. Expression of calcitonin gene-related peptide in the infrapatellar fat pad in knee osteoarthritis patients. *J Orthop Surg Res*. 2017;12(1):65. doi:10.1186/s13018-017-0568-1.
191. Torti FM, Torti S V. Regulation of ferritin genes and protein. *Blood*. 2002;99(10):3505-3516. http://www.ncbi.nlm.nih.gov/pubmed/11986201. Accessed July 31, 2018.
192. Li C, Zhou H-M. The Role of Manganese Superoxide Dismutase in Inflammation Defense. *Enzyme Res*. 2011;2011:1-6. doi:10.4061/2011/387176.
193. Dautry-Varsat A, Ciechanover A, Lodish HF. pH and the recycling of transferrin during receptor-mediated endocytosis. *Proc Natl Acad Sci U S A*. 1983;80(8):2258-2262. doi:10.1073/PNAS.80.8.2258.
194. Brissot P, Ropert M, Le Lan C, Loréal O. Non-transferrin bound iron: A key role in iron overload and iron toxicity. *Biochim Biophys Acta - Gen Subj*. 2012;1820(3):403-410. doi:10.1016/J.BBAGEN.2011.07.014.
195. Ji C, Kosman DJ. Molecular mechanisms of non-transferrin-bound and transferring-bound iron uptake in primary hippocampal neurons. *J Neurochem*. 2015;133(5):668-683. doi:10.1111/jnc.13040.
196. Tripathi AK, Karmakar S, Asthana A, et al. Transport of Non-Transferrin Bound Iron to the Brain: Implications for Alzheimer's Disease. *J Alzheimers Dis*. 2017;58(4):1109-1119. doi:10.3233/JAD-170097.
197. Coffey R, Knutson MD. The plasma membrane metal-ion transporter ZIP14 contributes to nontransferrin-bound iron uptake by human β-cells. *Am J Physiol Physiol*. 2017;312(2):C169-C175. doi:10.1152/ajpcell.00116.2016.
198. Prakash M. Role of non-transferrin-bound iron in chronic renal failure and other disease conditions. *Indian J Nephrol*. 2007;17(4):188. doi:10.4103/0971-4065.39169.
199. Bohnsack M, Wilharm A, Hurschler C, Rühmann O, Stukenborg-Colsman C, Wirth CJ. Biomechanical and kinematic influences of a total infrapatellar fat pad resection on the knee. *Am J Sports Med*. 2004;32(8):1873-1880. http://www.ncbi.nlm.nih.gov/pubmed/15572315. Accessed July 31, 2018.
200. McCulloch K, Litherland GJ, Rai TS. Cellular senescence in osteoarthritis pathology. *Aging Cell*. 2017;16(2):210-218. doi:10.1111/acel.12562.
201. Martel-Pelletier J, Barr AJ, Cicuttini FM, et al. Osteoarthritis. *Nat Rev Dis Prim*. 2016;2:16072. doi:10.1038/nrdp.2016.72.
202. Collaborators TG 2015 O. Health Effects of Overweight and Obesity in 195 Countries over 25 Years. *N Engl J Med*. June 2017:NEJMoa1614362. doi:10.1056/NEJMoa1614362.
203. Pottie P, Presle N, Terlain B, Netter P, Mainard D, Berenbaum F. Obesity and osteoarthritis: more complex than predicted! *Ann Rheum Dis*. 2006;65(11):1403-1405. doi:10.1136/ard.2006.061994.
204. Bliddal H, Leeds AR, Christensen R. Osteoarthritis, obesity and weight loss: evidence, hypotheses and horizons - a scoping review. *Obes Rev*. 2014;15(7):578-586. doi:10.1111/obr.12173.
205. Vuolteenaho K, Koskinen A, Moilanen E. Leptin - A Link between Obesity and Osteoarthritis. Applications for Prevention and Treatment. *Basic Clin Pharmacol Toxicol*. 2014;114(1):103-108. doi:10.1111/bcpt.12160.
206. Berenbaum F, Eymard F, Houard X. Osteoarthritis, inflammation and obesity. *Curr Opin*

Rheumatol. 2013;25(1):114-118. doi:10.1097/BOR.0b013e32835a9414.
207. Cancello R, Clément K. Review article: Is obesity an inflammatory illness? Role of low-grade inflammation and macrophage infiltration in human white adipose tissue. *BJOG An Int J Obstet Gynaecol*. 2006;113(10):1141-1147. doi:10.1111/j.1471-0528.2006.01004.x.
208. Herder C, Schneitler S, Rathmann W, et al. Low-Grade Inflammation, Obesity, and Insulin Resistance in Adolescents. *J Clin Endocrinol Metab*. 2007;92(12):4569-4574. doi:10.1210/jc.2007-0955.
209. Monteiro R, Azevedo I. Chronic inflammation in obesity and the metabolic syndrome. *Mediators Inflamm*. 2010;2010. doi:10.1155/2010/289645.
210. Magnuson A, Fouts J, Booth A, Foster M. Obesity-induced chronic low grade inflammation: Gastrointestinal and adipose tissue crosstalk. *Integr Obes Diabetes*. 2015;1(5). doi:10.15761/IOD.1000124.
211. Iwata M, Ochi H, Hara Y, et al. Initial responses of articular tissues in a murine high-fat diet-induced osteoarthritis model: pivotal role of the IPFP as a cytokine fountain. Fritz JH, ed. *PLoS One*. 2013;8(4):e60706. doi:10.1371/journal.pone.0060706.
212. Cordain L, Eaton SB, Sebastian A, et al. Origins and evolution of the Western diet: health implications for the 21st century. *Am J Clin Nutr*. 2005;81(2):341-354. http://www.ncbi.nlm.nih.gov/pubmed/15699220. Accessed July 18, 2017.
213. McNeill JN, Wu C-L, Rabey KN, Schmitt D, Guilak F. Life-long caloric restriction does not alter the severity of age-related osteoarthritis. *Age (Omaha)*. 2014;36(4):9669. doi:10.1007/s11357-014-9669-5.
214. Fontana L, Klein S. Aging, Adiposity, and Calorie Restriction. *JAMA*. 2007;297(9):986. doi:10.1001/jama.297.9.986.
215. Paolisso G, Rizzo MR, Mazziotti G, et al. Advancing age and insulin resistance: role of plasma tumor necrosis factor-alpha. *Am J Physiol*. 1998;275(2 Pt 1):E294-9. http://www.ncbi.nlm.nih.gov/pubmed/9688632. Accessed July 25, 2017.
216. Weiss EP, Fontana L. Caloric restriction: powerful protection for the aging heart and vasculature. *AJP Hear Circ Physiol*. 2011;301(4):H1205-H1219. doi:10.1152/ajpheart.00685.2011.
217. You T, Sonntag WE, Leng X, Carter CS. Lifelong caloric restriction and interleukin-6 secretion from adipose tissue: effects on physical performance decline in aged rats. *J Gerontol A Biol Sci Med Sci*. 2007;62(10):1082-1087. http://www.ncbi.nlm.nih.gov/pubmed/17921419. Accessed July 25, 2017.
218. Kealy RD, Lawler DF, Ballam JM, et al. Evaluation of the effect of limited food consumption on radiographic evidence of osteoarthritis in dogs. *J Am Vet Med Assoc*. 2000;217(11):1678-1680. http://www.ncbi.nlm.nih.gov/pubmed/11110459. Accessed July 25, 2017.
219. Runge JJ, Biery DN, Lawler DF, et al. The effects of lifetime food restriction on the development of osteoarthritis in the canine shoulder. *Vet Surg*. 2008;37(1):102-107. doi:10.1111/j.1532-950X.2007.00354.x.
220. Bendele AM, Hulman JF. Effects of body weight restriction on the development and progression of spontaneous osteoarthritis in guinea pigs. *Arthritis Rheum*. 1991;34(9):1180-1184. http://www.ncbi.nlm.nih.gov/pubmed/1930336. Accessed July 25, 2017.
221. Jimenez PA, Glasson SS, Trubetskoy O V, Haimes HB. Spontaneous osteoarthritis in Dunkin Hartley guinea pigs: histologic, radiologic, and biochemical changes. *Lab Anim*

Sci. 1997;47(6):598-601. http://www.ncbi.nlm.nih.gov/pubmed/9433695. Accessed July 18, 2017.
222. Podell BK, Ackart DF, Richardson MA, DiLisio JE, Pulford B, Basaraba RJ. A model of type 2 diabetes in the guinea pig using sequential diet-induced glucose intolerance and streptozotocin treatment. *Dis Model Mech*. 2017;10(2). http://dmm.biologists.org/content/10/2/151.long#sec-1. Accessed July 19, 2017.
223. West KL, Fernandez ML. Guinea pigs as models to study the hypocholesterolemic effects of drugs. *Cardiovasc Drug Rev*. 2004;22(1):55-70. http://www.ncbi.nlm.nih.gov/pubmed/14978518. Accessed July 25, 2017.
224. Madsen CS, Janovitz E, Zhang R, et al. The Guinea Pig as a Preclinical Model for Demonstrating the Efficacy and Safety of Statins. *J Pharmacol Exp Ther*. 2008;324(2). http://jpet.aspetjournals.org/content/324/2/576?ijkey=4b019e0e2f805e5b09e90609823822eb0d212453&keytype2=tf_ipsecsha. Accessed July 25, 2017.
225. Ensign WY, McNamara DJ, Fernandez ML. Exercise improves plasma lipid profiles and modifies lipoprotein composition in guinea pigs. *J Nutr Biochem*. 2002;13(12):747-753. http://www.ncbi.nlm.nih.gov/pubmed/12550059. Accessed July 25, 2017.
226. Fernandez ML, Wilson TA, Conde K, Vergara-Jimenez M, Nicolosi RJ. Hamsters and Guinea Pigs Differ in Their Plasma Lipoprotein Cholesterol Distribution when Fed Diets Varying in Animal Protein, Soluble Fiber, or Cholesterol Content. *J Nutr*. 1999;129(7):1323-1332. http://jn.nutrition.org/content/129/7/1323?ijkey=78e9dd394323a8562f3f2dfa2c6f849c9f56aae0&keytype2=tf_ipsecsha. Accessed July 25, 2017.
227. Ye P, Cheah IK, Halliwell B. High fat diets and pathology in the guinea pig. Atherosclerosis or liver damage? *Biochim Biophys Acta - Mol Basis Dis*. 2013;1832(2):355-364. doi:10.1016/j.bbadis.2012.11.008.
228. Tveden-Nyborg P, Birck MM, Ipsen DH, et al. Diet-induced dyslipidemia leads to nonalcoholic fatty liver disease and oxidative stress in guinea pigs. *Transl Res*. 2016;168:146-160. doi:10.1016/j.trsl.2015.10.001.
229. Bendele AM, White SL, Hulman JF. Osteoarthrosis in guinea pigs: histopathologic and scanning electron microscopic features. *Lab Anim Sci*. 1989;39(2):115-121. http://www.ncbi.nlm.nih.gov/pubmed/2709799. Accessed June 22, 2018.
230. Rose SR, Petersen NJ, Gardner TJ, Hamill RJ, Trautner BW. Etiology of thrombocytosis in a general medicine population: analysis of 801 cases with emphasis on infectious causes. *J Clin Med Res*. 2012;4(6):415-423. doi:10.4021/jocmr1125w.
231. Vahlensieck M, Linneborn G, Schild H, Schmidt H-M. Hoffa's recess: incidence, morphology and differential diagnosis of the globular-shaped cleft in the infrapatellar fat pad of the knee on MRI and cadaver dissections. *Eur Radiol*. 2002;12(1):90-93. doi:10.1007/s003300100982.
232. Diepold J, Ruhdorfer A, Dannhauer T, Wirth W, Steidle E, Eckstein F. Sex-differences of the healthy infra-patellar (Hoffa) fat pad in relation to intermuscular and subcutaneous fat content--data from the Osteoarthritis Initiative. *Ann Anat*. 2015;200:30-36. doi:10.1016/j.aanat.2014.12.004.
233. Ballegaard C, Riis RGC, Bliddal H, et al. Knee pain and inflammation in the infrapatellar fat pad estimated by conventional and dynamic contrast-enhanced magnetic resonance imaging in obese patients with osteoarthritis: a cross-sectional study. *Osteoarthr Cartil*. 2014;22(7):933-940. doi:10.1016/j.joca.2014.04.018.

234. Cortez M, Carmo LS, Rogero MM, Borelli P, Fock RA. A High-Fat Diet Increases IL-1, IL-6, and TNF-α Production by Increasing NF-κB and Attenuating PPAR-γ Expression in Bone Marrow Mesenchymal Stem Cells. *Inflammation*. 2013;36(2):379-386. doi:10.1007/s10753-012-9557-z.
235. Goldring MB, Otero M. Inflammation in osteoarthritis. *Curr Opin Rheumatol*. 2011;23(5):471-478. doi:10.1097/BOR.0b013e328349c2b1.
236. Foldager CB, Toh WS, Gomoll AH, Olsen BR, Spector M. Distribution of Basement Membrane Molecules, Laminin and Collagen Type IV, in Normal and Degenerated Cartilage Tissues. *Cartilage*. 2014;5(2):123-132. doi:10.1177/1947603513518217.
237. Foldager CB, Toh WS, Christensen BB, Lind M, Gomoll AH, Spector M. Collagen Type IV and Laminin Expressions during Cartilage Repair and in Late Clinically Failed Repair Tissues from Human Subjects. *Cartilage*. 2016;7(1):52-61. doi:10.1177/1947603515604022.
238. Scanzello CR. Chemokines and inflammation in osteoarthritis: Insights from patients and animal models. *J Orthop Res*. 2017;35(4):735-739. doi:10.1002/jor.23471.
239. Monibi F, Roller BL, Stoker A, Garner B, Bal S, Cook JL. Identification of Synovial Fluid Biomarkers for Knee Osteoarthritis and Correlation with Radiographic Assessment. *J Knee Surg*. 2016;29(3):242-247. doi:10.1055/s-0035-1549022.
240. Ramesh G. Novel Therapeutic Targets in Neuroinflammation and Neuropathic Pain. *Inflamm Cell Signal*. 2014;1(3). doi:10.14800/ics.111.
241. Borzì RM, Mazzetti I, Cattini L, Uguccioni M, Baggiolini M, Facchini A. Human chondrocytes express functional chemokine receptors and release matrix-degrading enzymes in response to C-X-C and C-C chemokines. *Arthritis Rheum*. 2000;43(8):1734-1741. doi:10.1002/1529-0131(200008)43:8<1734::AID-ANR9>3.0.CO;2-B.
242. Yuan GH, Masuko-Hongo K, Sakata M, et al. The role of C-C chemokines and their receptors in osteoarthritis. *Arthritis Rheum*. 2001;44(5):1056-1070. doi:10.1002/1529-0131(200105)44:5<1056::AID-ANR186>3.0.CO;2-U.
243. Appleton CTG, Usmani SE, Pest MA, Pitelka V, Mort JS, Beier F. Reduction in disease progression by inhibition of transforming growth factor α-CCL2 signaling in experimental posttraumatic osteoarthritis. *Arthritis Rheumatol (Hoboken, NJ)*. 2015;67(10):2691-2701. doi:10.1002/art.39255.
244. Yang M, Li K. The role of cytokines and transcription factors in megakaryocytopoiesis. *Zhongguo shi yan xue ye xue za zhi*. 2002;10(6):580-585. http://www.ncbi.nlm.nih.gov/pubmed/12513728. Accessed June 21, 2018.
245. Samocha-Bonet D, Justo D, Rogowski O, et al. Platelet counts and platelet activation markers in obese subjects. *Mediators Inflamm*. 2008;2008:834153. doi:10.1155/2008/834153.
246. Santangelo KS, Radakovich LB, Fouts J, Foster MT. Pathophysiology of obesity on knee joint homeostasis: Contributions of the infrapatellar fat pad. *Horm Mol Biol Clin Investig*. 2016;26(2). doi:10.1515/hmbci-2015-0067.